UNIVERSITY OF ILLINOIS AT CHICAGO CIRCLE

THE GRADUATE COLLEGE

June 30, 1982

I HEREBY RECOMMEND THAT THE THESIS PREPARED UNDER MY SUPERVISION BY MARIA HELENA DE AZAMBUJA VICCARO

ENTITLED THEORY OF OPTICAL AND MAGNETIC PROPERTIES OF DEEP CENTERS IN SEMICONDUCTORS

BE ACCEPTED IN PARTIAL FULFILLMENT OF THE REQUIREMENTS FOR THE DEGREE OF Doctor of Philosophy

R. R. Gamo
In Charge of Thesis

Recommendation concurred in

S. Sundaram
Cynthia J. Jameson
Ede Mon Kwan
H. Paquameuta
R. R. Gamo

Committee on Final Examination

D517

THEORY OF OPTICAL AND MAGNETIC PROPERTIES OF DEEP CENTERS IN SEMICONDUCTORS

BY

MARIA HELENA de AZAMBUJA VICCARO

B.S. Universidade Federal do Rio Grande do Sul, Brazil, 1972
M.S. Universidade Federal do Rio Grande do Sul, Brazil, 1975
M.S. University of Illinois at Chicago Circle, 1979

THESIS

Submitted in partial fulfillment of the requirements
for the degree of Doctor of Philosophy in Physics
in the Graduate College of the
University of Illinois at Chicago Circle, 1982

Chicago, Illinois

ACKNOWLEDGEMENTS

I thank Professor R. R. Sharma, my thesis advisor, for his encouragement and perseverance throughout my thesis research work. I also wish to thank Professor S. Sundaram, for his collaboration and kind assistance. Professor P. M. Raccah has my appreciation for showing interest in my progress as a graduate student in the Physics Department.

I am grateful to my fellow graduate students, who so often assisted me with their friendship. I am profoundly grateful to my dear husband, Jim, for his understanding and constant encouragement.

Finally, I acknowledge the research fellowship from CNPq-Brazil.

ABSTRACT

The present work is concerned with the theory of optical and magnetic properties of deep centers in various III-V semiconductors. The localized impurity levels of GaAs:Cr^{2+}, GaAs:Cr^{3+}, InP:Cr^{2+}, InP:Fe^{2+}, GaAs:Fe^{2+}, and GaP:Fe^{2+} materials are analyzed in the framework of a molecular cluster, taking into account the crystalline fields, Jahn-Teller distortion, and spin-orbit and spin-spin interactions. Cluster wave functions, compatible with tetrahedral and tetragonal symmetries, are constructed, using the best available self-consistent atomic wave functions for the impurity ion and the nearest-neighbors atoms. The multi-center integrals encountered in our calculations are evaluated using an available expression for the expansion of Slater orbitals from one center onto another.

A generalized treatment for electron-electron interactions of the impurity centers is presented, and the matrices for the d^2, d^3, d^4, and d^5 configurations are explicitly listed for the irreducible representations of the cubic crystal field. The general matrices are used to calculate the energy splittings of GaAs:Cr^{3+} and GaAs:Cr^{2+}. Our calculated value of the energy of the ^5E-$^5T_2$ transition for GaAs:Cr^{2+} is 0.65 eV, in good agreement with the experimental value, 0.68 eV. A comparison with previous theoretical calculations for these systems is also made. Calculations of the spin-Hamiltonian parameters are performed for GaAs:Cr^{2+} and InP:Cr^{2+}. We obtain, for InP:Cr^{2+}, $g_{\parallel} = 1.981$, $g_{\perp} = 2.010$, $D = -0.979\ cm^{-1}$,

and a = 0.089 cm^{-1}, in good agreement with the experimental values of $g_{||}$ = 1.981, $g_{\perp}$ = 2.010, D = -0.967 cm^{-1}, and a = 0.089 cm^{-1}. For GaAs:Cr^{2+}, our calculations result in $g_{||}$ = 1.975, $g_{\perp}$ = 1.995, and D = -1.865 cm^{-1}, compared to the values $g_{||}$ = 1.974, $g_{\perp}$ = 1.997, and D = -1.860 cm^{-1} determined experimentally. The calculated value of a = 0.0043 cm^{-1}, on the other hand, is an order of magnitude smaller than the experimental value of a = 0.031. An estimate of the tetragonal distortion on GaAs:Cr^{2+} is presented. The intensity ratio of two electric-dipole transitions in this system is predicted, using two contradictory sets of experimental values for the Jahn-Teller energies. The calculated ratios are found to be very different (135.1 and 7.45) for the two sets of data, implying that an experimental determination of the transition intensities could indicate which assignment is correct. Results are also presented for the case of Fe^{2+} in GaAs, GaP, and InP systems, for which we calculate the transition energies between the states $^5T_2$ and ^5E, taking into account spin-orbit and spin-spin interactions.

TABLE OF CONTENTS

TABLE OF CONTENTS (continued)

LIST OF TABLES

LIST OF TABLES (continued)

LIST OF FIGURES

I. INTRODUCTION

There is increasing interest in the III-V semiconductor materials containing transition-metal impurities, because of their important applications, such as in photoconductors, microwave detectors, and other optoelectronic devices. Chromium and iron doping of III-V semiconductors, such as GaAs, InP, and GaP, is known to produce deep acceptor levels in the forbidden band-gap of these systems, which compensate for shallow donor impurities and produce semi-insulating materials. Despite the great technological importance of Fe- and Cr-doped III-V compounds, little is known about the microscopic physical characteristics, such as the electronic structure of Fe and Cr impurities in GaAs, InP, and GaP. Although much progress has been made in studies of Cr- and Fe-doped III-V compounds, due to recent experimental work, there have been very few theoretical attempts to explain the experimental observations.

The scarcity of theoretical investigations on deep centers in III-V compounds has prompted us to make a systematic study of Cr^{2+}- and Fe^{2+}-doped GaAs, InP, and GaP. The theory of the electronic structure of the transition-metal ion impurities has not been well developed, because of the complexity of these systems. The electronic structure of the magnetic ion is no longer like that of a free ion, but is changed, due to interactions with the solid in which it is present as an impurity. Also, many additional electrons present in the solid interact with the magnetic ion, and among themselves, via various

interactions, such as electron-electron, spin-orbit, and spin-spin interactions. These interactions are complicated to deal with. It is obvious that a magnetic ion interacting with the solid constitutes a multi-particle system. Such a multi-particle problem cannot be solved exactly; therefore one has to resort to suitable approximations. As our interest lies in the localized impurity centers, we adopt a cluster approach, taking into account the crystal fields present in the solid, along with perturbations due to Jahn-Teller distortions and spin-orbit and spin-spin interactions.

For the GaAs and GaP systems, Fe^{2+} and Cr^{2+} impurities are substitutional on the Ga site, and for InP these impurities are substitutional on the In site. As the GaAs, GaP, and InP systems have a zinc-blende structure, the local symmetry around the transition-metal ions is tetrahedral. We have built up symmetry-adopted electronic wave functions for tetrahedral symmetry, and also for tetragonal symmetry, which is useful in case of strong Jahn-Teller distortion in these materials.

A generalized treatment for the d-electron interaction matrices is presented. These matrices for the d^2, d^3, d^4, and d^5 configurations are explicitly listed for the irreducible representations of the cubic crystal field. The method for obtaining d^6 to d^{10} and the general formula relating d^n to d^{10-n} are given. The interaction matrices have been evaluated for GaAs:Cr^{2+} and GaAs:Cr^{3+}, and compared with available experimental and theoretical results. The importance of the general matrix elements for designating correctly the energy levels, deducing the values of Coulomb and exchange integrals, and removing accidental degeneracy, is pointed out. Relative intensity calculations

for the Jahn-Teller split levels of GaAs:Cr^{2+} are presented, and an estimate of the Jahn-Teller tetragonal distortion is also made for this system. The explicit expressions for the spin-Hamiltonian parameters ($g_{\parallel}$, $g_{\perp}$, D, and a) for systems with local tetragonal symmetry are presented, and their values for GaAs:Cr^{2+} and InP:Cr^{2+} are calculated. The derived expressions for $g_{\parallel}$, $g_{\perp}$, and D take into account the Zeeman and spin-orbit interactions to the second order and spin-spin interaction to the first order in the ground state, including overlap and charge transfer. The expression for the cubic field parameter a includes fourth-order effects of the spin-orbit and second-order effects of the spin-spin interaction. The cubic crystal field and Jahn-Teller energy splittings are included in the present treatment. The transition energies between levels split by spin-orbit interaction to the second order, and spin-spin interaction in the first order, are obtained for GaAs:Fe^{2+}, GaP:Fe^{2+}, and InP:Fe^{2+}, including overlap and charge transfer covalency effects. We have evaluated exactly the multi-center integrals, which appear in our expressions for spin-orbit coupling constants, dipole transition moments, and in the cluster wave functions, using the available expression for the expansion of a function from one center onto the other. In our calculations of the several physical parameters mentioned above, we have used the best available self-consistent atomic wave functions for the transition-metal ions and ligands.

In Appendix I, we give details of Jahn-Teller interactions in tetrahedral configurations. In Appendix II, we present the

explicit form of the coefficients encountered in the expression for the expansion of Slater-type orbitals from one center onto another. In Chapter II we present a review of the existing experimental and theoretical results for III-V compounds doped with transition-metal ions. Chapter III contains the relevant theory needed to understand the systems under study. We construct wave functions of a cluster containing the central magnetic ion and the nearest neighbors, for both tetrahedral and tetragonal symmetries. The details of the generalized treatment for d-electron interaction matrices are presented in Section III.A. In Section III.B the spin-orbit and spin-spin interactions are handled. In Subsection III.B.1 the expressions for the spin-Hamiltonian parameters $g_{\parallel}$, $g_{\perp}$, D, and a pertinent to $GaAs:Cr^{2+}$ and $InP:Cr^{2+}$ are presented. In Subsection III.B.2 we present the energy splittings due to the spin-orbit and spin-spin interactions in the $GaAs:Fe^{2+}$, $GaP:Fe^{2+}$, and $InP:Fe^{2+}$ materials. The expressions for the electric dipole transition moments, which are useful for the calculation of intensity of transitions between the Jahn-Teller split levels $^5T_2$ and ^5E of Cr^{2+} in III-V materials, have been developed in Section III.C. Chapter IV contains our calculations of the various physical quantities presented in Chapter III. In particular, it contains the energy calculations of $GaAs:Cr^{2+}$ and $GaAs:Cr^{3+}$ using the generalized d-electron interaction matrices, in Section IV.A, where our results are also compared with the previous theoretical calculations and available experimental results; an estimate of the Jahn-Teller distortion for $GaAs:Cr^{2+}$ in Section IV.B; calculation of

overlap integrals in Section IV.C; calculation of spin-spin and spin-orbit constants in Section IV.D; spin-Hamiltonian parameters $g_{\parallel}$, $g_{\perp}$, D, and $\underline{a}$, for GaAs:Cr^{2+} and InP:Cr^{2+} in Section IV.E and comparisons with experimental results; prediction of relative intensities for GaAs:Cr^{2+} in Section IV.F; spin-orbit and spin-spin splitting energies of InP:Fe^{2+}, GaP:Fe^{2+}, and GaAs:Fe^{2+} in Section IV.G. Chapter V contains the discussion and conclusion of our work, an analysis of our results with the experimental data and the previous theoretical calculations; suggestions for future improvements are also indicated.

II. REVIEW OF THE EXISTING EXPERIMENTAL AND THEORETICAL RESULTS

The III-V semiconductor materials containing transition-metal impurities have been the subject of a considerable number of experimental and theoretical investigations. Optical and electron paramagnetic resonance (EPR) experiments have been extensively done with these semiconductor materials. The experimental results for chromium-doped GaAs, using photoluminescence[1-8], absorption[9], and photoconductivity[10-12] techniques, have shown peaks near 0.57 eV, 0.7 eV, 0.84 eV, and 0.9 eV. These lines have not been properly identified for a variety of reasons, such as the possible different charge states of Cr giving rise to mixed spectra, thereby making the analysis difficult.

Recently, White[13] has proposed a model for the 0.84 eV peak in GaAs:Cr as comprising a transition from a Cr^{3+} donor pair to a Cr^{2+} ionized donor pair. The Zeeman studies by Killoran *et al.*[14] seem to support White's model in GaAs:Cr, but still, the origin of the peak has not been clear. In fact, it is generally believed that the 0.84 eV peak corresponds to a transition in Cr^{2+} involving the ground state and the first excited state, with the spin S=2 as the ground state.

As mentioned above, transitions between different charge states of the impurity are possible, particularly, in photoinduced transitions[15-20]. The origin of the peaks at 0.57 eV, 0.7 eV, and 0.9 eV is debatable, since they may correspond to transitions related to intracenter Cr^{2+} or Cr^{3+}, or to transitions

from the bands of the solid to Cr impurity levels. Electron Paramagnetic Resonance experiments[15-18] indicate that a strong Jahn-Teller effect is present for the Cr^{2+} and Cr^{3+} impurity states in GaAs. For GaAs:Cr^{2+}, the impurity states undergo a strong Jahn-Teller distortion,[18] changing the symmetry at the Cr^{2+} site from tetrahedral (T_d) to tetragonal (D_{2d}), similar to the Cr^{2+}-doped II-VI compounds studied by Vallin et al.[21-23], as depicted in Fig. II.1. The free-ion term energy ^5D of d^4 is split by the tetrahedral crystal field into a ground state $^5T_2$ and an excited state ^5E. These levels split further, because of the Jahn-Teller distortion: the ground state $^5T_2$ (in T_d symmetry) splits into $^5B_2$ and ^5E (in D_{2d} symmetry), whereas the excited state ^5E (in T_d symmetry) splits into $^5A_1$ and $^5B_1$ (in D_{2d} symmetry). The magnitude of the Jahn-Teller splitting energy for GaAs:Cr^{2+} has been deduced by Krebs and Stauss[18] by analyzing stress measurements, by Tokumoto and Ishiguro[24] by ultrasonic attenuation, and by Hennel et al.[25] by optical absorption. Owing to the complexity of the system, the results from various experiments vary somewhat. Krebs and Stauss[18] have deduced a static Jahn-Teller distortion energy $E_{JT} = 1500\ cm^{-1}$; Tokumoto and Ishiguro[24] have obtained $E_{JT} = 399\ cm^{-1}$; Hennel et al.[25] have found that $360\ cm^{-1} < E_{JT} < 660\ cm^{-1}$.

In GaAs:Cr^{3+} there are some indications that an orthorhombic Jahn-Teller distortion may be present[15,16] (see Fig. II.2). The lowest-lying Cr^{3+} state under the cubic (T_d) crystal field is $^4T_1$. The ground state, $^4T_1$, further splits into three levels, under an orthorhombic Jahn-Teller distortion. Krebs and Stauss[15] have interpreted the EPR spectrum by means of the spin-Hamiltonian

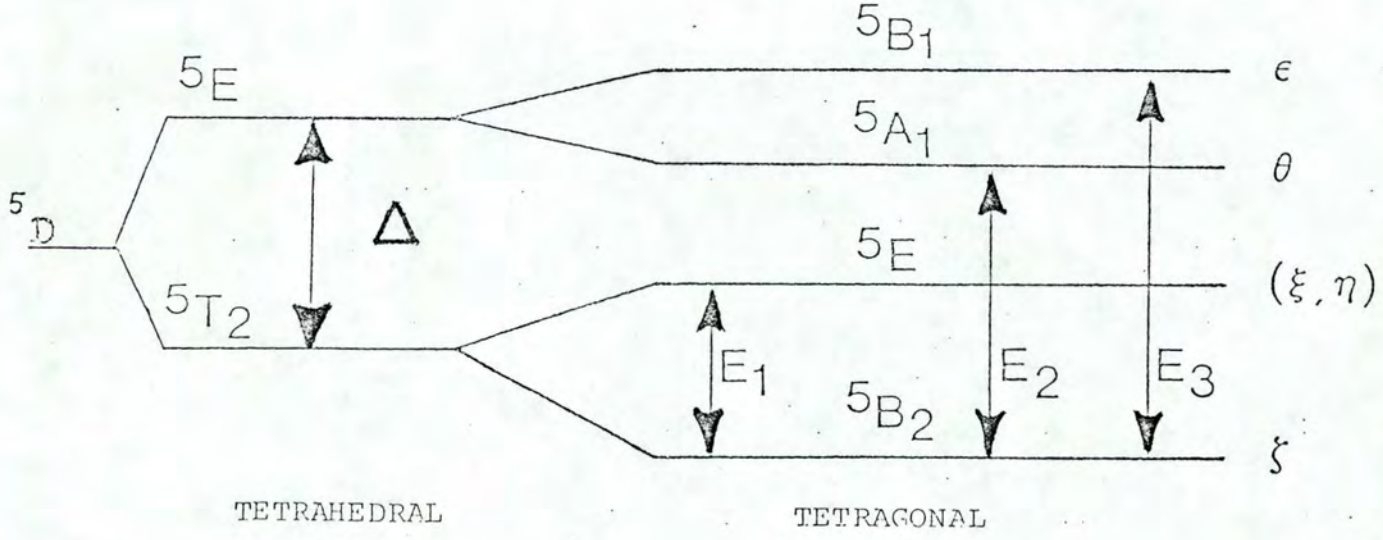

FIG.II.1

Splitting of the $Cr^{2+}(3d^4)$ free-ion ground state ^5D under combined action of the tetrahedral crystal field and the tetragonal Jahn-Teller distortion. The one-electron orbitals ζ, ξ, η, θ, and ε in the cubic field representation have been used to show the orbitals appropriate to the energy levels. The symmetry designations for each level are also shown.

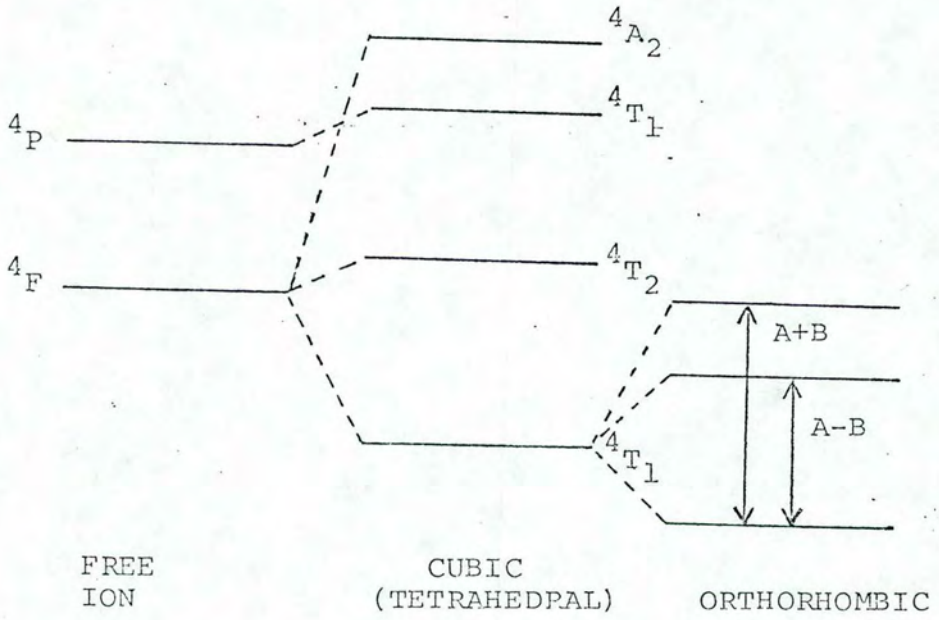

FIG.II.2

Splitting of the lowest states of $Cr^{3+}(3d^3)$ under the action of tetrahedral and orthorhombic $[A\ell_z^2 + B(\ell_x^2 - \ell_y^2)]$ crystal fields.

parameters g_x, g_y, g_z, and zero-field splitting parameters D and E, estimating the Jahn-Teller energy to be approximately 1867 cm^{-1}. More recently, Krebs and Stauss[16] reported the value of $E_{JT} \cong 2800\ cm^{-1}$, by analyzing stress measurements on GaAs:Cr^{3+}.

For GaP:Cr, EPR and infrared luminescence experiments have been reported by Kaufman and Koschel.[26] These authors have observed a 1.03 eV sharp line in photoluminescence measurements and an isotropic electron spin resonance signal with g = 1.999 in EPR measurements.

Experimental studies on iron-doped GaAs have been carried out for both Fe^{2+} and Fe^{3+}, using Acoustic Paramagnetic Resonance[27,28] and other techniques, such as the Hall effect, optical absorption, and photoluminescence[28-30]. In the photoluminescence and optical absorption spectra,[28,29] 0.32 eV and 0.5 eV peaks were observed for GaAs:Fe, giving an indication of intracenter transitions connected with the Fe impurity. Optical absorption experiments performed by Ippolitova et al.[30] in the range 0.37-0.5 eV have been attributed to intracenter transitions of Fe^{2+} in GaAs:Fe. The EPR measurements and optical results[31] in GaAs:Fe^{2+} and photoluminescence results[32] in GaP:Fe have been analyzed in terms of an externally introduced factor k, which has been termed the "covalency reduction factor".

Concerning iron- and chromium-doped InP, only a few experiments have been performed. The EPR results[33] show a cubic symmetry spectrum for InP:Fe^{3+}, and a tetragonal Jahn-Teller distortion for InP:Cr^{2+}. As for the optical data for iron-doped InP, by Koschel et al.[34], the luminescence peaks near 0.35 eV were

attributed to the intracenter Fe^{2+} transition, corresponding to transitions from the excited-state triplet ($^5T_2$) to the doublet (^5E) ground state (see Fig. II.3). The ground state of Fe^{2+} in InP is split by the second-order effect of the spin-orbit interaction. To analyze the experimental photoluminescense lines, Koschel et al.[34] introduced two external parameters into the expression that relates the split energy levels (see Fig. II.3) to the spin-orbit and spin-spin interactions without covalency and Jahn-Teller distortions[35-38]. One of the parameters introduced by Koschel et al.[34] is a multiplication factor, q, which reduces the energy-level spacings and accounts for a possible Jahn-Teller distortion. The other factor is k, which has been introduced to reduce the spin-orbit coupling associated with the impurity ions. The reduction factors, q and k, have been used for interpreting the experimental spectra, and do not give a clear indication of their physical origin in InP:Fe^{2+} and other related III-V compounds.

All the magnetic and optical experiments on GaAs:Cr, GaAs:Fe, InP:Cr, InP:Fe, and GaP:Fe clearly show that the impurity centers are strongly covalent in nature. It is this covalency effect which is roughly accounted for, by employment of the reduction factor k, by various authors.[31,32,34] Although this reduction factor is adjusted to explain the experimental data, it is not obvious how it appears as a simple multiplication factor.

As for the theory of deep-center impurity levels in semiconductors, not much progress has been made. The lack of knowledge of the correct wave functions for the transition-metal

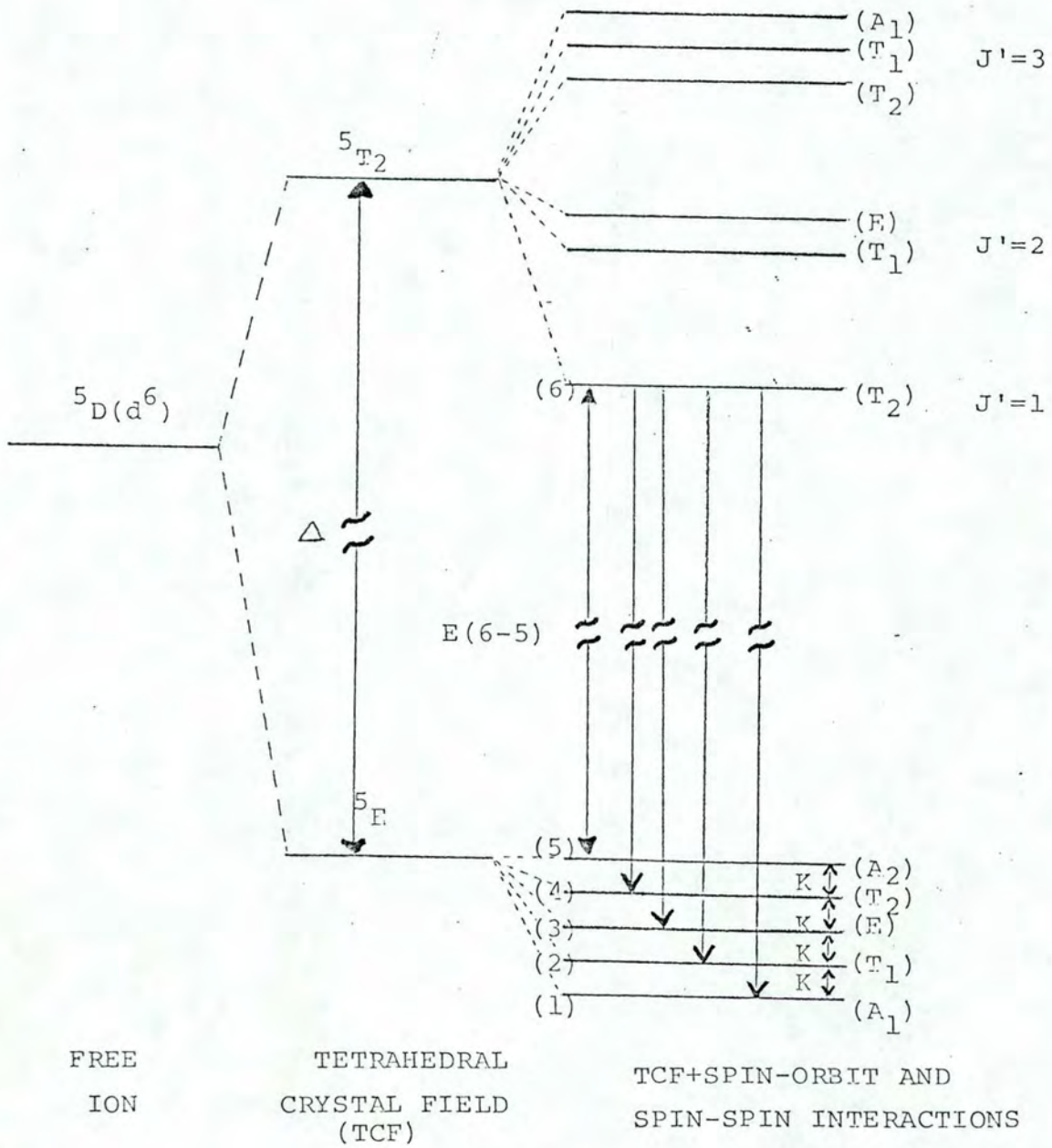

FIG.II.3

Fe^{2+} energy diagram, showing the effects of the tetrahedral crystal field, spin-orbit and spin-spin interactions. The allowed optical transitions are indicated by the arrows.

ions in a complex or a solid has been a stumbling block to real progress in the theoretical understanding of the experimental observations.

Hemstreet and Dimmock[39,40] and Sharma, Viccaro, and Sundaram[41] have calculated crystal-field term states for Cr^{2+} and Cr^{3+} in GaAs, using an approach that is a modification of the standard electron-electron interaction matrix elements, by introducing parameters (R_{ee}, R_{et}, and R_{tt}) accounting for the changes in the single-particle electronic states in the system. The parameters were deduced from the X_α scattered wave cluster calculations performed by Hemstreet et al.[39,42], which could not alone account for the electronic structure of Cr in GaAs. Recently, Sharma and Sundaram[43] have derived the explicit expressions for the generalized electron-electron interactions in a cubic field for d^n orbitals, in the process of investigating the electronic structures of Co^{2+} and Mn^{2+} in solids, and have been checked by Sharma, Viccaro, and Sundaram[41]. Reference [41] also gives the explicit expressions for electron-electron interaction matrices for electronic wave functions which are not of "pure" d character. With the pure d electron orbitals, such matrix elements had previously been derived by Tanabe and Sugano.[44] Sharma, Viccaro, and Sundaram[41,45] have also presented electronic energy levels arising from the electron-electron interactions in a cubic field in GaAs:Cr^{2+} and GaAs:Cr^{3+} which also correct the previous results obtained by Hemstreet and Dimmock[39,40]. This method, incorporating electron-electron interactions, has correctly predicted the ground state of Cr^{2+} in GaAs, and obtained 0.6 eV as the energy separation between the states $^5T_2$ and ^5E of Cr^{2+}, compared

to the corresponding experimental value of 0.68 eV for the cubic field splitting. The effects of the Jahn-Teller distortion, however, were not considered in these calculations.

The general electron-electron interaction matrix elements[41,43] have been shown to be useful for making the refined calculations of the transition-metal ions in solids, in order to obtain correct group-theoretical assignments to the observed energy levels of the impurity in solids. The refined treatment of the electron-electron interaction also predicts the values of the Coulomb and exchange interactions, which otherwise cannot be obtained from any other source. Also, the accidental degeneracy inherent in the B, C, Δ theory[44,46] (where B and C are known as "Racah's parameters" and Δ is the crystal field splitting energy) is automatically removed by this general treatment.

The charge states of Mn in the photoluminescence spectra of GaAs:Mn were studied by Srivastava, Sundaram, and Sharma[47]. These authors have performed multiple-scattered wave X_α calculations on pure GaAs, neutral Mn contained in GaAs, and GaAs:Mn^{2+}, and have found that Mn^{2+} is more strongly bound in GaAs than is neutral Mn. The binding energy of Mn^{2+} as calculated in reference [47] turned out to be 0.106 eV, which agrees with the photoluminescence[48,49] value 0.113 eV, also in conformation with the EPR observations[50].

The importance of covalency to the properties of transition-metal ions has been stressed by various authors.[51-53] The theoretical calculations on impurity systems are extremely difficult, owing to the complicated nature of the system. The wave functions of such systems are not exactly known, and only the

approximate methods can be employed.

Only recently, attempts have been made, by the present author and co-workers[54-58], to understand the overlap and charge-transfer covalency mechanisms for the transition-metal ions in the III-V compounds. Since these ions form deep center levels in the III-V semiconductors, a cluster approach to describing impurity states seems to be very appropriate. Deep center energy levels can be explained by using electronic wave functions involving the impurity and the surrounding atoms subjected to Jahn-Teller distortion, if present. In addition, owing to the inclusion of the neighboring ions along with the crystal fields, the method takes into account the influence of the surroundings not only on the optical levels but also on the magnetic splittings of the impurity, if spin-spin and spin-orbit interactions are considered. In other words, the important spin-Hamiltonian parameters g_x, g_y, g_z, zero field splitting parameter D, cubic field parameter a, etc., can be obtained by this treatment. Recently, the parameters $g_{\parallel}$, $g_{\perp}$, D, and $\underline{a}$ associated with GaAs:Cr^{2+} have been investigated theoretically by Viccaro, Sundaram, and Sharma,[54,55] using the cluster model, where the symmetry adopted wave functions were constructed, incorporating Jahn-Teller distortions. The calculations of the relative optical intensities have also been reported by Viccaro _et al._[56] in GaAs:Cr^{2+}, considering the Jahn-Teller effect.

For InP:Cr^{2+}, a similar cluster method, used for GaAs:Cr^{2+}, has also been reported by Viccaro, Sundaram, and Sharma,[57] considering the charge transfer covalency effects. Also, the observed optical spectra[34] for InP:Fe^{2+} have been studied with this approach, with symmetry adopted wave functions, by these

authors.[58]

The cluster approach, similar to the one used by Viccaro, Sundaram, and Sharma[54,55,57] in the study of the spin-Hamiltonian parameters $g_{||}$, $g_{\perp}$, D, and a of GaAs:Cr^{2+} and InP:Cr^{2+}, was adopted previously by Vallin and Watkins[23] for Cr^{2+}-doped II-VI compounds. However, one finds significant differences between the two treatments. For example, the s orbitals of the ligands have not been considered by Vallin and Watkins, and they have adopted an approximate treatment by taking a single parameter for estimating the orbital admixtures involved in the wave functions. Also, they have taken only the "local" and "distant" contributions into account; the "nonlocal" terms should be included, as is clear from the formalism developed by Sharma[53]. As far as the spin-orbit coupling constants are concerned, for estimating the spin-Hamiltonian parameters, one is required to use the first-principles method given by Sharma, Das, and Orbach,[52] and Sharma[59]. Also, for the overlap matrix elements one may use a general analytical expression derived by Sharma[60], for the overlap integrals between two Slater orbitals.

In the following chapters, we present details of the theory appropriate to GaAs:Cr^{2+}, GaAs:Cr^{3+}, GaAs:Fe^{2+}, InP:Cr^{2+}, InP:Fe^{2+}, and GaP:Fe^{2+}. The theory for these systems has not been available before. In chapter III, we present the theoretical details of symmetry, crystal fields, spin-orbit and spin-spin interactions, the spin-Hamiltonian, the derivation of spin-Hamiltonian parameters, and Jahn-Teller distortion using the cluster approach. In chapter IV, the calculations and

comparisons with experimental results are presented. Chapter V contains the discussion and conclusion, and suggestions are made for further improvements.

III. THEORY

In this chapter, we present a theory which we have developed to describe the optical and magnetic properties of transition-metal-doped III-V compounds. We are interested in obtaining the energy levels and wave functions of magnetic impurities in semiconductors, and in deriving expressions for the spin-Hamiltonian parameters ($g_{\parallel}$, $g_{\perp}$, D, and $\underline{a}$) and electric dipole moments for intensity calculations.

As mentioned previously, the theory of the electronic structure of the transition-metal impurities in semiconductors has not been well developed, because of the complex nature of the problem. In these complex systems, the electronic environment of the magnetic ion is no longer like that of free ions, but is changed because of interactions with the solid in which the impurity ion is present. Many additional electrons are present in the solid, and they interact via various interactions, such as electron-electron interaction and spin-orbit and spin-spin interactions. The abovementioned interactions are complicated. Furthermore, the electrons interact with the nuclei present in the solid. It is obvious that such a multi-particle problem cannot be solved exactly, and therefore one has to resort to some suitable procedure. There are methods, such as pseudo-potential[61] and Slater's self-consistent scattered wave X_{α} method[62], that concern themselves with treating the multi-particle systems. The pseudo-potential approximation uses a single particle potential determined by fitting with suitable data, usually optical excitations. Thus, in order to use this method, one is first required to determine pseudo-potentials. For magnetic ions in GaAs, GaP, and InP, the correct pseudo-potentials are not yet known.

The other approximate method, namely, the self-consistent scattered wave X_α method, requires the assumption of spherical average potential and a parameter known as the "α-parameter". Although many authors have given the α-parameters for different atoms and ions, it is usually adjusted to get good agreement with experiment. Also, for the spherical average potential, it is necessary to divide the relevant space into different spherical regions, which makes the method somewhat approximate and therefore not suitable for treating magnetic ions in semiconductors. Both the methods (pseudo-potential and X_α) are not expected to explain energy splittings of magnetic ions with the accuracy one desires, because one is involved in explaining small magnetic splittings as well as large splittings observed in optical transitions. Also, because of the interactions of the electrons on the magnetic impurity with the external environment in the solid, distortions of the immediate surroundings may occur, resulting in what is known as the "Jahn-Teller distortion". If one also has to include the Jahn-Teller distortions, one is further required to modify the theoretical methods. For the reasons discussed above, the pseudo-potential and X_α methods do not appear to be good approximations for application to transition-metal ions in semiconductors.

For calculations that consider finer details of the optical and electron paramagnetic resonance spectra, one may use a linear combination of atomic orbitals for the multielectronic systems. In this work, we adopt a "cluster" approach, in which the atomic wave functions of the magnetic ion and the surrounding atoms, constituting the cluster, are combined to form the

electronic cluster wave functions. The observed results of optical and electron paramagnetic experiments in transition-metal impurities in semiconductors GaAs, GaP, and InP are characteristic of the electrons present in the neighborhood of the transition-metal impurities. A cluster approach, then, is appropriate for describing the optical and magnetic properties of these systems, because of the localized nature of the d-electrons, which form the outermost shell of the transition-metal impurities. We will include in the cluster approach the effect of the crystal field, electron-electron interaction, spin-orbit, spin-spin, and Jahn-Teller effects, on the systems under investigation. In the present work we will deal specifically with GaAs:Cr^{2+}, GaAs:Cr^{3+}, GaAs:Fe^{2+}, InP:Cr^{2+}, and GaP:Fe^{2+} materials.

When atoms are brought together to form a solid, the atomic energy levels mix and form bands. In semiconductors, usually energy gaps occur between the valence and conduction bands, and are of the order of a few eV. In Table III.1 energy gaps for some semiconductors have been listed. For the energy gaps for other semiconductors, one can refer to the book by Bylander.[63] For GaAs, the energy gap between the valence and the conduction bands is 1.4 eV; for GaP it is 2.2 eV; and for InP it is 1.2 eV.

When transition-metal ions are added to the pure systems as impurities, the new energy levels characteristic of the impurities arise, in addition to the bands for the pure systems. These impurities in semiconductors (GaAs, GaP, and InP) form discrete levels near the center of the gap. Being near the

Table III.1

ENERGY GAPS FOR SOME SEMICONDUCTOR MATERIALS

Material	Energy gap(eV)
GaAs	1.4
GaP	2.2
InP	1.2
ZnSe	2.6
ZnTe	2.2
CdSe	1.7
CdTe	1.4
Si	1.1

center of the gap, these levels are referred to as "deep levels".

The outermost electronic configurations of different charge states of Cr and Fe are $Cr^{3+}(3d^3)$, $Cr^{2+}(3d^4)$, and $Fe^{2+}(3d^6)$. The electronic levels in the energy gap are characteristic of these d-electrons, and are localized, owing to the low electronic mobility of the d-electrons. The Cr^{3+}, Cr^{2+}, and Fe^{2+} impurity ions act as acceptors in GaAs, GaP, and InP semiconductors, because these transition-metal ions tend to accept electrons from the valence band to fill their unfilled d-shells.

Experimentally, doping is done to control the characteristics (such as resistivity, and other properties) of semiconductors. Such controlled properties are very important for industrial applications of semiconductor materials.

Theoretically, as discussed above, it is difficult to describe the electronic interactions of impurities in semiconductors. The band theories used to explain the electronic structure of pure systems cannot be applied to impure systems, because of the lack of translational symmetry in the impure systems, and because the crystal environment affects the energy levels of the impurities, with the result that the observed spectra are very different from the pure ionic spectra. In fact, the electrons in the d-shell of the impurity ion take part in bonding in the system, and are no longer pure d-electrons. Besides, the electron-electron interactions between the electrons of the impurity and those near the impurity in the solid become important. Furthermore, the spin-orbit and spin-spin interactions are significant for explaining the relative positions of the optical levels and the spin-Hamiltonian parameters.

The multiparticle Hamiltonian, for the interacting electrons and nuclei present in the system, may be written as

$$H = H(\alpha) + H(\beta) + H(\alpha,\beta) \tag{1}$$

In this equation, "α" designates the region in the neighborhood of the impurity, which may be a cluster containing the impurity and a limited number of surrounding ions, and "β" designates the region of the rest of the solid. The interactions occurring in the region near the impurity may be expressed as

$$H(\alpha) = -\frac{\hbar}{2m}\sum_{i\in\alpha}\nabla_i^2 - \sum_{\substack{q_\alpha,\\ i\in\alpha}}\frac{Z_{q_\alpha}e^2}{r_{\alpha i}}$$

$$+\frac{1}{2}\sum_{q_\alpha\, q_{\alpha'}}\frac{Z_{q_\alpha}Z_{q_{\alpha'}}e^2}{R_{\alpha\alpha'}} + \frac{1}{2}\sum_{i,j\in\alpha}{}'\frac{e^2}{r_{ij}}$$

$$+\sum_{i\in\alpha}\varsigma(r_i)\,\vec{l}_i\cdot\vec{s}_i$$

$$+\frac{\hbar^2e^2}{m^2c^2}\sum_{i,j\in\alpha}{}'\left\{\frac{\vec{s}_i\cdot\vec{s}_j}{r_{ij}^3} - \frac{3(\vec{s}_i\cdot\vec{r}_{ij})(\vec{s}_j\cdot\vec{r}_{ij})}{r_{ij}^5}\right\} \tag{2}$$

The interaction terms of H(α), described by equation (2), contain the kinetic energy of the electrons (first term), the attractive potential between the electrons and the nuclei of charge $Z_{q_\alpha}e$ (second term), where e is the absolute value of the electron charge, and $r_{\alpha i}$ is the distance between the

electron i and the nucleus q_α; the nucleus-nucleus interaction (third term), with a distance $R_{\alpha\alpha'}$ between nucleus q_α and nucleus $q_{\alpha'}$; the electron-electron interaction (fourth term), with r_{ij} being the distance between electrons i and j (the factor 1/2 appears to avoid double counting, and the primed summation sign implies that $i \neq j$); the spin-orbit interaction (fifth term), where $\zeta(\vec{r}_i)$ is the spin-orbit operator, $\vec{\ell}_i$ is the angular momentum of electron i, and $\vec{s}_i$ is its spin; the spin-spin interaction (sixth term), where the electrons i and j interact via their spin, or magnetic dipoles, and the constant $\hbar$ is Planck's constant divided by 2π, e is the electronic charge, m is the electronic mass, and c is the velocity of light.

An expression similar to Eq. (2) holds for region β, with $H(\beta)$ containing the interactions for the electrons in the crystal excluding the electrons and nuclei in the cluster containing the impurity. The interactions of the electrons and nuclei near the impurity in region α with the electrons and nuclei of the rest of the crystal in region β is $H(\alpha,\beta)$:

$$
\begin{aligned}
H(\alpha,\beta) = &- \sum_{\substack{i \in \beta \\ q_\alpha}} \frac{Z q_\alpha e^2}{r_{\alpha i}} - \sum_{\substack{i \in \alpha \\ q_\beta}} \frac{Z q_\beta e^2}{r_{\beta i}} \\
&+ \sum_{q_\alpha, q_\beta} \frac{Z q_\alpha Z q_\beta e^2}{R_{\alpha\beta}} + \sum_{\substack{i \in \alpha \\ j \in \beta}} \frac{e^2}{r_{ij}} \\
&+ \sum_{\substack{i \in \alpha \\ j \in \beta}} [\zeta(\vec{r}_i) + \zeta(\vec{r}_j)](\vec{\ell}_i \cdot \vec{s}_j + \vec{\ell}_j \cdot \vec{s}_i) \\
&+ \frac{\hbar^2 e^2}{m^2 c^2} \sum_{\substack{i \in \alpha \\ j \in \beta}} \left\{ \frac{\vec{s}_i \cdot \vec{s}_j}{r_{ij}^3} - \frac{3(\vec{s}_i \cdot \vec{r}_{ij})(\vec{s}_j \cdot \vec{r}_{ij})}{r_{ij}^5} \right\} \qquad (3)
\end{aligned}
$$

The interaction terms contained in $H(\alpha,\beta)$ have meanings similar to the ones described for Eq. (2), but the interactions taking place in Eq. (3) are among particles located in different regions (α and β).

We observe that the spin-orbit and spin-spin interactions of the electrons near the impurity with the electrons of the rest of the crystal, in Eq. (3) [$H(\alpha,\beta)$], are negligible compared with the Coulomb interaction terms. Furthermore, as we are interested in the localized energy levels corresponding to the impurity, we consider electronic interactions in the cluster of atoms containing the impurity, with the effect of the rest of the crystal accounted for appropriately. The effect of the crystal fields on the cluster will be accounted for in two steps, first by subjecting the cluster to the (cubic) crystal field, and second by incorporating directly in calculations the Jahn-Teller splittings of the energy levels observed in crystals. Thus, the Hamiltonian can be written as

$$H = \sum_i \left\{ \frac{-\hbar^2 \nabla_i^2}{2m} - \frac{Ze^2}{r_i} + V_c(\vec{r}_i) \right\} + V_{JT}$$

$$+ \frac{1}{2} \sum_{i,j}{}' \frac{e^2}{r_{ij}} + \sum_i \zeta(\vec{r}_i)\, \vec{\ell}_i \cdot \vec{s}_i$$

$$+ \frac{\hbar^2 e^2}{m^2 c^2} \sum_{i,j}{}' \left\{ \frac{\vec{s}_i \cdot \vec{s}_j}{r_{ij}^3} - \frac{3(\vec{s}_j \cdot \vec{r}_{ij})(\vec{s}_j \cdot \vec{r}_{ij})}{r_{ij}^5} \right\} \qquad (4)$$

where $V_c(\vec{r}_i)$ represents the crystal fields[64] and V_{JT} accounts for a possible Jahn-Teller interaction[64,65]. The Jahn-Teller effect distorts an orbitally degenerated ground state and removes its digeneracy. For explicit expressions of V_{JT}, see Appendix I.

The basic idea of the crystal field, $V_c(\vec{r}_i)$ in Eq. (4), is that the transition-metal ion in crystals is subjected to an electric field originating in the rest of the crystal. Considering the environment to be represented by a charge distribution ρ, which is a general function of position, the potential energy $V_c(\vec{r}_i)$ is

$$V_c(\vec{r}_i) = -\int \frac{e\rho(\vec{R})}{|\vec{R} - \vec{r}_i|} \, d\zeta \qquad (5)$$

where $\vec{r}_i$ is the position of electron i, $\vec{R}$ is the position of a general point of the environment, as indicated in Figure III.1, and the integral is over the volume of the rest of the crystal. The $1/|\vec{R} - \vec{r}_i|$ operator may be expanded in terms of spherical harmonics, and depending on the symmetry that surrounds the transition-metal ion, the expansion for the crystal field may be greatly simplified. For tetrahedral symmetry, the potential for identical nearest neighbors of transition-metal ions is, besides a constant factor, equal to

$$V_c(\vec{r}_i) = -D_4 r^4 [Y_4^0(\theta,\phi) + \sqrt{\frac{15}{4}} (Y_4^4(\theta,\phi) + Y_4^{-4}(\theta,\phi))] \qquad (6)$$

where r, θ, and ϕ are the spherical coordinates of $\vec{r}_i$. For ionic materials, D_4 can be estimated by a point charge model. For semiconductors, however, accurate charge distribution

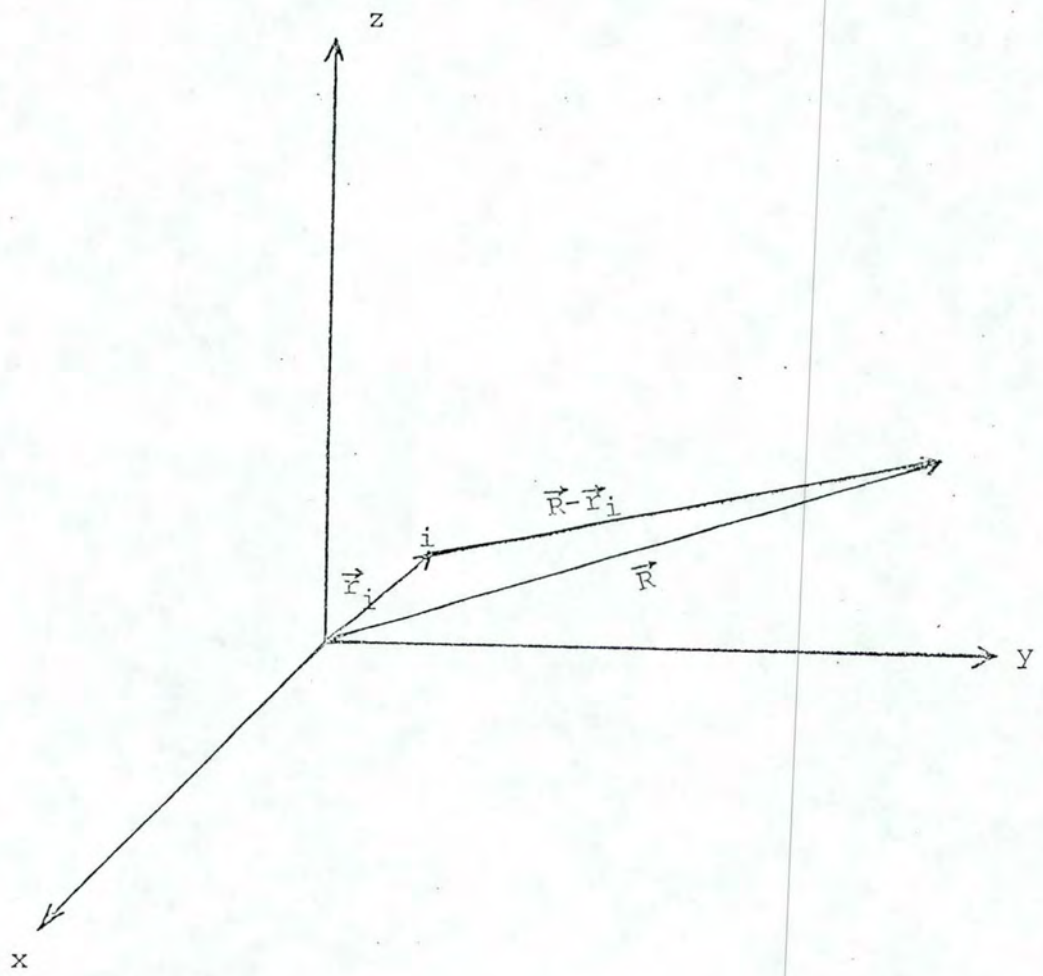

FIG.III.1

Position vector of an electron i, $\vec{r}_i$, and position vector $\vec{R}$ of a general point of the environment.

has to be taken into account, and estimation of the crystal field cannot be done straightforwardly. One way to have information about the strength of the crystal field is through experimental observations. The cubic crystal field-splitting energies of Fe^{2+} and Cr^{2+} in GaAs, GaP, and InP semiconductors are on the order of 3000 cm^{-1}. This is a strong interaction, compared to other interactions expressed in the Hamiltonian (Eq. 4). The electron-electron interaction is of comparable order, 10^3 cm^{-1}, whereas the spin-orbit interaction is of the order of 10^2 cm^{-1}, and the spin-spin interaction is about 10 cm^{-1}.

As mentioned previously, in order to handle the Hamiltonian, Eq. (4), we consider an appropriate cluster approach. Because of the localized nature of the impurity levels, we consider the cluster wave function as a linear combination of the atomic wave function of the impurity and the surrounding atoms. The one-electron cluster orbitals are, then, expressed as

$$\Psi = N(\Phi_d + \sum_{i,\ell} c_\ell^i \chi_{\ell i}) \quad , \tag{7}$$

where N is a normalization constant, Φ_d is the impurity atomic wave function, $\chi_{\ell i}$ is the atomic wave function of surrounding atoms i with orbital ℓ, c_ℓ^i stands for the admixture coefficients for the linear combination of atomic orbitals. The atomic wave functions Φ_d and $\chi_{\ell i}$ with quantum numbers n, ℓ, m, can be expressed in terms of Slater-type orbitals with principal quantum number $n_{\ell i}$:

$$\Phi_{n\ell m}(\vec{r}) = \sum_i C_{n\ell_i} \frac{(2\zeta_{\ell_i})^{n_{\ell_i}+\frac{1}{2}}}{\sqrt{(2n_{\ell_i})!}} r^{n_{\ell_i}-1} e^{-\zeta_{\ell_i} r} Y_\ell^m(\theta,\phi) \tag{8}$$

Table III.2

LIST FOR GaAs, GaP, AND InP OF
LATTICE CONSTANTS a AND THE NEAREST NEIGHBOR DISTANCES R

(see Figure III.2)

[in Ångstrom units (Å);
R is also listed in units of Bohr radius (a_0)]

Material	a (Å)	R (Å)	R (a_0)
GaAs	5.635	2.43	4.5918
GaP	5.436	2.36	4.4596
InP	5.861	2.54	4.7997

and the parameters $C_{n\ell_i}$, ζ_{ℓ_i}, and n_{ℓ_i} can be obtained by self-consistent field calculations[66,67]. We have used the best available self-consistent wave functions calculated by Clementi[66] and by Gilbert et al.[67]. The cluster wave functions, Eq. (7), have to be built in such a way that they satisfy the symmetry requirements of the environment.

For GaAs and GaP, the Fe^{n+} and Cr^{n+} (n = 2,3) impurities are substitutional on the Ga site, and for InP these impurities are substitutional on the In site. As the GaAs, GaP, and InP systems have a zinc-blende structure, the local symmetry around the impurity is, then, tetrahedral (see Fig. III.2). In Table III.2 the crystal structure parameters are listed for GaAs, GaP, and InP.

For convenience, we use real atomic wave functions, to be combined in Eq. (7) to form the cluster wave functions. The angular part of the atomic orbitals may be written as combinations of spherical harmonics (Y_ℓ^m) as follows:

$$\phi_s = Y_0^0(\theta,\phi) \tag{9-a}$$

$$\phi_{p_x} = \frac{-1}{\sqrt{2}}\left[Y_1^1(\theta,\phi) - Y_1^{-1}(\theta,\phi)\right] \tag{9-b}$$

$$\phi_{p_y} = \frac{i}{\sqrt{2}}\left[Y_1^1(\theta,\phi) + Y_1^{-1}(\theta,\phi)\right] \tag{9-c}$$

$$\phi_{p_z} = Y_1^0(\theta,\phi) \tag{9-d}$$

$$\phi_{d(3z^2-r^2)} = Y_2^0(\theta,\phi) \tag{9-e}$$

$$\phi_{d(x^2-y^2)} = \frac{1}{\sqrt{2}}\left[Y_2^2(\theta,\phi) + Y_2^{-2}(\theta,\phi)\right] \tag{9-f}$$

$$\phi_{d_{xy}} = \frac{-i}{\sqrt{2}}\left[Y_2^2(\theta,\phi) - Y_2^{-2}(\theta,\phi)\right] \tag{9-g}$$

$$\phi_{d_{yz}} = \frac{i}{\sqrt{2}}\left[Y_2^1(\theta,\phi) + Y_2^{-1}(\theta,\phi)\right] \tag{9-h}$$

$$\phi_{d_{xz}} = \frac{-1}{\sqrt{2}}\left[Y_2^1(\theta,\phi) - Y_2^{-1}(\theta,\phi)\right] \tag{9-i}$$

For tetrahedral symmetry, the symmetric combinations of atomic orbitals, according to Fig. III.3, are listed in Table III.3. These symmetric combinations were obtained by using group-theoretical techniques.[68] For other symmetry groups, one can refer to Ballhausen and Gray.[68] For the tetrahedral symmetry, the anti-bonding cluster wave functions which form the basis for the irreducible representations E and T_2 are

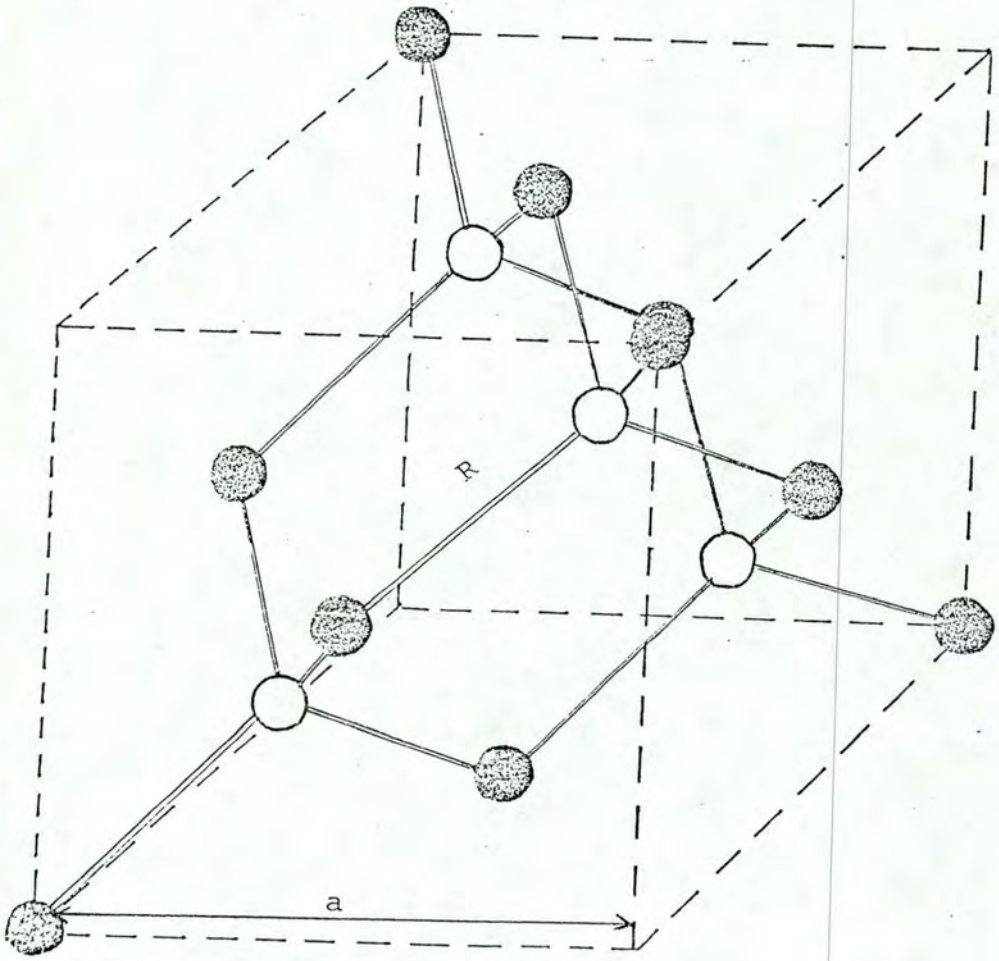

FIG.III.2

Zinc-blende structure. In GaAs, GaP, and InP compounds, the As and P atoms are located at (0,0,0);(0,1/2,1/2);(1/2,0,1/2);(1/2,1/2,0) the Ga and In atoms are located at (1/4,1/4,1/4);(1/4,3/4,3/4) ; (3/4,1/4,3/4);(3/4,3/4,1/4). The lattice constant a and the nearest neighbor distance R, for the compounds mentioned above, are listed in Table III.2.

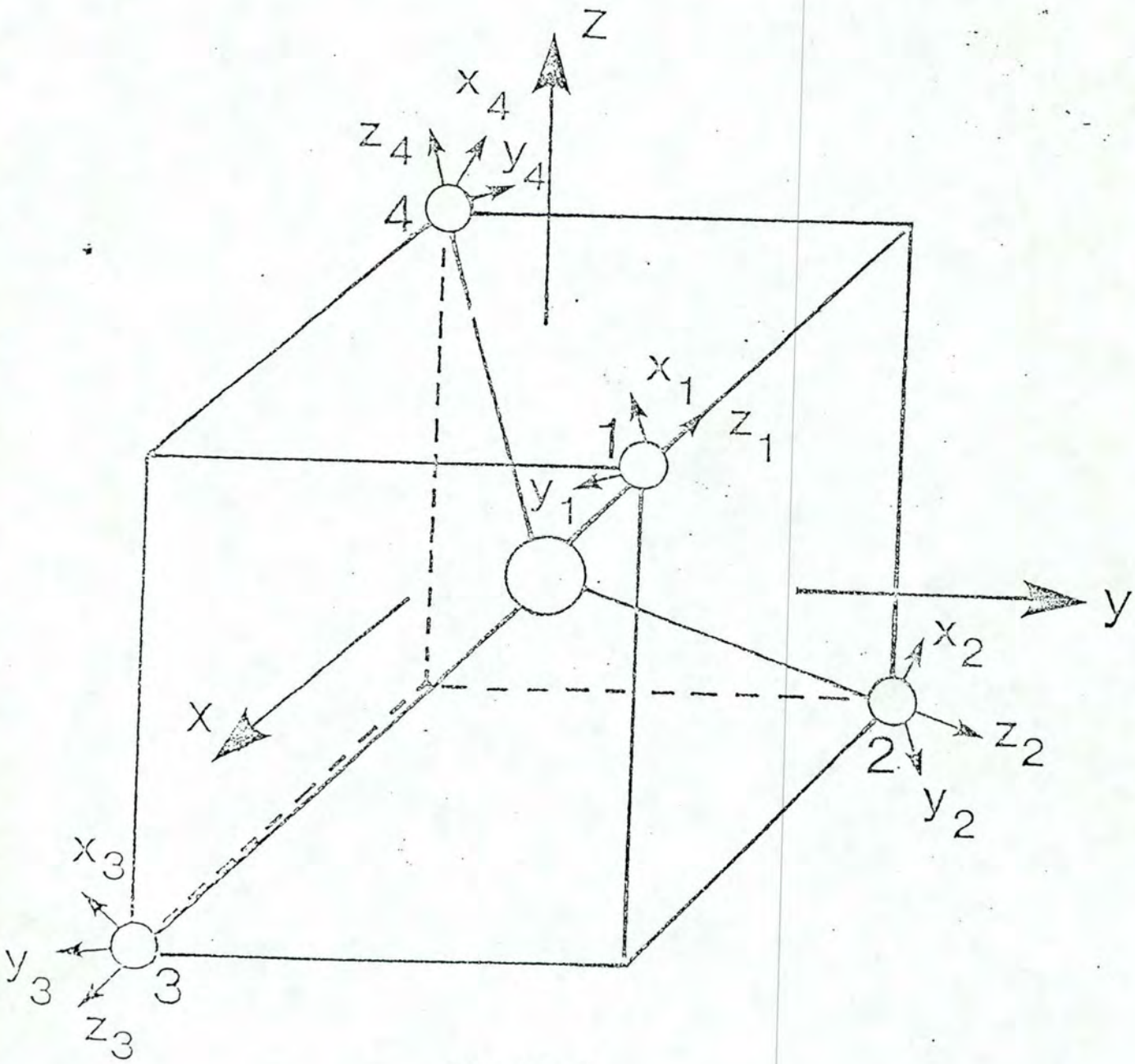

FIG.III.3

Tetrahedral configuration, with ligand atoms numbered 1,2,3 and 4, at alternate vertices of the cube.

$$\Psi_{\theta} = N_E \{ \phi_{d(3z^2-r^2)} - \lambda'_{d,p_\pi} \frac{1}{2} (\chi_{p_{x_1}} - \chi_{p_{x_2}} - \chi_{p_{x_3}} + \chi_{p_{x_4}}) \} \quad (10)$$

$$\Psi_{\epsilon} = N_E \{ \phi_{d(x^2-y^2)} - \lambda'_{d,p_\pi} \frac{1}{2} (\chi_{p_{y_1}} - \chi_{p_{y_2}} - \chi_{p_{y_3}} + \chi_{p_{y_4}}) \} \quad (11)$$

$$\begin{aligned} \Psi_{\xi} = N_{T_2} \{ & \phi_{d_{yz}} - \lambda_{d,s} \frac{1}{2} (\chi_{s_1} - \chi_{s_2} + \chi_{s_3} - \chi_{s_4}) \\ & - \lambda_{d,p_\sigma} \frac{1}{2} (\chi_{p_{z_1}} - \chi_{p_{z_2}} + \chi_{p_{z_3}} - \chi_{p_{z_4}}) \\ & - \lambda_{d,p_\pi} \frac{1}{4} [\chi_{p_{x_1}} + \chi_{p_{x_2}} - \chi_{p_{x_3}} - \chi_{p_{x_4}} \\ & + \sqrt{3} (-\chi_{p_{y_1}} - \chi_{p_{y_2}} + \chi_{p_{y_3}} + \chi_{p_{y_4}})] \} \end{aligned} \quad (12)$$

$$\Psi_{\eta} = N_{T_2}\{\phi_{d_{xz}} - \lambda_{d,s}\frac{1}{2}(\chi_{s_1} + \chi_{s_2} - \chi_{s_3} - \chi_{s_4})$$

$$- \lambda_{d,p_\sigma}\frac{1}{2}(\chi_{p_{z_1}} + \chi_{p_{z_2}} - \chi_{p_{z_3}} - \chi_{p_{z_4}})$$

$$- \lambda_{d,p_\pi}\frac{1}{4}[\chi_{p_{x_1}} - \chi_{p_{x_2}} + \chi_{p_{x_3}} - \chi_{p_{x_4}}$$

$$+\sqrt{3}(\chi_{p_{y_1}} - \chi_{p_{y_2}} + \chi_{p_{y_3}} - \chi_{p_{y_4}})]\} \qquad (13)$$

$$\Psi_{\zeta} = N_{T_2}\{\phi_{d_{xy}} - \lambda_{d,s}\frac{1}{2}(\chi_{s_1} - \chi_{s_2} - \chi_{s_3} + \chi_{s_4})$$

$$- \lambda_{d,p_\sigma}\frac{1}{2}(\chi_{p_{z_1}} - \chi_{p_{z_2}} - \chi_{p_{z_3}} + \chi_{p_{z_4}})$$

$$- \lambda_{d,p_\pi}\frac{(-1)}{2}(\chi_{p_{x_1}} + \chi_{p_{x_2}} + \chi_{p_{x_3}} + \chi_{p_{x_4}})\} \qquad (14)$$

Table III.3

BASIS FUNCTIONS USED FOR FORMING LINEAR COMBINATIONS TO OBTAIN CLUSTER ORBITALS. ϕ_{dj} ARE THE 3d ORBITALS OF THE CENTRAL MAGNETIC ION AND χ_{sj}, $\chi_{p_\pi j}$ AND $\chi_{p_\sigma j}$ ARE TETRAHEDRAL-SYMMETRY COMBINATIONS OF s AND p ORBITALS OF THE LIGANDS, s_i, p_{x_i} AND p_{y_i} DENOTE THE s, p_x AND p_y ORBITALS OF THE LIGANDS AT SITE i.

j	ϕ_{dj}	χ_{s_j}	$\chi_{p_{\pi j}}$	$\chi_{p_{\sigma j}}$
θ	$\phi_{d(3z^2-r^2)}$		$\frac{1}{2}(p_{x_1}-p_{x_2}-p_{x_3}+p_{x_4})$	
ϵ	$\phi_{d(x^2-y^2)}$		$\frac{1}{2}(p_{y_1}-p_{y_2}-p_{y_3}+p_{y_4})$	
ξ	$\phi_{d_{yz}}$	$\frac{1}{2}(s_1-s_2+s_3-s_4)$	$\frac{1}{4}[p_{x_1}+p_{x_2}-p_{x_3}-p_{x_4}$ $+\sqrt{3}(-p_{y_1}-p_{y_2}+p_{y_3}+p_{y_4})]$	$\frac{1}{2}(p_{z_1}-p_{z_2}+p_{z_3}-p_{z_4})$
η	$\phi_{d_{xz}}$	$\frac{1}{2}(s_1+s_2-s_3-s_4)$	$\frac{1}{4}[p_{x_1}-p_{x_2}+p_{x_3}-p_{x_4}$ $+\sqrt{3}(p_{y_1}-p_{y_2}+p_{y_3}-p_{y_4})]$	$\frac{1}{2}(p_{z_1}+p_{z_2}-p_{z_3}-p_{z_4})$
ζ	$\phi_{d_{xy}}$	$\frac{1}{2}(s_1-s_2-s_3+s_4)$	$-\frac{1}{2}(p_{x_1}+p_{x_2}+p_{x_3}+p_{x_4})$	$\frac{1}{2}(p_{z_1}-p_{z_2}-p_{z_3}+p_{z_4})$

The cluster wave functions Ψ_θ and Ψ_ε (Eqs. 10 and 11) transform like the irreducible representation E in tetrahedral symmetry, and the wave functions Ψ_ξ, ψ_η, and ψ_ζ (Eqs. 12-14) transform like the irreducible representation T_2, in the same symmetry group. The central-ion atomic wave functions Φ_{d_j} [$j \equiv (3z^2 - r^2)$, $(x^2 - y^2)$, yz, xz, xy] correspond to the x, y, z axis system located at the central ion, whereas the ligand χ_{s_i}, $\chi_{p_{x_i}}$, $\chi_{p_{y_i}}$, and $\chi_{p_{z_i}}$ atomic orbitals correspond to the local x_i, y_i, z_i axis systems situated at the i^{th} ligand (see Fig. III.3). The numerical factors appearing in Eqs. (10)-(14) are included to have conveniently normalized symmetric combinations of orbitals. In Eqs. (10)-(14) the coefficients $\lambda_{d,s}$, λ_{d,p_σ}, λ_{d,p_π} and λ'_{d,p_π} are admixture coefficients. The bonding orbitals may also be constructed in a similar way. The normalization constants N_E and N_{T_2} are found upon integration of the wave functions, and are equal to

$$N_E = \left[1 + \lambda'^2_{d,p_\pi} - 2\,\lambda'_{d,p_\pi} G_E(d,p_\pi)\right]^{-1/2} \qquad (15)$$

$$N_{T_2} = \left[1 + \lambda^2_{d,s} + \lambda^2_{d,p_\sigma} + \lambda^2_{d,p_\pi} - 2\lambda_{d,s}\, G_{T_2}(d,s)\right.$$

$$\left. -2\,\lambda_{d,p_\sigma} G_{T_2}(d,p_\sigma) - 2\,\lambda_{d,p_\pi} G_{T_2}(d,p_\pi)\right]^{-1/2} \qquad (16)$$

The group overlap integrals, G, in Eqs. (15) and (16) are, explicitly,

$$G_E(d,p_\pi) = \langle \phi_{d(3z^2-r^2)} | \frac{1}{2}(\chi_{p_{x_1}} - \chi_{p_{x_2}} - \chi_{p_{x_3}} + \chi_{p_{x_4}}) \rangle \quad (17)$$

$$G_{T_2}(d,s) = \langle \phi_{d_{xy}} | \frac{1}{2}(\chi_{s_1} - \chi_{s_2} - \chi_{s_3} + \chi_{s_4}) \rangle \quad (18)$$

$$G_{T_2}(d,p\ ) = \langle \phi_{d_{xy}} | \frac{1}{2}(\chi_{p_{z_1}} - \chi_{p_{z_2}} - \chi_{p_{z_3}} + \chi_{p_{z_4}}) \rangle \quad (19)$$

$$G_{T_2}(d,p\ ) = \langle \phi_{d_{xy}} | \frac{-1}{2}(\chi_{p_{x_1}} + \chi_{p_{x_2}} + \chi_{p_{x_3}} + \chi_{p_{x_4}}) \rangle \quad (20)$$

Because of the symmetry (see Fig. III.3), $G_E(d,p_\pi)$, $G_{T_2}(d,s)$, $G_{T_2}(d,p_\sigma)$, and $G_{T_2}(d,p_\pi)$ are reduced to

$$G_E(d,p_\pi) = 2 \langle \phi_{d(3z^2-r^2)} | \chi_{p_{x_1}} \rangle \quad (21\text{-a})$$

$$G_{T_2}(d,s) = 2 \langle \phi_{d_{xy}} | \chi_{s_1} \rangle \quad (21\text{-b})$$

$$G_{T_2}(d,p_\sigma) = 2 \langle \phi_{d_{xy}} | \chi_{p_{z_1}} \rangle \quad (21\text{-c})$$

$$G_{T_2}(d,p_\pi) = -2 \langle \phi_{d_{xy}} | \chi_{p_{x_1}} \rangle \qquad (21\text{-}d)$$

which are two-center in nature. It is convenient to rotate the x,y,z coordinate system into x'y'z', such that x'y'z' is parallel to the coordinates $x_1y_1z_1$ (see Fig. III.3 and Fig. III.4), and express the Φ_{d_j} wave functions in terms of the rotated coordinates x'y'z'. This is achieved by using the rotation matrix elements[69], defined in terms of the Euler angles[70] α, β, and γ. The rotation of the spherical harmonics is given[71] by

$$Y_\ell^m(\theta,\phi) = \sum_{m'=-\ell}^{\ell} \mathcal{D}^\ell_{m',m}(\alpha,\beta,\gamma)\ Y_\ell^{m'}(\theta',\phi') \qquad (22)$$

The Euler angle α is the center of rotation around the z-axis, β is the rotation angle around the new y-axis, and γ is the rotation angle around the latter new z-axis. The angles are here defined as positive when rotated in the counterclockwise direction. The rotation matrix elements $\mathcal{D}^\ell_{m',m}(\alpha,\beta,\gamma)$ may be expressed in terms of the "reduced" matrix elements $d^\ell_{m',m}(\gamma)$[69]:

$$\mathcal{D}^\ell_{m',m}(\alpha,\beta,\gamma) = e^{im'\gamma}\ d^\ell_{m',m}(\beta)\ e^{im\alpha} \qquad (23)$$

where

$$d^\ell_{m',m}(\beta) = \sum_k \frac{(-1)^k (\ell+m)!(\ell-m)!(\ell+m')!(\ell-m')!}{k!(\ell+m-k)!(\ell-m'-k)!(k+m'-m)!} \cdot$$

$$(\cos\beta/2)^{2\ell-2k-m'+m}\ (\sin\beta/2)^{2k+m'-m} \qquad (24)$$

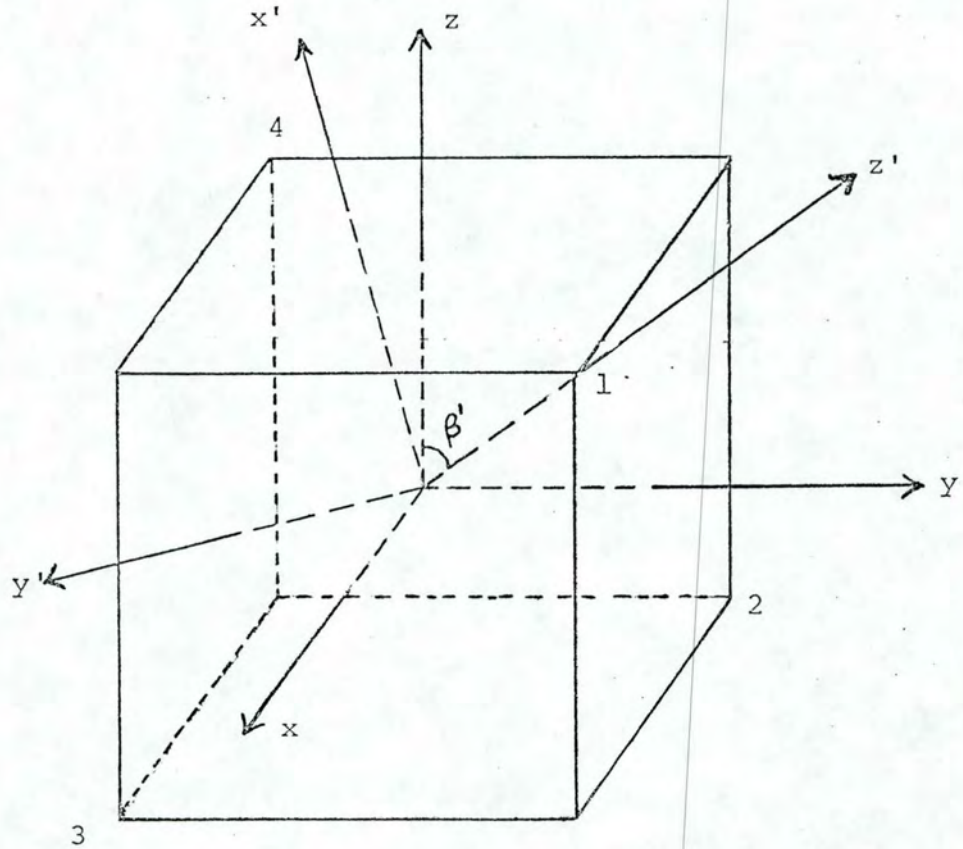

FIG.III.4

Transformed coordinate system for evaluation of an overlap integral.

Table III.4

REDUCED ROTATION MATRIX ELEMENTS $d^{1}_{m',m}(\beta)$

[WHERE $s=\sin\beta$ AND $t=\cos\beta$]

m' \ m	1	0	-1
1	$\frac{1}{2}(1+t)$	$\frac{1}{\sqrt{2}}s$	$\frac{1}{2}(1-t)$
0	$-\frac{1}{\sqrt{2}}s$	t	$\frac{1}{\sqrt{2}}s$
-1	$\frac{1}{2}(1-t)$	$-\frac{1}{\sqrt{2}}s$	$\frac{1}{2}(1+t)$

Table III.5

REDUCED ROTATION MATRX ELEMENTS $d^{2}_{m',m}(\beta)$

[WHERE $s=\sin\beta$ AND $t=\cos\beta$]

m' \ m	2	1	0	-1	-2
2	$\frac{1}{4}(1+t)^2$	$\frac{1}{2}(1+t)$	$\frac{\sqrt{6}}{4}s^2$	$\frac{1}{2}s(1-t)$	$\frac{1}{4}(1-t)^2$
1	$-\frac{1}{2}s(1+t)$	$\frac{1}{2}(1+t)(2t-1)$	$\frac{\sqrt{6}}{2}st$	$\frac{1}{2}(1-t)(2t+1)$	$\frac{1}{2}s(1-t)$
0	$\frac{\sqrt{6}}{4}s^2$	$-\frac{\sqrt{6}}{2}st$	$\frac{1}{2}(3t^2-1)$	$\frac{\sqrt{6}}{2}st$	$\frac{\sqrt{6}}{4}s^2$
-1	$-\frac{1}{2}s(1-t)$	$\frac{1}{2}(1-t)(2t+1)$	$-\frac{\sqrt{6}}{2}st$	$\frac{1}{2}(1+t)(2t-1)$	$\frac{1}{2}s(1+t)$
-2	$\frac{1}{4}(1-t)^2$	$-\frac{1}{2}s(1-t)$	$\frac{\sqrt{6}}{4}s^2$	$-\frac{1}{2}s(1+t)$	$\frac{1}{4}(1+t)^2$

Table III.6

REDUCED ROTATION MATRIX ELEMENTS $d^3_{m',m}(\beta)$, WHERE $s=\sin\beta$, $t=\cos\beta$, $T_+=1+t$, $T_-=1-t$. THIS MATRIX IS SYMMETRIC WITH RESPECT TO THE ANTI-DIAGONAL, THE SYMMETRIC MATRIX ELEMENTS ARE OMITTED.

m' \ m	3	2	1	0	-1	-2	-3
3	$\frac{T_+^3}{8}$	$\frac{\sqrt{6}sT_+^2}{8}$	$\frac{\sqrt{15}}{8}s^2T_+$	$\frac{\sqrt{20}s^3}{8}$	$\frac{\sqrt{15}s^2T_-}{8}$	$\frac{\sqrt{6}sT_-^2}{8}$	$\frac{T_-^3}{8}$
2	$-\frac{\sqrt{6}sT_+^2}{8}$	$\frac{T_+}{4}(T_+-3s^2)$	$-\frac{\sqrt{10}s(3s^2-2T_+)}{8}$	$\frac{\sqrt{30}ts^2}{4}$	$-\frac{\sqrt{10}s(-3s^2+2T_-)}{8}$	$\frac{T_-}{4}(3s^2-T_-)$	
1	$\frac{\sqrt{15}s^2T_+}{8}$	$\frac{\sqrt{10}s(3s^2-2T_+)}{8}$	$\frac{T_+^3}{8}-s^2\frac{(1+7t)}{4}$	$-\frac{\sqrt{3}s(-4+5s^2)}{4}$	$\frac{T_-^3}{8}-s^2\frac{(1-7t)}{4}$		
0	$-\frac{\sqrt{20}s^3}{8}$	$\frac{\sqrt{30}ts^2}{4}$	$\frac{\sqrt{3}s(-4+5s^2)}{4}$	$\frac{t(2-5s^2)}{2}$			
-1	$\frac{\sqrt{15}s^2T_-}{8}$	$\frac{\sqrt{10}s(-3s^2+2T_-)}{8}$	$\frac{T_-^3}{8}-\frac{s^2(1-7t)}{4}$				
-2	$-\frac{\sqrt{6}sT_-^2}{8}$	$\frac{T_-}{4}(3s^2-T_-)$					
-3	$\frac{T_-^3}{8}$						

The sum in Eq. (24) spans all integral values of k for which the denominator is not infinite (the factorial of a negative integer is taken to be infinite). The reduced matrix elements $d^{\ell}_{m',m}(\beta)$ are tabulated for β = 1, 2, and 3, in Tables III.4, III.5, and III.6. At present, we will make use of the $d^{\ell}_{m',m}(\beta)$ matrix element for ℓ = 2 (Table III.5), in order to express the Φ_{d_j} wave functions in terms of a rotated frame of reference. In Section C, when we deal with transition moment calculations, we will make use of the matrix elements $d^{\ell}_{m',m}(\beta)$ for ℓ = 1 and ℓ = 3 (Tables III.4 and III.6), to perform rotations of spherical harmonics involving ℓ = 1 and ℓ = 3 values. The spherical harmonics with ℓ = 2, of which the Φ_{d_j} are linear combinations (see Eq. 9), transform under rotation according to Eq. (22), as follows:

$$Y_2^0(\theta,\phi) = \mathcal{D}^2_{0,0}(\alpha,\beta,\gamma)\,Y_2^0(\theta',\phi') + \mathcal{D}^2_{2,0}(\alpha,\beta,\gamma)\,Y_2^2(\theta',\phi') + \mathcal{D}^2_{-2,0}(\alpha,\beta,\gamma)\,Y_2^{-2}(\theta',\phi')$$

$$+\mathcal{D}^2_{1,0}(\alpha,\beta,\gamma)\,Y_2^1(\theta',\phi') + \mathcal{D}^2_{-1,0}(\alpha,\beta,\gamma)\,Y_2^{-1}(\theta',\phi') \qquad (25\text{-a})$$

$$Y_2^2(\theta,\phi) = \mathcal{D}^2_{0,2}(\alpha,\beta,\gamma)\,Y_2^0(\theta',\phi') + \mathcal{D}^2_{2,2}(\alpha,\beta,\gamma)\,Y_2^2(\theta',\phi') + \mathcal{D}^2_{-2,2}(\alpha,\beta,\gamma)\,Y_2^{-2}(\theta',\phi')$$

$$+\mathcal{D}^2_{1,2}(\alpha,\beta,\gamma)\,Y_2^1(\theta',\phi') + \mathcal{D}^2_{-1,2}(\alpha,\beta,\gamma)\,Y_2^{-1}(\theta',\phi') \qquad (25\text{-b})$$

$$Y_2^{-2}(\theta,\phi) = \mathcal{D}^2_{0,2}(\alpha,\beta,\gamma)\, Y_2^0(\theta',\phi') + \mathcal{D}^2_{2,-2}(\alpha,\beta,\gamma)\, Y_2^2(\theta',\phi') + \mathcal{D}^2_{-2,-2}(\alpha,\beta,\gamma)\, Y_2^{-2}(\theta',\phi')$$

$$+ \mathcal{D}^2_{1,-2}(\alpha,\beta,\gamma)\, Y_2^1(\theta',\phi') + \mathcal{D}^2_{-1,-2}(\alpha,\beta,\gamma)\, Y_2^{-1}(\theta',\phi') \qquad (25\text{-c})$$

$$Y_2^1(\theta,\phi) = \mathcal{D}^2_{0,1}(\alpha,\beta,\gamma)\, Y_2^0(\theta',\phi') + \mathcal{D}^2_{2,1}(\alpha,\beta,\gamma)\, Y_2^2(\theta',\phi') + \mathcal{D}^2_{-2,1}(\alpha,\beta,\gamma)\, Y_2^{-2}(\theta',\phi')$$

$$+ \mathcal{D}^2_{1,1}(\alpha,\beta,\gamma)\, Y_2^1(\theta',\phi') + \mathcal{D}^2_{-1,1}(\alpha,\beta,\gamma)\, Y_2^{-1}(\theta',\phi') \qquad (25\text{-d})$$

$$Y_2^{-1}(\theta,\phi) = \mathcal{D}^2_{0,-1}(\alpha,\beta,\gamma)\, Y_2^0(\theta',\phi') + \mathcal{D}^2_{2,-1}(\alpha,\beta,\gamma)\, Y_2^2(\theta',\phi') + \mathcal{D}^2_{-2,-1}(\alpha,\beta,\gamma)\, Y_2^{-2}(\theta',\phi')$$

$$+ \mathcal{D}^2_{1,-1}(\alpha,\beta,\gamma)\, Y_2^1(\theta',\phi') + \mathcal{D}^2_{-1,-1}(\alpha,\beta,\gamma)\, Y_2^{-1}(\theta',\phi') \qquad (25\text{-e})$$

One notices that for the symmetry displayed in Fig. III.4, it is always possible to obtain the rotated axes x'y'z' parallel to the ligand's axes $x_i y_i z_i$ (see Fig. III.3), with the Euler angle $\gamma = 0$ ($\alpha \neq 0$, $\beta \neq 0$). Taking advantage of this simplification, we can express the functions Φ_{d_j} [$j \equiv (3z^2 - r^2)$, $(x^2 - y^2)$, yz, xz, xy] in terms of rotated functions $\Phi_{d_{i'}}$, [$i' \equiv (3z'^2 - r'^2)$, $(x'^2 - y'^2)$, y'z', x'z', x'y'] and coefficients $A_{j,i'}(\alpha,\beta)$, using Eqs. (9) and (25):

$$\Phi_{d_j} = \sum_{i'} A_{j,i'}(\alpha,\beta)\ \Phi_{d_{i'}} \qquad (26)$$

Table III.7

COEFFICIENTS $A_{j,i'}(\alpha,\beta)$ (WHERE α AND β ARE EULER ANGLES) OF THE TRANSFORMATION $\phi_{d_j} = \sum_{i'} A_{j,i'}(\alpha,\beta)\phi_{di'}$, WHERE $s=\sin\beta$, $t=\cos\beta$, $s_\alpha=\sin\alpha$, $t_\alpha=\cos\alpha$.

ϕ_{d_j} \ $\phi_{di'}$	$\phi_{d(3z'^2-r'^2)}$	$\phi_{d(x'^2-y'^2)}$	$\phi_{d_{x'y'}}$	$\phi_{d_{y'z'}}$	$\phi_{d_{x'z'}}$
$\phi_{d(3z^2-r^2)}$	$\frac{(3t^2-1)}{2}$	$\frac{\sqrt{3}}{2}s^2$	0	0	$-3st$
$\phi_{d(x^2-y^2)}$,	$\frac{\sqrt{3}}{2}s^2(t_\alpha^2-s_\alpha^2)$	$\frac{(1+t^2)(t_\alpha^2-s_\alpha^2)}{2}$	$-2ts_\alpha t_\alpha$	$-2ss_\alpha t_\alpha$	$st(t_\alpha^2-s_\alpha^2)$
$\phi_{d_{xy}}$	$\sqrt{3}s^2 s_\alpha t_\alpha$	$(1+t^2)s_\alpha t_\alpha$	$t(t_\alpha^2-s_\alpha^2)$	$s(t_\alpha^2-s_\alpha^2)$	$2sts_\alpha t_\alpha$
$\phi_{d_{yz}}$	$\sqrt{3}sts_\alpha$	$-sts_\alpha$	$-st_\alpha$	tt_α	$-(1-2t^2)s_\alpha$
$\phi_{d_{xz}}$	$\sqrt{3}stt_\alpha$	$-stt_\alpha$	ss_α	$-ts_\alpha$	$-(1-2t^2)t_\alpha$

The coefficients $A_{j,i'}(\alpha,\beta)$ are obtained upon substitution of the $\mathcal{D}^2_{m',m}(\alpha,\beta,\sigma)$ matrix elements (see Eqs. 9, 23, 25, and Table III.5), and are listed in Table III.7. The central ion's atomic wave functions which contribute to the overlap integrals expressed by Eqs. (21-a) through (21-d), are expressed in terms of the rotated wave functions and the Euler angles α and β as (see Table III.7)

$$\phi_{d(3z^2-r^2)} = \frac{1}{2}(3\cos^2\beta - 1)\phi_{d(3z'^2-r'^2)} + \frac{\sqrt{3}}{2}\sin^2\beta\,\phi_{d(x'^2-y'^2)}$$

$$-\sqrt{3}\,\sin\beta\cos\beta\,\phi_{d_{x'z'}} \qquad (27)$$

$$\phi_{d_{xy}} = \sqrt{3}\,\sin^2\beta\,\sin\alpha\cos\alpha\,\phi_{d(3z'^2-r'^2)} + (1+\cos^2\beta)\sin\alpha\cos\alpha\,\phi_{d(x'^2-y'^2)}$$

$$+\cos\beta(\cos^2\alpha - \sin^2\alpha)\phi_{d_{x'y'}} + \sin\beta(\cos^2\alpha - \sin^2\alpha)\phi_{d_{y'z'}}$$

$$+2\sin\beta\cos\beta\sin\alpha\cos\alpha\,\phi_{d_{x'z'}} \qquad (28)$$

The Euler angles α and β ($\gamma = 0$), required for the rotation of the axes xyz into x'y'z' as illustrated in Fig. III.4, are

$$\alpha = -\frac{3\pi}{4} \qquad (29\text{-a})$$

$$\beta = -\beta' \qquad (29\text{-b})$$

$$\gamma = 0 \tag{29-c}$$

where (see Fig. III.4) β' is such that

$$\cos\beta' = \frac{1}{\sqrt{3}} \tag{30-a}$$

$$\sin\beta' = \frac{2}{\sqrt{3}} \tag{30-b}$$

Equations (27) and (28) are simplified when one substitutes the Euler angles α, β, as given by Eqs. (29) and (30), into the following expressions:

$$\phi_{d(3z^2-r^2)} = \frac{1}{\sqrt{3}}\phi_{d(x'^2-y'^2)} + \frac{\sqrt{2}}{\sqrt{3}}\phi_{d_{x'z'}} \tag{31}$$

$$\phi_{d_{xy}} = \frac{1}{\sqrt{3}}\phi_{d(3z'^2-r'^2)} + \frac{2}{3}\phi_{d(x'^2-y'^2)} - \frac{\sqrt{2}}{3}\phi_{d_{x'z'}} \tag{32}$$

With Eqs. (31) and (32), the overlap integrals expressed by Eqs. (21-a) through (21-d) are reduced to

$$G_E(d, p_\pi) = \frac{2}{\sqrt{3}}\langle\phi_{d(x'^2-y'^2)} | \chi_p\rangle_{x_1} + \frac{2\sqrt{2}}{\sqrt{3}}\langle\phi_{d_{x'z'}} | \chi_p\rangle_{x_1} \tag{33}$$

$$G_{T_2}(d,s) = \frac{2}{\sqrt{3}} \langle \phi_{d(3z'^2-r'^2)} | \chi_{s_1} \rangle + \frac{4}{3} \langle \phi_{d(x'^2-y'^2)} | \chi_{s_1} \rangle$$

$$-\frac{2\sqrt{2}}{3} \langle \phi_{d_{x'z'}} | \chi_{s_1} \rangle \qquad (34)$$

$$G_{T_2}(d,p_\sigma) = \frac{2}{\sqrt{3}} \langle \phi_{d(3z'^2-r'^2)} | \chi_{p_{z_1}} \rangle + \frac{4}{3} \langle \phi_{d(x'^2-y'^2)} | \chi_{p_{z_1}} \rangle$$

$$-\frac{2\sqrt{2}}{3} \langle \phi_{d_{x'z'}} | \chi_{p_{z_1}} \rangle \qquad (35)$$

$$G_{T_2}(d,p_\pi) = \frac{-2}{\sqrt{3}} \langle \phi_{d(3z'^2-r'^2)} | \chi_{p_{x_1}} \rangle \frac{-4}{\sqrt{3}} \langle \phi_{d(x'^2-y'^2)} | \chi_{p_{x_1}} \rangle$$

$$+\frac{2\sqrt{2}}{3} \langle \phi_{d_{x'z'}} | \chi_{p_{x_1}} \rangle \qquad (36)$$

Some of the integrals contained in Eqs. (33)-(36) are equal to zero, as one can verify by direct integration, or simply by using symmetry arguments. Specifically, these integrals are

$$\langle \phi_{d(x'^2-y'^2)} | \chi_{p_{x_1}} \rangle = 0 \qquad (37\text{-a})$$

$$\langle \phi_{d(x'^2-y'^2)} | \chi_{s_1} \rangle = 0 \qquad (37\text{-b})$$

$$\langle \phi_{d_{x'z'}} | \chi_{s_1} \rangle = 0 \qquad (37\text{-c})$$

$$\langle \phi_{d(x'^2-y'^2)} | \chi_{p_{z_1}} \rangle = 0 \qquad (37\text{-d})$$

$$\langle \phi_{d_{x'z'}} | \chi_{p_{z_1}} \rangle = 0 \qquad (37\text{-e})$$

$$\langle \phi_{d(3z'^2-r'^2)} | \chi_{p_{x_1}} \rangle = 0 \qquad (37\text{-f})$$

To simplify the notation, we define the integrals which appear in Eqs. (33)-(36) as

$$S_{d,p_\pi} = \langle \phi_{d_{x'z'}} | \chi_{p_{x_1}} \rangle \qquad (38\text{-a})$$

$$S_{d,s} = \langle \phi_{d(3z'^2-r'^2)} | \chi_{s_1} \rangle \qquad (38\text{-b})$$

$$S_{d,p_\sigma} = \langle \phi_{d(3z'^2-r'^2)} | \chi_{p_{z_1}} \rangle \qquad (38\text{-c})$$

The overlap integrals (eqs. 33-36) are simplified, using eqs. (37) and (38), to

$$G_E(d,p_\pi) = \frac{2\sqrt{2}}{\sqrt{3}} S_{d,p_\pi} \tag{39}$$

$$G_{T_2}(d,s) = \frac{2}{\sqrt{3}} S_{d,s} \tag{40}$$

$$G_{T_2}(d,p_\sigma) = \frac{2}{\sqrt{3}} S_{d,p_\sigma} \tag{41}$$

$$G_{T_2}(d,p_\pi) = \frac{2\sqrt{2}}{3} S_{d,p_\pi} \tag{42}$$

The overlap integrals $S_{d,s}$, S_{d,p_σ}, and S_{d,p_π} (see Eq. 38) are two-center integrals, with one wave function centered at the central ion with the x'y'z' coordinate system, which is parallel to (and z-colinear with) the coordinate system $x_1y_1z_1$ (see Fig. III.4) at ligand site 1, where the other function is centered. These two-center integrals can be evaluated using the α-function technique.[60,72-75] The details of such calculations will be made clear in Chapter IV, where the results of various overlap integrals Fe^{2+} and Cr^{2+} in GaAs, GaP, and InP will also be presented. The substitution of the group overlap integrals, Eqs. (39)-(42), into the normalization constants (Eqs. 15 and 16) of the cluster wave functions results in the expressions

$$N_E = \left[1+ \lambda'^{2}_{d,p_\pi} - \frac{4\sqrt{2}}{\sqrt{3}} \lambda'_{d,p_\pi} S_{d,p_\pi}\right]^{-1/2} \tag{43}$$

$$N_{T_2} = \left[1+ \lambda^2_{d,s} + \lambda^2_{d,p_\sigma} + \lambda^2_{d,p_\pi} - \frac{4}{\sqrt{3}} \lambda_{d,s} S_{d,s}\right.$$

$$\left. - \frac{4}{\sqrt{3}} \lambda_{d,p_\sigma} S_{d,p_\sigma} - \frac{4\sqrt{2}}{3} \lambda_{d,p_\pi} S_{d,p_\pi}\right]^{-1/2} \tag{44}$$

We have presented, so far, a cluster wave function for a transition-metal ion surrounded by the four nearest neighbors, in a tetrahedral symmetry. Equations (10)-(14) were deduced by group-theoretical techniques. Another, alternative method for deriving cluster wave functions, developed by Sharma[76], is by directly investigating the symmetry of the overlap integrals between the central ion's wave functions and the orbitals of the various ligands. This method, which will be termined the "overlap-symmetry" method, allows more generality than the previous one, because the linear combination of the atomic orbitals can be expressed in terms of the rotation matrices. The explicit dependence of the cluster wave function on the Euler angles allows for deviations from the cubic symmetry. For example, in the case of an elongation or contraction of the tetrahedron, the angle β' (see Fig. III.4) is no longer given by $\sin\beta' = \sqrt{2}/\sqrt{3}$ and $\cos\beta' = 1/\sqrt{3}$. We shall use the overlap-symmetry method[76] to consider a cluster composed of the central ion (d-orbitals) and the four surrounding

atoms (s and p orbitals), which will be useful for evaluating the transition matrix elements for obtaining optical intensities in Section C. According to this method, the linear combination of the d-orbitals' wave functions Φ_j [$j \equiv d_{(3z^2 - r^2)}$, $d_{(x^2 - y^2)}$, d_{yz}, d_{xz}, d_{xy}) and the surrounding atomic wave functions χ_{ik} (where $i \equiv 1,2,3,4$ designates the position of the surrounding atoms, as in Fig. III.3, and k designates the s, p_x, p_y, and p_z orbitals) is first expressed as

$$\Psi_j = N_j(\phi_j - \sum_{i,k} C^i_{kj} \chi_{ki}) \tag{45}$$

N_j is the normalization constant, and C^i_{kj} is the coefficient that mixes the wave functions of the surrounding atoms with the wave functions of the central ion. One may also write the bonding orbitals in a manner similar to that of the antibonding orbitals of Eq. (45). Subject to the condition that the bonding and antibonding orbitals are orthogonal, one obtains, in the first-order approximation[76],

$$C^i_{kj} = \langle \chi_{ki} \mid \phi_j \rangle + \gamma^i_{kj} \tag{46}$$

where $\gamma^i_{k,j}$ is the corresponding coefficient for the bonding orbital, and is known as "charge transfer". Equation (46) means that the c^i_{kj} coefficient transforms as the overlap $\langle \chi_{ki} | \Phi_j \rangle$. This information is helpful in building up the symmetric combinations of the ligands and the central ion's orbitals. To investigate the various overlap integrals, one

has to make use of rotations (through the Euler angles), so that the coordinate system of the rotated wave functions of the central ion is parallel to and z-colinear with the coordinate system of the ligand i. Relative to the four ligands (see Figs. III.3 and III.4), the Euler angles are

$$\alpha_1 = -\frac{3\pi}{4} \quad , \quad \beta_1 = -\beta' \quad , \quad \gamma_1 = 0 \tag{47-a}$$

$$\alpha_2 = -\frac{\pi}{4} \quad , \quad \beta_2 = -(\pi - \beta') \quad , \quad \gamma_2 = 0 \tag{47-b}$$

$$\alpha_3 = \frac{3\pi}{4} \quad , \quad \beta_3 = -(\pi - \beta') \quad , \quad \gamma_3 = 0 \tag{47-c}$$

$$\alpha_4 = \frac{\pi}{4} \quad , \quad \beta_4 = -\beta' \quad , \quad \gamma_4 = 0 \tag{47-d}$$

The central ion's atomic function $\Phi_{d_{(3z^2 - r^2)}}$ [$j \equiv d_{(3z^2 - r^2)}$ in Eq. (45)] can be obtained in terms of a rotated system parallel to $x_i y_i z_i$ ($i \equiv 1,2,3,4$), by the use of Table III.7 and Eq.(47). The contributing coefficients (which would lead to a non-zero overlap) for the admixture of the $\Phi_{d_{(3z^2 - r^2)}}$ and the χ_{s_i} wave functions are

$$C^i_{s,d_{(3z^2 - r^2)}} = \frac{3\cos^2\beta_i - 1}{2} \Lambda_{d,s} \tag{48}$$

where $\Lambda_{d,s}$ is an admixture coefficient. Similarly, for the mixture of the $\Phi_{d_{(3z^2 - r^2)}}$ orbitals with the χ_{p_z}, χ_{p_x}, and χ_{p_y} ligand orbitals, one obtains

$$C^{i}_{p_z, d_{(3z^2-r^2)}} = \frac{3\cos^2\beta_i - 1}{2} \Lambda_{d,p_\sigma} \qquad (49)$$

$$C^{i}_{p_x, d_{(3z^2-r^2)}} = -\sqrt{3}\, \sin\beta_i \cos\beta_i \Lambda_{d,p_\pi} \qquad (50)$$

$$C^{i}_{p_y, d_{(3z^2-r^2)}} = 0 \quad . \qquad (51)$$

By substitution of Eqs. (48)-(51) into Eq. (45), the cluster wave function can be explicitly written, because the Euler angles for the different ligands are listed in Eq. (47). The same procedure can be followed to derive the combinations of the $\Phi_{d_{(x^2-y^2)}}$, $\Phi_{d_{yz}}$, $\Phi_{d_{xz}}$, and $\Phi_{d_{xy}}$ with the surrounding atomic orbitals. The derived expressions are, in terms of the angle β' (see Fig. III.4),

$$\Psi_\theta = N_\theta \Big\{ \phi_{d(3z^2-r^2)} - \frac{(3\cos^2\beta'-1)}{2} \Lambda_{d,s} (\chi_{s_1} + \chi_{s_2} + \chi_{s_3} + \chi_{s_4})$$

$$- \frac{(3\cos^2\beta'-1)}{2} \Lambda_{d,p} (\chi_{p_{z_1}} + \chi_{p_{z_2}} + \chi_{p_{z_3}} + \chi_{p_{z_4}})$$

$$- \sqrt{3}\, \cos\beta' \sin\beta' \Lambda_{d,p} (\chi_{p_{x_1}} - \chi_{p_{x_2}} - \chi_{p_{x_3}} + \chi_{p_{x_4}}) \Big\} \qquad (52)$$

$$\Psi_{\epsilon} = N_{\epsilon}\{\phi_{d(x^2-y^2)} - \sin\beta' \Lambda_{d,p_\pi}(\chi_{p_{y_1}} - \chi_{p_{y_2}} - \chi_{p_{y_3}} + \chi_{p_{y_4}})\} \quad (53)$$

$$\Psi_{\xi} = N_{\xi}\{\phi_{d_{yz}} - \frac{\sqrt{6}\cos\beta'\sin\beta'}{2}\Lambda_{d,s}(\chi_{s_1} - \chi_{s_2} + \chi_{s_3} - \chi_{s_4})$$

$$- \frac{\sqrt{6}\cos\beta'\sin\beta'}{2}\Lambda_{d,p_\sigma}(\chi_{p_{z_1}} - \chi_{p_{z_2}} + \chi_{p_{z_3}} - \chi_{p_{z_4}})$$

$$- \frac{(\sin^2\beta' - \cos^2\beta')}{\sqrt{2}}\Lambda_{d,p_\pi}(\chi_{p_{x_1}} + \chi_{p_{x_2}} - \chi_{p_{x_3}} - \chi_{p_{x_4}})$$

$$- \frac{\cos\beta'}{\sqrt{2}}\Lambda_{d,p_\pi}(-\chi_{p_{y_1}} - \chi_{p_{y_2}} + \chi_{p_{y_3}} + \chi_{p_{y_4}})\} \quad (54)$$

$$\Psi_{\eta} = N_{\eta}\{\phi_{d_{xz}} - \frac{\sqrt{6}\cos\beta'\sin\beta'}{2}\Lambda_{d,s}(\chi_{s_1} + \chi_{s_2} - \chi_{s_3} - \chi_{s_4})$$

$$- \frac{\sqrt{6}\cos\beta'\sin\beta'}{2}\Lambda_{d,p_\sigma}(\chi_{p_{z_1}} + \chi_{p_{z_2}} - \chi_{p_{z_3}} - \chi_{p_{z_4}})$$

$$- \frac{(\sin^2\beta' - \cos^2\beta')}{\sqrt{2}}\Lambda_{d,p_\pi}(\chi_{p_{x_1}} - \chi_{p_{x_2}} + \chi_{p_{x_3}} - \chi_{p_{x_4}})$$

$$- \frac{\cos\beta'}{\sqrt{2}}\Lambda_{d,p}(\chi_{p_{y_1}} - \chi_{p_{y_2}} + \chi_{p_{y_3}} - \chi_{p_{y_4}})\} \quad (55)$$

$$\Psi_\xi = N_\xi\{\phi_{d_{xy}} - \frac{\sqrt{3}\sin^2\beta'}{2}\Lambda_{d,s}(\chi_{s_1} - \chi_{s_2} - \chi_{s_3} + \chi_{s_4})$$

$$- \frac{\sqrt{3}\sin^2\beta'}{2}\Lambda_{d,p_\sigma}(\chi_{p_{z_1}} - \chi_{p_{z_2}} - \chi_{p_{z_3}} + \chi_{p_{z_4}})$$

$$- (-\sin\beta'\cos\beta')\Lambda_{d,p_\pi}(\chi_{p_{x_1}} + \chi_{p_{x_2}} + \chi_{p_{x_3}} + \chi_{p_{x_4}})\} \quad (56)$$

In Eqs. (52)-(56), N_θ, N_ε, N_ξ, N_η, and N_ζ are obtained upon normalization of these wave functions. The normalization constants, in terms of the angle β' and the overlap integrals $S_{d,s}$, S_{d,p_σ}, and S_{d,p_π} as defined in Eq. (38) are

$$N_\theta = \{1-(3\cos^2\beta' - 1)[2\Lambda_{d,s}S_{d,s} + 2\Lambda_{d,p_\sigma}S_{d,p_\sigma} - \Lambda^2_{d,s} - \Lambda^2_{d,p_\sigma}]$$

$$-12(\sin\beta'\cos\beta')^2[2\Lambda_{d,p_\pi}S_{d,p_\pi} - \Lambda^2_{d,p_\pi}]\}^{-1/2} \quad (57)$$

$$N_\epsilon = \{1-8\sin^2\beta'\Lambda_{d,p_\pi}S_{d,p_\pi} + 4\sin^2\beta'\Lambda_{d,p_\pi}\}^{-1/2} \quad (58)$$

$$N_\xi = N_\eta = \{ 1 - 6\sin^2\beta' \cos^2\beta' [2 \Lambda_{d,s} S_{d,s} + 2 \Lambda_{d,p_\sigma} S_{d,p_\sigma} - \Lambda^2_{d,s} - \Lambda^2_{d,p_\sigma}] - 2 [(\sin^2\beta' - \cos^2\beta')^2 + \cos^2\beta'] \cdot [2 \Lambda_{d,p_\pi} S_{d,p_\pi} - \Lambda^2_{d,p_\pi}] \}^{-1/2} \quad (59)$$

$$N_\zeta = \{ 1 - 3\sin^4\beta' [2 \Lambda_{d,s} S_{d,s} + 2 \Lambda_{d,p_\sigma} S_{d,p_\sigma} - \Lambda^2_{d,s} - \Lambda^2_{d,p_\sigma} - 4\sin^2\beta' \cos^2\beta' [2 \Lambda_{d,p_\pi} S_{d,p_\pi} - \Lambda^2_{d,p_\pi}] \}^{-1/2} \quad (60)$$

We notice that the cluster wave functions (52)-(56) are also valid for tetragonal (D_{2d}) symmetry, as the angle β' may be such that $\sin\beta' \neq \sqrt{2}/\sqrt{3}$ and $\cos\beta' \neq 1/\sqrt{3}$. In the more general case, the wave functions Ψ_θ and Ψ_ε (Eqs. 52 and 53) are no longer degenerate, and this is confirmed by group theory. In the limiting case of $\sin\beta' = \sqrt{2}/\sqrt{3}$ and $\cos\beta' = 1/\sqrt{3}$, Ψ_θ and Ψ_ε become degenerate, as required by tetrahedral symmetry. Also, the Ψ_ξ and Ψ_η functions remain degenerate (Eqs. 54 and 55), but not Ψ_ζ (Eq. 56), and this is consistent with the group-theoretical treatment of D_{2d} symmetry. In the limiting case of tetrahedral symmetry, as expected, Ψ_ξ, Ψ_η, and Ψ_ζ become degenerate. Comparing Eqs. (52)-(56) with Eqs. (10)-(14), one sees that in the proper limit ($\sin\beta' = \sqrt{2}/\sqrt{3}$ and $\cos\beta' = 1/\sqrt{3}$) both sets give the same symmetric combinations, and the admixture coefficients λs of Eqs. (10)-(14) are related to the admixture coefficients Λs of Eqs. (52)-(56) as follows:

$$\lambda_{d,s} = \frac{2}{\sqrt{3}} \Lambda_{d,s} \tag{61}$$

$$\lambda_{d,p_\sigma} = \frac{2}{\sqrt{3}} \Lambda_{d,p_\sigma} \tag{62}$$

$$\lambda_{d,p_\pi} = \frac{2\sqrt{2}}{3} \Lambda_{d,p_\pi} \tag{63}$$

$$\lambda'_{d,p_\pi} = \frac{2\sqrt{2}}{\sqrt{3}} \Lambda_{d,p_\pi} \tag{64}$$

Actually, Eqs. (63) and (64) show that the admixture coefficients λ'_{d,p_π} and λ_{d,p_π} of Eqs. (10)-(14) are not independent, but are related by a $\sqrt{3}$ factor:

$$\lambda'_{d,p_\pi} = \sqrt{3}\ \lambda_{d,p_\pi} \tag{65}$$

Group theory alone does not predict a proportionality between λ'_{d,p_π} and λ_{d,p_π}, although such proportionality has its roots in symmetry properties (which we have investigated through the overlap integrals). Indeed, one expects λ'_{d,p_π} and λ_{d,p_π} to be proportional, since both admixture coefficients describe a chemical bond of the same nature (π-bonding).

At this point, we are equipped with the multi-electronic Hamiltonian (Eq. 4), and the cluster orbitals (Eqs. 10-14 or Eqs. 52-56). In the following sections, we will work out the different interactions in the Hamiltonian. In Section A, we will focus our attention on the electron-electron interaction term of the Hamiltonian. The effect of the cubic crystal field

interaction will also be included in this section, as part of the treatment of the Coulomb interaction terms of the Hamiltonian.

A. Electron-electron interactions: Generalized d-electron matrices

In order to explain the spectra of free ions, Racah[77] introduced three basic Electron Coulomb repulsion parameters, A, B, and C, for pure d-electrons. Tanabe and Sugano[44] extended Racah's treatment to the case of transition-metal ions in solids and complexes, by considering the effect of the crystal field in terms of the splitting parameter Δ, assuming that the electrons retain their pure d-character. In the absence of a more nearly exact theory, the model above has been used to interpret the optical spectra of transition-metal ions in solids and complexes. It has the obvious advantage of involving only three parameters, B, C, and Δ (the parameter A represents an overall shift of the energy levels). While this theory brings forth useful simplifications, it suffers from the serious drawback of neglecting the important solid-state effects, such as the modifications of the electron wave functions from the pure d-character.

In order to obtain a more nearly exact theory, one has to remove the restriction of the pure d-nature from the electronic wave functions. This improvement has been made recently by Sharma and Sundaram[43], and the resulting theory has been checked and compared with existing results by Sharma, Viccaro, and Sundaram[41]. To this end, one may conceive of the one-

electron orbitals as sets of orbitals which form bases for irreducible representations of the symmetry group of the crystal potential. In the strong field coupling scheme[46,64], where many physical cases of interest occur, the functions θ, ε, ξ, η, and ζ are used to denote the set of one-electron orbitals in the cubic field representation. These orbitals are no longer of the pure d-character, if cluster wave functions are employed. In a cubic crystal field, the sets $\{\theta,\varepsilon\}$ and $\{\xi,\eta,\zeta\}$ are split by the crystal field parameter Δ (see Fig. III.1 for T_d symmetry), and form a basis for the irreducible representations E and T_2, respectively. Employing the strong-field scheme, the allowed terms for all possible configurations $e^{\ell}t_2^m$ of d^n (where $n = \ell + m$) can be obtained by group theory[64], and are listed in Table III.8. As the allowed terms were obtained by group theory, there is no restriction to pure d-orbitals, and Table III.8 can be used for the more general case of non-pure d-electrons.

The Coulomb repulsion is a two-electron interaction term, which operates on the wave functions of electrons i and j. This electron-electron interaction is given by

$$V_n = \sum_{i>j}^{n} \frac{e^2}{r_{ij}} \qquad (66)$$

To evaluate the energy eigenvalues of the Coulomb interaction, one is required to evaluate the matrix elements of V_n. The matrix elements of the electron-electron interaction can be expressed in terms of the integrals

Table III.8

DISTRIBUTION OF d^n LEVELS IN STRONG CRYSTALLINE FIELDS[64] .

d	e : ^2E t_2 : $^2T_2$
d^2	e^2 : $^1A_1 + {}^3A_2 + {}^1E$ et_2: $^1T_1 + {}^3T_1 + {}^1T_2 + {}^3T_2$ $(t_2)^2$: $^1A_1 + {}^1E + {}^3T_1 + {}^1T_2$
d^3	e^3 : ^2E e^2t_2: $2{}^2T_1 + {}^4T_1 + 2{}^2T_2$ $e(t_2)^2$: $^2A_1 + {}^2A_2 + 2{}^2E + 2{}^2T_1 + {}^4T_1 + 2{}^2T_2 + {}^4T_2$ $(t_2)^3$: $^4A_2 + {}^2E + {}^2T_1 + {}^2T_2$
d^4	e^4 : $^1A_1$ e^3t_2: $^1T_1 + {}^3T_1 + {}^1T_2 + {}^3T_2$ $e^2(t_2)^2$: $2{}^1A_1 + {}^1A_2 + {}^3A_2 + 3{}^1E + {}^3E + {}^1T_1 + 3{}^3T_1 + 3{}^1T_2 + 2{}^3T_2 + {}^5T_2$ $e(t_2)^3$: $^1A_1 + {}^3A_1 + {}^1A_2 + {}^3A_2 + {}^1E + 2{}^3E + {}^5E + 2{}^1T_1 + 2{}^3T_1 + 2{}^1T_2 + 2{}^3T_2$ $(t_2)^4$: $^1A_1 + {}^1E + {}^3T_1 + {}^1T_2$
d^5	t_2e^4 : $^2T_2$ $(t_2)^2e^3$: $^2A_1 + {}^2A_2 + 2{}^2E + 2{}^2T_1 + {}^4T_1 + 2{}^2T_2 + {}^4T_2$ $(t_2)^3e^2$: $2{}^2A_1 + {}^4A_1 + {}^6A_1 + {}^2A_2 + {}^4A_2 + 3{}^2E + 2{}^4E + 4{}^2T_1 + {}^4T_1 + 4{}^2T_2 + {}^4T_2$ $(t_2)^4e$: $^2A_1 + {}^2A_2 + 2{}^2E + 2{}^2T_1 + {}^4T_1 + 2{}^2T_2 + {}^4T_2$ $(t_2)^5$: $^2T_2$

$$V = \langle f(i)g(j)|\frac{e^2}{r_{ij}}|h(i)k(j)\rangle \quad , \tag{67}$$

where f(i), h(i), and g(j), k(j) are one-electron wave functions of electrons i and j. For cubic symmetry, in the most general case of non-pure d-electrons, the one-electron basic orbitals θ, ε, ξ, η, and ζ are used, and there are ten non-vanishing independent integrals[46] (a, b, c, . . ., j) of the type expressed by Eq. (67). Omitting the i and j indices from the one-electron wave functions in Eq. (67), the independent integrals can be written as

$$a = \langle \xi\xi|\frac{e^2}{r_{ij}}|\xi\xi\rangle \tag{68-a}$$

$$b = \langle \xi\eta|\frac{e^2}{r_{ij}}|\xi\eta\rangle \tag{68-b}$$

$$c = \langle \theta\xi|\frac{e^2}{r_{ij}}|\varepsilon\xi\rangle \tag{68-c}$$

$$d = \langle \varepsilon\xi|\frac{e^2}{r_{ij}}|\varepsilon\xi\rangle \tag{68-d}$$

$$e = \langle \theta\theta|\frac{e^2}{r_{ij}}|\theta\theta\rangle \tag{68-e}$$

$$f = \langle \theta\theta|\frac{e^2}{r_{ij}}|\varepsilon\varepsilon\rangle \tag{68-f}$$

$$g = \langle \theta\theta|\frac{e^2}{r_{ij}}|\eta\eta\rangle \tag{68-g}$$

$$h = \langle \theta\varepsilon|\frac{e^2}{r_{ij}}|\eta\eta\rangle \tag{68-h}$$

$$i = \langle \theta\eta | \frac{e^2}{r_{ij}} | \xi\zeta \rangle \tag{68-i}$$

$$j = \langle \xi\xi | \frac{e^2}{r_{ij}} | \eta\eta \rangle \tag{68-j}$$

One way to obtain the matrix elements of the electron-electron interactions is to use the wave functions directly for each irreducible representation (see Table III.8) of every electronic configuration $e^{\ell}t_2^m$. These matrix elements are expressed as

$$\langle t_2^m(S_1\Gamma_1)e^{\ell}(S_2\Gamma_2)S\Gamma | \sum_{i>j}^{n} \frac{e^2}{r_{ij}} | t_2^{m'}(S_3\Gamma_3)e^{\ell'}(S_4\Gamma_4)S\Gamma \rangle \tag{69}$$

where

$$n = m + \ell = m' + \ell' \tag{70}$$

The states $|t_2^m(S_1\Gamma_1)\ e^{\ell}(S_2\Gamma_2)\ S\ \Gamma\rangle$ and $|t_2^{m'}(S_3\Gamma_3)\ e^{\ell'}(S_4\Gamma_4)\ S\ \Gamma\rangle$ are wave functions which transform according to the irreducible representation Γ. The symbols Γ_1, Γ_2, Γ_3, and Γ_4 also denote irreducible representations, and Γ is generated by the group-theoretical direct products $\Gamma_1 \times \Gamma_2$ and $\Gamma_3 \times \Gamma_4$. S is the total spin, consistent with the addition of S_1 and S_2 as well as with S_3 and S_4 spin states. This method of derivation of the electronic matrix elements has been described in detail by Griffith.[46] Tanabe and Sugano[44] have used a recurrence relation between matrix elements of a d^n configuration and those of a d^{n-1} configuration, to generate the electron-electron matrix elements for d-electrons in a cubic field symmetry. The matrix

elements of V_n (see Eq. 66) can be generated by the recurrence relation[44,46]:

$$\langle t_2^m(S_1\Gamma_1)e^{\ell}(S_2\Gamma_2)S\Gamma \mid V_n \mid t_2^{m'}(S_3\Gamma_3)e^{\ell'}(S_4\Gamma_4)S\Gamma\rangle$$

$$= \frac{\sqrt{\ell\ell'}}{n-2} \sum_{\substack{S'S''\bar{S} \\ \Gamma'\Gamma''\bar{\Gamma}}} \langle e^{\ell}S_2\Gamma_2\{ \mid e^{\ell-1}(S'\Gamma')e\rangle\langle S_1\Gamma_1, S'\Gamma' e(S_2\Gamma_2)S\Gamma|$$

$$|S_1\Gamma_1 S'\Gamma'(\bar{S}\bar{\Gamma})eS\Gamma\rangle \langle t_2^m(S_1\Gamma_1)e^{\ell-1}(S'\Gamma')\bar{S}\bar{\Gamma} \mid V_{n-1} \mid$$

$$|t_2^{m'}(S_3\Gamma_3)e^{\ell'-1}(S''\Gamma'')S'\Gamma'\rangle \langle S_3\Gamma_3 S''\Gamma''(\bar{S}\bar{\Gamma})eS\Gamma|$$

$$|S_3\Gamma_3, S''\Gamma'' e(S_4\Gamma_4)S\Gamma\rangle \langle e^{\ell'-1}(S''\Gamma'')e|\}\ e^{\ell'}S_4\Gamma_4\rangle$$

$$+ \frac{\sqrt{mm'}}{n-2} \sum_{\substack{S'S''\bar{S} \\ \Gamma'\Gamma''\bar{\Gamma}}} \langle t_2^m S_1\Gamma_1\{ \mid t_2, t_2^{m-1}(S'\Gamma')S_1\Gamma_1\rangle \langle t_2 S'\Gamma'(S_1\Gamma_1)$$

$$S_2\Gamma_2 S\Gamma \mid t_2, S'\Gamma' S_2\Gamma_2(\bar{S}\bar{\Gamma})S\Gamma\rangle \langle t_2^{m-1}(S'\Gamma')e^{\ell}(S_2\Gamma_2)\bar{S}\bar{\Gamma} \mid V_{n-1} \mid$$

$$|t_2^{m'-1}(S''\Gamma'')e^{\ell}(S_4\Gamma_4)\bar{S}\bar{\Gamma}\rangle \langle t_2, S''\Gamma'' S_4\Gamma_4(\bar{S}\bar{\Gamma})S\Gamma|$$

$$|t_2 S''\Gamma''(S_3\Gamma_3)S_4\Gamma_4 S\Gamma\rangle \langle t_2, t_2^{m'-1}(S''\Gamma'')S_3\Gamma_3|\}\ t_2^m S_3\Gamma_3\rangle \qquad (71)$$

In order to calculate this matrix element for the n-electron system, it is necessary to know, in addition to the matrix elements for the (n-1)-electron system, the transformation matrices of the type $\langle S_1\Gamma_1, S'\Gamma' e(S_2\Gamma_2)S\Gamma | S_1\Gamma_1 S'\Gamma'(\bar{S}\bar{\Gamma})eS\Gamma\rangle$ and the coefficients of fractional parentage of the type $\langle e^{\ell} S_2\Gamma_2 \{ | e^{\ell-1}(S'\Gamma')e\rangle$. Both transformation matrices and the coefficients of fractional parentage are available in the form of tables.[44,46]

The laborious work of deriving the matrix elements given by Eq. (71) in terms of the general two-electron matrix elements a, b, c, . . ., j (see Eq. 68) was done by Sharma and Sundaram[43], and reviewed by Sharma, Viccaro, and Sundaram[41]. It was shown[41,43] that the generalized expressions for the electron-electron interactions have important consequences, such as the removal of accidental degeneracies in the energy spectrum, and the possibility of deducing the Coulomb and exchange parameters in conjunction with experimental optical spectra. The derived results of the electron-electron matrix elements for d^n electrons (n = 2, 3, 4, and 5), in terms of the generalized parameters a, b, c, . . ., j, are listed in Tables III.9-III.12.

As expected, the matrix elements in Tables III.9-12 reduce to the Tanabe-Sugano[44] matrix elements in the limiting condition that the θ, ε, ξ, η, and ζ orbitals are pure d-type orbitals. Those matrix elements in Tables III.9-12 which, on reduction to the pure d-orbital case, differ in sign from the corresponding matrix elements by Tanabe and Sugano[44] (or by Griffith[46]), have been marked by an asterisk. Although

Griffith's phase conventions have been followed consistently, we have not been able to trace out why Griffith's[46] matrix elements disagree in sign with ours.

In the limiting case of pure d-orbitals, the ten independent integrals (a, b, c, . . ., j) are reduced into Racah's three parameters A, B, and C, as follows[46]:

$$a = \left\langle \xi\xi \left| \frac{e^2}{r_{ij}} \right| \xi\xi \right\rangle = A + 4B + 3C \qquad (72\text{-a})$$

$$b = \left\langle \xi\eta \left| \frac{e^2}{r_{ij}} \right| \xi\eta \right\rangle = A - 2B + C \qquad (72\text{-b})$$

$$c = \left\langle \theta\xi \left| \frac{e^2}{r_{ij}} \right| \varepsilon\xi \right\rangle = 2\sqrt{3}\, B \qquad (72\text{-c})$$

$$d = \left\langle \varepsilon\xi \left| \frac{e^2}{r_{ij}} \right| \varepsilon\xi \right\rangle = A - 2B + C \qquad (72\text{-d})$$

$$e = \left\langle \theta\theta \left| \frac{e^2}{r_{ij}} \right| \theta\theta \right\rangle = A + 4B + 3C \qquad (72\text{-e})$$

$$f = \left\langle \theta\theta \left| \frac{e^2}{r_{ij}} \right| \varepsilon\varepsilon \right\rangle = 4B + C \qquad (72\text{-f})$$

$$g = \left\langle \theta\theta \left| \frac{e^2}{r_{ij}} \right| \eta\eta \right\rangle = B + C \qquad (72\text{-g})$$

$$h = \left\langle \theta\varepsilon \left| \frac{e^2}{r_{ij}} \right| \eta\eta \right\rangle = \sqrt{3}\, B \qquad (72\text{-h})$$

$$i = \left\langle \theta\eta \left| \frac{e^2}{r_{ij}} \right| \xi\zeta \right\rangle = \sqrt{3}\, B \qquad (72\text{-i})$$

$$j = \left\langle \xi\xi \left| \frac{e^2}{r_{ij}} \right| \eta\eta \right\rangle = 3B + C \qquad (72\text{-j})$$

Table III.9

ELECTRON-ELECTRON MATRIX ELEMENTS FOR d^2 ELECTRONS IN TERMS OF THE COULOMB AND EXCHANGE INTEGRALS a,b,.....,j.ASTERISK DENOTES THE CHANGE IN SIGN WITH RESPECT TO TANABE-SUGANO MATRIX ELEMENTS BECAUSE OF THE PHASE CONVENTIONS[41].

$^1A_1(d^2)$	$e^2(^1A_1)$	$t_2^2(^1A_1)$
$e^2(^1A_1)$	$e+f$	$\sqrt{6}g+\sqrt{2}h$
$t_2^2(^1A_1)$	$\sqrt{6}g+\sqrt{2}h$	$a+2j$
$^1E(d^2)$	$e^2(^1E)$	$t_2^2(^1E)$
$e^2(^1E)$	$e-f$	$2h^*$
$t_2^2(^1E)$	$2h^*$	$a-j$
$^1T_2(d^2)$	$t_2^2(^1T_2)$	$t_2(^2T_2)e(^2E)$
$t_2^2(^1T_2)$	$b+j$	$-2i^*$
$t_2(^2T_2)e(^2E)$	$-2i^*$	$d+g+\sqrt{3}h$
		$-c/\sqrt{3}$
$^3T_1(d^2)$	$t_2^2(^3T_1)$	t_2e
$t_2^2(^3T_1)$	$b-j$	$-2\sqrt{3}i^*$
t_2e	$-2\sqrt{3}i^*$	$d-g+\sqrt{3}c+h/\sqrt{3}$

$^3A_2(e^2) = e-3f$

$^3T_2(et_2) = d-g-(1/\sqrt{3})c-\sqrt{3}h$

$^1T_1(et_2) = d+g+\sqrt{3}c-(1/\sqrt{3})h$

Table III.10

ELECTRON-ELECTRON MATRIX ELEMENTS FOR d^3 ELECTRONS. ASTERISK DENOTES THE CHANGE IN SIGN WITH RESPECT TO GRIFFITH'S MATRIX ELEMENTS[41].

^2E	$t_2^3(^2E)c^0(^1A_1)$	$t_2^2(^1A_1)e^1(^2E)$	$t_2^2(^1E)e^1(^2E)$	$t^0(^1A_1)c^3(^2E)$
$t_2^3(^2E)c^0(^1A_1)$	$3b$	$-2\sqrt{6}i$	$-\sqrt{6}i^*$	0
$t_2^2(^1A_1)e^1(^2E)$	$-2\sqrt{6}i$	$a+(2/\sqrt{3})c+2d$ $-g-(1/\sqrt{3})h+2j$	$(4/\sqrt{3})c+(2/\sqrt{3})h^*$	$\sqrt{3}g+h$
$t_2^2(^1E)e^1(^2E)$	$-\sqrt{6}i^*$	$4c/\sqrt{3}+(2/\sqrt{3})h^*$	$a+(2/\sqrt{3})c+2d$ $-g-(1/\sqrt{3})h-j$	$2h^*$
$t^0(^1A_1)e^3(^2E)$	0	$\sqrt{3}g+h$	$2h^*$	$3e-5f$

$^2T_1$	t_2^3	$t_2^2(^3T_1)e$	$t_2^2(^1T_2)e$	$t_2e^2(^3A_2)$	$t_2e^2(^1E)$
t_2^3	$a+2b-2j$	$-\sqrt{3}i^*$	$\sqrt{3}i^*$	0	$-2h$
$t_2^2(^3T_1)e$		$b+(4/\sqrt{3})c+2d$ $+g-j$	$-\sqrt{3}h$	$\sqrt{3}i$	$3i^*$
$t_2^2(^1T_2)e$			$b+2d-g$ $-(2/\sqrt{3})h+j$	$-\sqrt{3}i$	$-i^*$
$t_2e^2(^3A_2)$				$(2/\sqrt{3})c+2d+e$ $-3f+g+(1/\sqrt{3})h$	$+2h^*$
$t_2e^2(^1E)$					$e+2d+(2/\sqrt{3})c$ $-g-(h/\sqrt{3})-f$

$^2T_2$	t_2^3	$t_2^2(^3T_1)e$	$t_2^2(^1T_2)e$	$t_2e^2(^1A_1)$	$t_2e^2(^1E)$
t_2^3	$a+2b$	$-3i$	$-5i^*$	$2g+2h/\sqrt{3}$	$2h/\sqrt{3}$
$t_2^2(^3T_1)e$		$b-j+2d+g$ $+2h/\sqrt{3}$	$\sqrt{3}h^*$	$-3i$	$-3i$
$t_2^2(^1T_2)e$			$b+4c/\sqrt{3}+2d$ $-g+j$	$-i^*$	$+i^*$
$t_2e^2(^1A_1)$				$e+2d+2c/\sqrt{3}$ $-g+f-h/\sqrt{3}$	$4c/\sqrt{3}+2h/\sqrt{3}$
$t_2e^2(^1E)$					$2c/\sqrt{3}+2d+e-f$ $-g-h/\sqrt{3}$

$^4T_1$	$t_2^2(^3T_1)e$	$t_2e^2(^3A_2)$
$t_2^2(^3T_1)e$	$b+4c/\sqrt{3}+2d$ $-2g-j$	$2\sqrt{3}i$
$t_2e^2(^3A_2)$	$2\sqrt{3}i$	$2c/\sqrt{3}+2d+e$ $-3f-2g$ $-2h/\sqrt{3}$

$t_2^2(^1E)e$: $^2A_1 = a-2c/\sqrt{3}+2d-g-\sqrt{3}h-j$

$t_2^2(^1E)e$: $^2A_2 = a+2\sqrt{3}c+2d-g+h/\sqrt{3}-j$

t_2^3: $^4A_2 = 3b-3j$

$t_2^2(^3T_1)e$: $^4T_2 = b+2d-2g-4h/\sqrt{3}-j$

Table III.11

ELECTRON-ELECTRON MATRIX ELEMENTS FOR d^4 ELECTRONS. ASTERISK DENOTES CHANGE IN SIGN WITH RESPECT TO GRIFFITH'S MATRIX ELEMENTS[41].

$^3T_1$	t_2^4	$t_2^3(^2T_1)e$	$t_2^3(^2T_2)e$	$t_2^2(^3T_1)e^2(^1A_1)$	$t_2^2(^3T_1)e^2(^1E)$	$t_2^2(^1T_2)e^2(^3A_2)$	$t_2e^3(^2E)$
t_2^4	$a+5b-3j$	$-\sqrt{2}i$	$-\sqrt{6}i$	$\sqrt{2}g+\frac{\sqrt{2}}{\sqrt{3}}h^*$	$-\frac{2\sqrt{2}}{\sqrt{3}}h^*$	0	0
$t_2^3(^2T_1)e$		$a+2b+\sqrt{3}c$ $+3d-2g$ $-\sqrt{3}h-2j$	$2c+h$	$+i^*$	$-i^*$	$\sqrt{3}i$	$\sqrt{2}h$
$t_2^3(^2T_2)e$			$a+2b+\sqrt{3}c$ $+3d-2g$ $-\frac{1}{\sqrt{3}}h$	$-\sqrt{3}i^*$	$-\sqrt{3}i^*$	$5i$	$+\sqrt{2}g$
$t_2^2(^3T_1)e^2(^1A_1)$				$b+\frac{4}{\sqrt{3}}c+4d$ $+e+f-2g$ $-\frac{2}{\sqrt{3}}h-j$	$-\frac{4}{\sqrt{3}}c-\frac{2}{\sqrt{3}}h$	0	$\sqrt{6}i^*$
$t_2^2(^3T_1)e^2(^1E)$					$b+\frac{4}{\sqrt{3}}c+4d$ $+e-f-2g$ $-\frac{2}{\sqrt{3}}h-j$	$-2h^*$	$-\sqrt{6}i^*$
$t_2^2(^1T_2)e^2(^3A_2)$						$b+\frac{4}{\sqrt{3}}c+4d$ $+e-3f-2g$ $-\frac{2}{\sqrt{3}}h+j$	$\sqrt{2}i$
$t_2e^3(^2E)$							$\frac{1}{\sqrt{3}}c+3d+3e$ $-5f-2g-\frac{2}{\sqrt{3}}h$

$^1T_2$	t_2^4	$t_2^3(^2T_1)e$	$t_2^3(^2T_2)e$	$t_2^2(^3T_1)e^2(^3A_2)$	$t_2^2(^1T_2)e^2(^1E)$	$t_2^2(^1T_2)e^2(^1A_1)$	t_2e^3
t_2^4	$a+5b-j$	$\sqrt{6}i^*$	$-5\sqrt{2}i$	0	$-\frac{2\sqrt{2}}{\sqrt{3}}h^*$	$\sqrt{2}g+\frac{\sqrt{2}}{\sqrt{3}}h^*$	0
$t_2^3(^2T_1)e$		$a+2b+\sqrt{3}c$ $+3d-\sqrt{3}h-2j$	$-2c-h^*$	$\sqrt{3}i$	$-\sqrt{3}i$	$-\sqrt{3}i$	$-\sqrt{2}h^*$
$t_2^3(^2T_2)e$			$a+2b+\sqrt{3}c$ $+3d+\sqrt{3}h$	$-3i^*$	$+5i^*$	$-5i^*$	$\sqrt{2}g+\frac{2\sqrt{2}}{\sqrt{3}}h$
$t_2^2(^3T_1)e^2(^3A_2)$				$b+\frac{4}{\sqrt{3}}c+4d+e$ $-3f+2g+\frac{2}{\sqrt{3}}h$ $-j$	$-2\sqrt{3}h$	0	$-3\sqrt{2}i^*$
$t_2^2(^1T_2)e^2(^1E)$					$b+\frac{4}{\sqrt{3}}c+4d+e$ $-f-2g-\frac{2}{\sqrt{3}}h$ $+j$	$-\frac{4}{\sqrt{3}}c-\frac{2}{\sqrt{3}}h$	$+\sqrt{2}i^*$
$t_2^2(^1T_2)e^2(^1A_1)$						$b+\frac{4}{\sqrt{3}}c+4d$ $+e+f-2g$ $-\frac{2}{\sqrt{3}}h+j$	$+\sqrt{2}i^*$
t_2e^3							$\frac{5}{\sqrt{3}}c+3d+3e$ $-5f+\frac{4}{\sqrt{3}}h$

Table III.11 (Continued)

$^1A_1$	t_2^4	$t_2^3(^2E)e$	$t_2^2(^1A_1)e^2(^1A_1)$	$t_2^2(^1E)e^2(^1E)$	e^4
t_2^4	$2a+4b$	$-4\sqrt{6}i$	$2\sqrt{2}g+\frac{2\sqrt{2}}{\sqrt{3}}h$	$+\frac{2\sqrt{2}}{\sqrt{3}}h^*$	0
$t_2^3(^2E)e$		$3b+\sqrt{3}c+3d+2\sqrt{3}h$	$-4\sqrt{3}i$	$-2\sqrt{3}i^*$	0
$t_2^2(^1A_1)e^2(^1A_1)$			$a+\frac{4}{\sqrt{3}}c+4d+e+f-2g-\frac{2}{\sqrt{3}}h+2j$	$+\frac{8}{\sqrt{3}}c+\frac{4}{\sqrt{3}}h^*$	$\sqrt{6}g+\sqrt{2}h$
$t_2^2(^1E)e^2(^1E)$				$a+\frac{4}{\sqrt{3}}c+4d+e-f-2g-\frac{2}{\sqrt{3}}h-j$	$+2\sqrt{2}h^*$
e^4					$6e-10f$

^1E	t_2^4	$t_2^3(^2E)e$	$t_2^2(^1E)e^2(^1A_1)$	$t_2^2(^1A_1)e^2(^1E)$	$t_2^2(^1E)e^2(^1E)$
t_2^4	$2a+4b-3j$	$2\sqrt{3}i$	$\sqrt{2}g+\frac{\sqrt{2}}{\sqrt{3}}h^*$	$-\frac{2}{\sqrt{3}}h$	$-\frac{4}{\sqrt{3}}h^*$
$t_2^3(^2E)e$		$3b+\sqrt{3}c+3d$	$-\sqrt{6}i^*$	$-4\sqrt{3}i$	0
$t_2^2(^1E)e^2(^1A_1)$			$a+\frac{4}{\sqrt{3}}c+4d+e+f-2g-\frac{2}{\sqrt{3}}h-j$	$\frac{4\sqrt{2}}{\sqrt{3}}c+\frac{2\sqrt{2}}{\sqrt{3}}h^*$	$-\frac{4\sqrt{2}}{\sqrt{3}}c-\frac{2\sqrt{2}}{\sqrt{3}}h$
$t_2^2(^1A_1)e^2(^1E)$				$a+\frac{4}{\sqrt{3}}c+4d+e-f-2g-\frac{2}{\sqrt{3}}h+2j$	0
$t_2^2(^1E)e^2(^1E)$					$a+\frac{4}{\sqrt{3}}c+4d+e-f-2g-\frac{2}{\sqrt{3}}h-j$

$^1T_1$	$t_2^3(^2T_1)e$	$t_2^3(^2T_2)e$	$t_2^2(^1T_2)e^2$	t_2e^3
$t_2^3(^2T_1)e$	$a+2b+\sqrt{3}c+3d+\sqrt{3}h-2j$	$2c+h$	$\sqrt{3}i^*$	$\sqrt{2}h$
$t_2^3(^2T_2)e$		$a+2b+\sqrt{3}c+3d-\sqrt{3}h$	$-5i^*$	$\sqrt{2}g$
$t_2^2(^1T_2)e^2$			$b+\frac{4}{\sqrt{3}}c+4d+e-f-2g-\frac{2}{\sqrt{3}}h+j$	$-\sqrt{2}i^*$
t_2e^3				$\frac{c}{\sqrt{3}}+3d+3e-5f-\frac{4}{\sqrt{3}}h$

$^3T_2$	$t_2^3(^2T_1)e$	$t_2^3(^2T_2)e$	$t_2^2(^3T_1)e^2(^3A_2)$	$t_2^2(^3T_1)e^2(^1E)$	t_2e^3
$t_2^3(^2T_1)e$	$a+2b+\sqrt{3}c+3d-2g-\frac{h}{\sqrt{3}}-2j$	$-2c-h^*$	$\sqrt{2}i$	i^*	$-\sqrt{2}h^*$
$t_2^3(^2T_2)e$		$a+2b+\sqrt{3}c+3d-2g-\sqrt{3}h$	$-\sqrt{6}i^*$	$\sqrt{3}i$	$\sqrt{2}g+\frac{2\sqrt{2}h}{\sqrt{3}}$
$t_2^2(^3T_1)e^2(^3A_2)$			$b+\frac{4}{\sqrt{3}}c+4d+e-3f-j$	$-\frac{2\sqrt{2}}{\sqrt{3}}h^*$	$-2\sqrt{3}i^*$
$t_2^2(^3T_1)e^2(^1E)$				$b+\frac{4}{\sqrt{3}}c+4d+e-f-2g-\frac{2}{\sqrt{3}}h-j$	$\sqrt{6}i$
t_2e^3					$\frac{5}{\sqrt{3}}c+3d+3e-5f-2g-\frac{2}{\sqrt{3}}h$

Table III.11 (Continued)

^3E	$t_2^3(^4A_2)e$	$t_2^3(^2E)e$	$t_2^2(^1E)e^2(^3A_2)$
$t_2^3(^4A_2)e$	$3b+\sqrt{3}c+3d$ $+g+\frac{h}{\sqrt{3}}-3j$	$-\frac{4}{\sqrt{3}}h$	0
$t_2^3(^2E)e$		$3b+\sqrt{3}c+3d$ $-2g-\frac{2}{\sqrt{3}}h$	$-\sqrt{6}i^*$
$t_2^2(^1E)e^2(^3A_2)$			$a+\frac{4}{\sqrt{3}}c+4d$ $+e-3f-2g-\frac{2}{\sqrt{3}}h-j$

$^3A_2$	$t_2^3(^2E)e$	$t_2^2(^1A_1)e^2(^3A_2)$
$t_2^3(^2E)e$	$3b+\sqrt{3}c$ $+3d-2g$	$-4\sqrt{3}i$
$t_2^2(^1A_1)e^2(^3A_2)$		$a+\frac{4}{\sqrt{3}}c+4d$ $+e-3f-2g-\frac{2}{\sqrt{3}}h+2j$

$^1A_2$	$t_2^3(^2E)e$	$t_2^2(^1E)e^2(^1E)$
$t_2^3(^2E)e$	$3b+\sqrt{3}c+3d$ $-2\sqrt{3}h$	$2\sqrt{3}i^*$
$t_2^2(^1E)e^2(^1E)$		$a+\frac{4}{\sqrt{3}}c+4d$ $+e-f-2g$ $-\frac{2}{\sqrt{3}}h-j$

$t_2^3(^2E)e$	$^3A_1 = 3b+\sqrt{3}c+3d$ $-2g-4h/\sqrt{3}$
$t_2^3(^4A_2)e$	$^5E = 3b+\sqrt{3}c+3d$ $-3g-\sqrt{3}h-3j$
$t_2^2(^3T_1)e^2(^3A_2)$	$^5T_2 = b+4c/\sqrt{3}+4d$ $+e-3f-4g$ $-4h/\sqrt{3}-j$

Table III.12

ELECTRON-ELECTRON MATRIX ELEMENTS FOR d^5 ELECTRONS. ASTERISK DENOTES THE CHANGE IN SIGN WITH RESPECT TO GRIFFTH'S MATRIX ELEMENTS[41].

$^2A_1$	$t_2^4(^1E)e$	$t_2^3(^2E)e^2(^1E)$	$t_2^3(^4A_2)e^2(^3A_2)$	$t_2^2(^1E)e^3$
$t_2^4(^1E)e$	$2a+4b+\frac{8}{\sqrt{3}}c+4d-2g-3j$	$-\sqrt{6}i$	0	$g+\frac{5}{\sqrt{3}}h^*$
$t_2^3(^2E)e^2(^1E)$		$3b+2\sqrt{3}c+6d$ $+e-f-3g$ $-\sqrt{3}h$	$-4h^*$	$\sqrt{6}i^*$
$t_2^3(^4A_2)e^2(^3A_2)$			$3b+2\sqrt{3}c+6d$ $+e-3f+2g+\frac{2}{\sqrt{3}}h-3j$	0
$t_2^2(^1E)e^3$				$a+\frac{10}{\sqrt{3}}c+6d$ $+3e-5f-3g-\frac{1}{\sqrt{3}}h-j$

$^2A_2$	$t_2^4(^1E)e$	$t_2^3(^2E)e^2(^1E)$	$t_2^2(^1E)e^3$
$t_2^4(^1E)e$	$2a+4b+4d$ $-2g-\frac{4}{\sqrt{3}}h$ $-3j$	$\sqrt{6}i$	$g-\sqrt{3}h^*$
$t_2^3(^2E)e^2(^1E)$		$3b+2\sqrt{3}c+6d$ $+e-f-3g$ $-\sqrt{3}h$	$-\sqrt{6}i^*$
$t_2^2(^1E)e^3$			$a+\frac{2}{\sqrt{3}}c+6d$ $+3e-5f-3g$ $-\frac{5}{\sqrt{3}}h-j$

^2E	$t_2^4(^1A_1)e$	$t_2^4(^1E)e$	$t_2^3(^2E)e^2(^1A_1)$	$t_2^3(^2E)e^2(^3A_2)$	$t_2^3(^2E)e^2(^1E)$	$t_2^2(^1E)e^3$	$t_2^2(^1A_1)e^3$
$t_2^4(^1A_1)e$	$2a+4b+\frac{4}{\sqrt{3}}c$ $+4d-2g-\frac{2}{\sqrt{3}}h$	$\frac{4}{\sqrt{3}}c+\frac{2}{\sqrt{3}}h$	$2\sqrt{3}i$	$6i$	$2\sqrt{6}i$	$-\frac{2}{\sqrt{3}}h^*$	$2g+\frac{2}{\sqrt{3}}h$
$t_2^4(^1E)e$		$2a+4b+\frac{4}{\sqrt{3}}c$ $+4d-2g$ $-\frac{2}{\sqrt{3}}h-3j$	$-\sqrt{3}i$	$3i$	0	$g+\frac{h^*}{\sqrt{3}}$	$\frac{2}{\sqrt{3}}h$
$t_2^3(^2E)e^2(^1A_1)$			$3b+2\sqrt{3}c+6d$ $+e+f-3g$ $-\sqrt{3}h$	0	0	$-\sqrt{3}i^*$	$-2\sqrt{3}i$
$t_2^3(^2E)e^2(^3A_2)$				$3b+2\sqrt{3}c$ $+6d+e-3f-g$ $-\frac{h}{\sqrt{3}}$	$2\sqrt{2}h$	$-3i^*$	$6i$
$t_2^3(^2E)e^2(^1E)$					$3b+2\sqrt{3}c+6d$ $+e-f-3g$ $-\sqrt{3}h$	0	$2\sqrt{6}i$
$t_2^2(^1E)e^3$						$a+2\sqrt{3}c+6d$ $+3e-5f-3g$ $-\sqrt{3}h-j$	$-\frac{4}{\sqrt{3}}c-\frac{2}{\sqrt{3}}h^*$
$t_2^2(^1A_1)e^3$							$a+2\sqrt{3}c+6d$ $+3e-5f-3g$ $-\sqrt{3}h+2j$

Table III.12 (Continued)

^4E	$t_2^3(^2E)e^2(^3A_2)$	$t_2^3(^4A_2)e^2(^1E)$
$t_2^3(^2E)e^2(^3A_2)$	$3b+2\sqrt{3}c+6d$ $+e-3f-4g$ $-\frac{4}{\sqrt{3}}h$	$-2h$
$t_2^3(^4A_2)e^2(^1E)$		$3b+2\sqrt{3}c+6d$ $+e-f-3g$ $-\sqrt{3}h-3j$

$^4T_1$	$t_2^4(^3T_1)e$	$t_2^3(^2T_2)e^2(^3A_2)$	$t_2^2(^3T_1)e^3$
$t_2^4(^3T_1)e$	$a+5b+\frac{2}{\sqrt{3}}c$ $+4d-3g-\sqrt{3}h$ $-3j$	$-\sqrt{6}i^*$	$g-\frac{1}{\sqrt{3}}h^*$
$t_2^3(^2T_2)e^2(^3A_2)$		$a+2b+2\sqrt{3}c$ $+6d+e-3f$ $-4g-\frac{4}{\sqrt{3}}h$	$-\sqrt{6}i$
$t_2^2(^3T_1)e^3$			$b+\frac{4}{\sqrt{3}}c+6d$ $+3e-5f-4g$ $-\frac{4}{\sqrt{3}}h-j$

$^4T_2$	$t_2^4(^3T_1)e$	$t_2^3(^2T_1)e^2(^3A_2)$	$t_2^2(^3T_1)e^3$
$t_2^4(^3T_1)e$	$a+5b+2\sqrt{3}c$ $+4d-3g-\sqrt{3}h$ $-3j$	$\sqrt{2}i^*$	$g+\sqrt{3}h^*$
$t_2^3(^2T_1)e^2(^3A_2)$		$a+2b+2\sqrt{3}c$ $+6d+e-3f$ $-4g-\frac{4}{\sqrt{3}}h$ $-2j$	$-\sqrt{2}i$
$t_2^2(^3T_1)e^3$			$b+\frac{8}{\sqrt{3}}c+6d$ $+3e-5f-4g$ $-\frac{4}{\sqrt{3}}h-j$

Table III.12 (Continued)

$^2T_1$	$t_2^5(^3T_1)e$	$t_2^5(^1T_2)e$	$t_2^3(^2T_1)e^2(^1A_1)$	$t_2^3(^2T_1)e^2(^1E)$	$t_2^3(^2T_2)e^2(^3A_2)$	$t_2^3(^2T_2)e^2(^1E)$	$t_2^3(^1T_2)e^3$	$t_2^3(^3T_1)e^3$
$t_2^5(^3T_1)e$	$a+5b+\frac{2}{\sqrt{3}}c$ $+4d-\sqrt{3}h-3j$	$-\sqrt{3}h$	$-\frac{\sqrt{6}}{2}i$	$\frac{1}{2}\sqrt{6}i$	$-\frac{1}{2}\sqrt{6}i^*$	$-\frac{3}{\sqrt{2}}i$	0	$g-\frac{h^*}{\sqrt{3}}$
$t_2^5(^1T_2)e$		$a+5b+2\sqrt{3}c$ $+4d-2g$ $-\frac{h}{\sqrt{3}}-j$	$\frac{1}{2}\sqrt{6}i$	$\frac{1}{2}\sqrt{6}i$	$\frac{1}{2}\sqrt{6}i^*$	$\frac{5}{\sqrt{2}}i$	$g+\sqrt{3}h^*$	0
$t_2^3(^2T_1)e^2(^1A_1)$			$a+2b+2\sqrt{3}c$ $+6d+e+f$ $-3g-\sqrt{3}h-2j$	0	0	$4c+2h$	$\frac{\sqrt{6}}{2}i^*$	$-\frac{\sqrt{6}}{2}i^*$
$t_2^3(^2T_1)e^2(^1E)$				$a+2b+2\sqrt{3}c$ $+6d+e-f$ $-3g-\sqrt{3}h-2j$	0	0	$-\frac{\sqrt{6}}{2}i^*$	$-\frac{\sqrt{6}}{2}i^*$
$t_2^3(^2T_2)e^2(^3A_2)$					$a+2b+2\sqrt{3}c$ $+6d+e-3f$ $-g-\frac{h}{\sqrt{3}}$	$2h^*$	$\frac{5}{2}\sqrt{6}i$	$-\frac{\sqrt{6}}{2}i$
$t_2^3(^2T_2)e^2(^1E)$						$a+2b+2\sqrt{3}c$ $+6d+e-f$ $-3g-\sqrt{3}h$	$\frac{5}{\sqrt{2}}i^*$	$-\frac{3}{\sqrt{2}}i^*$
$t_2^2(^1T_2)e^3$							$b+\frac{8}{\sqrt{3}}c+6d$ $+3e-5f-3g$ $-\frac{2h}{\sqrt{3}}+j$	$-\sqrt{3}h$
$t_2^2(^3T_1)e^3$								$b+\frac{4}{\sqrt{3}}c+6d$ $+3e-5f-g$ $-\frac{4}{\sqrt{3}}h-j$

Table III.12 (Continued)

$^2T_2$	t_2^5	$t_2^4(^3T_1)e$	$t_2^4(^1T_2)e$	$t_2^3(^2T_1)e^2(^3A_2)$	$t_2^3(^2T_1)e^2(^1E)$	$t_2^3(^2T_2)e^2(^1A_1)$	$t_2^3(^2T_2)e^2(^1E)$	$t_2^2(^1T_2)e^3$	$t_2^2(^3T_1)e^3$	t_2e^4
t_2^5	$2a+8b$ $-4j$	$3\sqrt{2}i^*$	$\sqrt{2}i$	0	$-2h^*$	$2g+\frac{2h}{\sqrt{3}}$	$\frac{2h}{\sqrt{3}}$	0	0	0
$t_2^4(^3T_1)e$		$a+5b+2\sqrt{3}c$ $+4d+\sqrt{3}h-3j$	$\sqrt{3}h^*$	$\frac{i}{\sqrt{2}}^*$	$-\frac{\sqrt{6}}{2}i$	$\frac{3}{\sqrt{2}}i^*$	$\frac{3}{\sqrt{2}}i^*$	0	$g+\sqrt{3}h^*$	0
$t_2^4(^1T_2)e$			$a+5b+\frac{2}{\sqrt{3}}c$ $+4d-2g-\sqrt{3}h-j$	$\frac{3}{\sqrt{2}}i$	$-\frac{\sqrt{6}}{2}i^*$	$\frac{5}{\sqrt{2}}i$	$-\frac{5}{\sqrt{2}}i$	$g-\frac{h}{\sqrt{3}}^*$	0	0
$t_2^3(^2T_1)e^2(^3A_2)$				$a+2b+2\sqrt{3}c$ $+6d+e-3f$ $-g-\frac{h}{\sqrt{3}}-2j$	$2h^*$	0	0	$-\frac{3}{\sqrt{2}}i^*$	$-\frac{1}{\sqrt{2}}i$	0
$t_2^3(^2T_1)e^2(^1E)$					$a+2b+2\sqrt{3}c$ $+6d+e-f$ $-3g-\sqrt{3}h-2j$	$-4c-2h^*$	0	$\frac{\sqrt{6}}{2}i$	$\frac{\sqrt{6}}{2}i^*$	$-2h^*$
$t_2^3(^2T_2)e^2(^1A_1)$						$a+2b+2\sqrt{3}c$ $+6d+e+f$ $-3g-\sqrt{3}h$	0	$-\frac{5}{\sqrt{2}}i^*$	$-\frac{3}{\sqrt{2}}i$	$2g+\frac{2}{\sqrt{3}}h$
$t_2^3(^2T_2)e^2(^1E)$							$a+2b+2\sqrt{3}c$ $+6d+e-f$ $-3g-\sqrt{3}h$	$-\frac{5}{\sqrt{2}}i^*$	$\frac{3}{\sqrt{2}}i$	$-\frac{2}{\sqrt{3}}h$
$t_2^2(^1T_2)e^3$								$b+\frac{4}{\sqrt{3}}c$ $+6d+3e-5f$ $-3g-\frac{4}{\sqrt{3}}h+j$	$\sqrt{3}h^*$	$-\sqrt{2}i^*$
$t_2^2(^3T_1)e^3$									$b+\frac{8}{\sqrt{3}}c+6d$ $+3e-5f-g$ $+\frac{2}{\sqrt{3}}h-j$	$-3\sqrt{2}i$
t_2e^4										$\frac{4}{\sqrt{3}}c+4d+6e$ $-10f-2g-\frac{2}{\sqrt{3}}h$

$t_2^3(^4A_2)e^2(^3A_2)$: $^4A_1 = 3b+2\sqrt{3}c+6d+e-3f-g-\frac{h}{\sqrt{3}}-3j$

$t_2^3(^4A_2)e^2(^1A_1)$: $^4A_2 = 3b+2\sqrt{3}c+6d+e+f-3g-\sqrt{3}h-3j$

$t_2^3(^4A_2)e^2(^3A_2)$: $^6A_1 = 3b+2\sqrt{3}c+6d+e-3f-6g-2\sqrt{3}h-3j$

For the matrix elements of the complementary states d^{10-n} (n = 2, 3, 4, 5), the nondiagonal matrix elements remain the same as in d^n matrices. The diagonal matrix elements of d^{10-n} states differ from the corresponding ones of d^n by a function which is a linear combination of a, b, c, . . ., j, as derived by Sharma and Sundaram[41]:

$$\langle t_2^{6-m}(S_1\Gamma_1)e^{4-\ell}(S_2\Gamma_2)S\Gamma M_S M_\Gamma \,|(e^2/r_{ij})\,|$$

$$|t_2^{6-m}(S_1\Gamma_1)e^{4-\ell}(S_2\Gamma_2)S\Gamma M_S M_\Gamma\rangle - \langle t_2^{m}(S_1\Gamma_1)e^{\ell}(S_2\Gamma_2)$$

$$S\Gamma M_S M_\Gamma \,|(e^2/r_{ij})|\, t_2^{m}(S_1\Gamma_1)e^{\ell}(S_2\Gamma_2)S\Gamma M_S M_\Gamma\rangle$$

$$= (3-m)a + 4(3-m)b + (24-4m-6\ell)(c/\sqrt{3} + d)$$

$$+ (6-3\ell)e + (5\ell-10)f + (2m+3\ell-12)g$$

$$+ (2m+3\ell-12)h/\sqrt{3} - 2(3-m)j \qquad (73)$$

where the integers m and ℓ are connected to n by the relation

$$m + \ell = n \text{ or } 10-n \qquad (74)$$

In Eq. (73), t_2 represents the orbitals ξ, η, and ζ, and e represents the orbitals θ and ε. S_i and S are the total spin quantum numbers and the Γ_i and Γ are the irreducible representations of the cubic group. The difference between the diagonal element of d^n and that of d^{10-n} as given by Eq. (73)

reduces, as expected, for the pure d-electron case to

$$\langle t_2^{6-m}(S_1\Gamma_1)e^{4-\ell}(S_2\Gamma_2)S\Gamma M_S M_\Gamma | (e^2/r_{ij}) |$$

$$| t_2^{6-m}(S_1\Gamma_1)e^{4-\ell}(S_2\Gamma_2)S\Gamma M_S M_\Gamma \rangle - \langle t_2^m(S_1\Gamma_1)$$

$$e^\ell(S_2\Gamma_2)S\Gamma M_S M_\Gamma | (e^2/r_{ij}) | t_2^m(S_1\Gamma_1)e^\ell(S_2\Gamma_2)S\Gamma M_S M_\Gamma \rangle$$

$$= (45\ A - 70\ B + 35\ C) -$$

$$(9\ A - 14\ B + 7\ C)(m + \ell) \qquad (75)$$

where A, B, and C are the standard Racah parameters. One notes that in the case of pure d-orbitals, expression (75) depends only on the sum $(m + \ell)$, which, according to Eq. (74), is n or 10-n, and hence, for a given n (with whatever appropriate values of the set m, ℓ), the difference between the diagonal elements in Eq. (75) is constant. The formula above, Eq. (73), is particularly significant because it reveals that the diagonal elements of the d^{10-n} configuration change by different amounts from the corresponding ones for the d^n configuration. As an example, for the configuration d^3 the diagonal element

$$\langle t_2^3(^2E)e^0(^1E)\,^2E | (e^2/r_{ij}) | t_2^3(^2E)e^0(^1E)\,^2E \rangle$$

and the corresponding one in the configuration d^7 differ by the amount

$$[-12(c/\sqrt{3} + d) - 6e + 10f + 6g + 2\sqrt{3}\, h] \quad ,$$

whereas the diagonal element

$$\langle t^0({}^1A_1)e^3({}^2E)^2E|(e^2/r_{ij})|t^0({}^1A_1)e^3({}^2E)^2E\rangle$$

in the configuration d^3 differs from the corresponding one in the d^7 configuration by

$$[-3a - 12b - 6(e/\sqrt{3} + d) + 3e - 5f + 3g + \sqrt{3}\, h + 6j].$$

Also, in the configuration d^3 the diagonal element

$$\langle t_2^2({}^3T_1)e^1({}^2E)^2T_1|(e^2/r_{ij})|t_2^2({}^3T_1)e^1({}^2E)^2T_1\rangle$$

differs from the corresponding diagonal element in the d^7 configuration by

$$[-a - 4b - 10(c/\sqrt{3} \pm d) - 3e + 5f + 5g + 5h/\sqrt{3} + 2j].$$

It is clear from the examples above that the various diagonal elements are changed by different amounts in going from the d^n to the d^{10-n} configuration. On the other hand, if pure d-orbitals are involved, all the diagonal elements of the d^3 configuration differ from the corresponding diagonal elements of the d^7 configuration by the constant amount (-18A + 28B - 14C), which agrees with the result given by Griffith[46]. Thus, in general, the present results from the improved treatment differ from the corresponding results in the simplified

theory of the pure d-orbitals. In particular, the extended theory shows that the matrix elements of complementary configurations are not related by a constant factor.

It must be recalled that in cubic-crystal fields the diagonal matrix elements for the states $|t_2^m e^\ell\rangle$ are further admixed, as usual, by the crystal field term $(0.4\ell - 0.6m)\Delta$, where $\Delta = 10$ Dq is the cubic-field splitting parameter. The splitting parameter Δ is positive for the octahedral symmetry, and in that case the t_2 level lies below the e level in energy. On the other hand, in the case of tetrahedral symmetry it has been shown by Griffith[46] that the parameter Δ changes sign, thereby inverting the t_2 and e levels. Also, the diagonal matrix elements of the d^n configuration are related to those of the d^{10-n} configuration in a given symmetry (octahedral or tetrahedral). This is a very important result concerning the improved theory, since the diagonal elements no longer change by the same amount, as shown by Eq. (73). Thus, in several cases, based solely on this type of change in the diagonal elements, the energy levels in the new treatment are expected to be different, and certain levels which are degenerate in the old treatment are predicted in the extended theory to have split components.

At first glance, the full import of the generalized matrices (Tables III.9-12) may not be obvious, owing to the fact that one now has eleven parameters (a, b, c, . . ., j, and Δ) replacing four parameters (A, B, C, and Δ) of the old theory. The large number of parameters makes the theory apparently less attractive, but it is important to note that it includes the

effect of the surroundings in the correct way. The new theory, however, is very significant, since it has been able to test the calculations[39,40] made on GaAs:Cr^{2+} and GaAs:Cr^{3+} and make comparisons, which we will discuss in detail in Chapter IV. Also, this generalized treatment gives correct group-theoretical assignments to the observed energy levels of the impurity in solids. Furthermore, using this refined treatment, Sharma and Sundaram[43] have shown the importance of these matrices by using it for the prediction of the Coulomb and exchange interaction constants for MgF_2:$Co^{2+}(d^7)$ and MgF_2:$Mn^{2+}(d^5)$, which turn out to be significantly different from the free-ion values. Moreover, the general treatment is helpful for removing the accidental degeneracy observed in certain areas.[41,43]

We now proceed, in Section B, to consider the other interaction terms contained in the Hamiltonian (Eq. 4), namely, the spin-orbit and spin-spin interactions. Also, the spin-Hamiltonian parameters will be derived in the next section, making use of the cluster wave functions already presented (Eqs. 10-14).

B. Spin-orbit and spin-spin interactions

This section will be separated into two parts. In subsection B.1 we will discuss the spin-Hamiltonian parameters for the GaAs:Cr^{2+} and InP:Cr^{2+} materials. In subsection B.2 we will discuss the energy splittings due to the spin-orbit and spin-spin interactions in the GaAs:Fe^{2+}, GaP:Fe^{2+}, and InP:Fe^{2+} materials.

B.1 Spin-Hamiltonian parameters for GaAs:Cr^{2+} and InP:Cr^{2+}

For the GaAs:$Cr^{2+}(3d^4)$ and InP:$Cr^{2+}(3d^4)$ semiconductors,

the localized impurity energy levels[18;22] are shown in the diagram depicted in Figure II.1. In a cubic crystal field, the wave functions Ψ_ξ, Ψ_η, and Ψ_ζ are degenerate cluster orbitals representing the ground state $^5T_2$ (for T_d symmetry), and the cluster orbitals Ψ_θ and Ψ_ε represent the degenerate excited state ^5E. Because the ground state is orbitally degenerated, the system undergoes a Jahn-Teller distortion[64,65] (see Appendix I). Experimental evidence in the EPR spectra of GaAs:Cr^{2+} (Ref. 18) and InP:Cr^{2+} (Ref. 33) indicates that a tetragonal Jahn-Teller distortion occurs in these materials. The tetragonal Jahn-teller distortion lowers the local symmetry from tetrahedral (T_d) to tetragonal (D_{2d}). Consequently, the ground state $^5T_2$ (in T_d symmetry) splits into $^5B_2$ and ^5E (in D_{2d} symmetry), whereas the excited state ^5E (in T_d symmetry) splits into $^5A_1$ and $^5B_1$ (in D_{2d} symmetry), as explained in Appendix I and depicted in Fig. II.1.

We may assume, as a first approximation, that the wave functions of the cluster are not altered significantly in going from tetrahedral to tetragonal symmetry. This assumption is valid in the case of a small tetragonal distortion, so that the angle β' (see Fig. III.4) does not deviate appreciably from the values of $\cos\beta' = 1/\sqrt{3}$ and $\sin\beta' = \sqrt{2}/\sqrt{3}$. In Chapter IV, we give the estimate of the Jahn-Teller distortion for GaAs:Cr^{2+}. The main effect of this interaction, however small its effect on the wave functions might be, is to split the energy levels of T_2 and E symmetry of the tetrahedron in the manner mentioned previously. With the energy-levels diagram, incorporating the effects of crystal-field and Jahn-

Teller distortion, and the cluster wave functions, we can proceed to analyze the magnetic properties of GaAs:Cr^{2+} and InP:Cr^{2+}. Although the spin-orbit and spin-spin interactions are small in the $3d^n$ systems, their presence has significant consequences for the single-ion magnetic properties, such as the g-factors and the zero-field and cubic-field parameters, as measured by EPR.

For a system with axial symmetry (such as D_{2d}), the spin-Hamiltonian is expressed by[64,78]

$$H_S = \mu_B[g_{\parallel} S_z H_z + g_{\perp}(S_x H_x + S_y H_y)]$$

$$+ D[S_z^2 - \frac{1}{3} S(S+1)] + \frac{a}{6}(S_x^4 + S_y^4 + S_z^4) \qquad (76)$$

where μ_B is the Bohr magneton ($\mu_B = \hbar e/2mc$), S_x, S_y, and S_z are the x-, y-, and z-components of the total spin $\vec{S}$ of the system. $\vec{H}$ is an externally applied magnetic field, with components H_x, H_y, and H_z. The g-factors are designated with a parallel subscript for the g_{zz} tensor-component and with a perpendicular subscript for the g_{xx} or g_{yy} tensor-components ($g_{\parallel} = g_{zz}$, $g_{\perp} = g_{xx} = g_{yy}$). The parameter D is known as the "zero-field splitting parameter", and $\underline{a}$, as the "cubic-field parameter". In order to obtain the g, D, and $\underline{a}$ parameters in the spin-Hamiltonian (Eq. 76) for GaAs:Cr^{2+} and InP:Cr^{2+}, one perturbs the ground state $^5B_2$ (see Fig. II.1) by the spin-orbit, Zeeman, and spin-spin interactions:

$$V_{SO} = \sum_i \zeta(\vec{r}_i)\ \vec{\ell}_i \cdot \vec{s}_i \tag{77}$$

$$V_Z = \mu_B \left(\sum_i \vec{\ell}_i + g_0 \sum_i \vec{s}_i \right) \cdot \vec{H} \tag{78}$$

$$V_{SS} = 4\mu_B^2 \sum_{i\ j} \left\{ \frac{\vec{s}_i \cdot \vec{s}_j}{r_{ij}^3} - \frac{3(\vec{s}_i \cdot \vec{r}_{ij})(\vec{s}_j \cdot \vec{r}_{ij})}{r_{ij}^5} \right\} \tag{79}$$

where g_o (= 2.0023) is the free-electron g-factor.

Within a manifold of states originating from a ^{2S+1}L term (^5D in our case), the spin-orbit (V_{SO}), Zeeman (V_Z), and spin-spin (V_{SS}) terms can be represented by the equivalent operators[78]

$$V_{SO} = \lambda\ \vec{L} \cdot \vec{S} \tag{80}$$

$$V_Z = \mu_B (\vec{L} + g_o \vec{S}) \cdot \vec{H} \tag{81}$$

$$V_{SS} = -\rho [(\vec{L} \cdot \vec{S})^2 + \tfrac{1}{2} \vec{L} \cdot \vec{S} - \tfrac{1}{3} \vec{L}^2 \vec{S}^2] \tag{82}$$

$\vec{L}$ and $\vec{S}$ are the total angular momentum and spin operators. In Eq. (80) λ is the effective spin-orbit coupling of the system, and for systems which obey Hund's rule, it is related to the one-electron spin-orbit coupling constant ζ by[78,79]

$$\lambda = \pm \frac{\zeta}{2S} \tag{83}$$

In Eq. (83) the positive sign stands for a configuration of a

less than half-filled shell (i.e., d^1, d^2, d^3, d^4), and the negative sign for a more than half-filled shell[79] (i.e., d^5, d^6, d^7, d^8). The ground term of d^5 is ^6S, and this cannot be split by spin-orbit coupling operator alone to any order (similarly for the d^{10} configuration). The d-electron spin-spin parameter ρ, in eq. (82), for a ^{2S+1}L term which obeys Hund's rule is given by Pryce[80] to be

$$\rho = \frac{4\mu_B^2}{7S(2L+1)} \left\{ (4S + 5)p_{1,2} + \frac{1}{7}(100 - 62S)p_{3,4} \right\} \qquad (84)$$

where

$$p_{n,m} = \int_0^\infty \frac{1}{r^n} \phi_d^2(r) \int_0^r r'^m \phi_d^2(r')\, dr' dr \qquad (85)$$

and $\phi_d(r)$ is the radial wave function of the magnetic ion. In Eqs. (84) and (85), only the "local" terms are considered.[52]

One obtains the g-factors, D, and $\underline{a}$ parameters of the spin-Hamiltonian (eq. 76) by treating the spin-orbit, Zeeman, and spin-spin interactions by perturbation theory. In the case of GaAs:Cr^{2+} and InP:Cr^{2+}, the ground state $\Psi_0 = \Psi_\zeta$ (see Fig. II.1) is non-degenerate (in D_{2d} symmetry), and in first-order perturbation theory one obtains

$$\langle \Psi_0 | V_{SO} + V_Z + V_{SS} | \Psi_0 \rangle = g_0 \mu_B \vec{S}.\vec{H}$$

$$- \rho \langle \Psi_0 | (L.S)^2 - \frac{1}{3} \vec{L}^2 \vec{S}^2 | \Psi_0 \rangle \qquad (86)$$

since

$$\langle \Psi_0 | L_x | \Psi_0 \rangle = 0 \qquad (87\text{-a})$$

$$\langle \Psi_0 | L_y | \Psi_0 \rangle = 0 \qquad (87\text{-b})$$

$$\langle \Psi_0 | L_z | \Psi_0 \rangle = 0 \qquad (87\text{-c})$$

In the second-order perturbation of the spin-orbit and Zeeman interactions we get, calling the excited states Ψ_n (Ψ_n = Ψ_ξ, Ψ_η, Ψ_θ, Ψ_ε in Fig. II.1), a correction to the energy:

$$E^{(1)} = - \sum_{n \neq 0} \frac{| \langle \Psi_0 | \lambda \vec{L}.\vec{S} + \mu_B (\vec{L} + g_0 \vec{S}).\vec{H} | \Psi_n \rangle |^2}{E_n - E_0} \qquad (88)$$

By collecting the terms in first- and second-order (Eqs. 86 and 88, respectively) which are linear in $S_i H_j$ ($i, j \equiv x, y, z$), we obtain

$$E(S_i H_j) = \mu_B \left(g_0 \delta_{ij} - 2 \sum_{n \neq 0} \frac{\langle \Psi_0 | \lambda L_i | \Psi_n \rangle \langle \Psi_n | L_j | \Psi_0 \rangle}{E_n - E_0} \right) S_i H_j \qquad (89)$$

The term in parentheses in Eq. (89) is the tensor component g_{ij}. In axial symmetry (such as D_{2d}), one can write

$$g_{xx} = g_{yy} = g_\perp \qquad (90\text{-a})$$

$$g_{zz} = g_\parallel \quad , \qquad (90\text{-b})$$

the other tensor components being zero. By comparison of Eq. (89) with the spin-Hamiltonian (Eq. 76), and with Eqs. (90),

one identifies the g-factors as

$$g_{\parallel} = g_0 - 2 \sum_{n \neq 0} \frac{\langle \Psi_0 | \lambda L_z | \Psi_n \rangle \langle \Psi_n | L_z | \Psi_0 \rangle}{} \tag{91}$$

$$g_{\perp} = g_0 - 2 \sum_{n \neq 0} \frac{\langle \Psi_0 | \lambda L_x | \Psi_n \rangle \langle \Psi_n | L_x | \Psi_0 \rangle}{E_n - E_0} \tag{92}$$

By collecting the first-order perturbation of the spin-spin interaction (see Eq. 86) and the second-order perturbation term of the spin-orbit interaction which is proportional to $S_i S_j$ (see Eq. 88), one obtains, after some mathematical manipulation, the following expression for the zero-field splitting:

$$D = -\rho \langle \Psi_0 | (\vec{L}.\vec{S})^2 - \frac{1}{3} \vec{L}^2 \vec{S}^2 | \Psi_0 \rangle$$

$$+ \sum_{n \neq 0} \frac{\langle \Psi_0 | \lambda L_x | \Psi_n \rangle \langle \Psi_n | \lambda L_x | \Psi_0 \rangle}{E_n - E_0}$$

$$- \sum_{n \neq 0} \frac{\langle \Psi_0 | \lambda L_z | \Psi_n \rangle \langle \Psi_n | \lambda L_z | \Psi_0 \rangle}{E_n - E_0} \tag{93}$$

In order to derive an explicit expression for the cubic term in the spin-Hamiltonian, a, one has to consider the fourth-rder effects of the spin-orbit interaction and the second-order

effects of the spin-spin interaction.

For GaAs:Cr^{2+} and InP:Cr^{2+}, the ground state Ψ_0 is given by Ψ_ζ, and the excited states Ψ_n are given by Ψ_ξ, Ψ_η, Ψ_θ, and Ψ_ε (see Fig. II.1), with the energy separations, $E_n - E_0$, between the excited states and the ground state indicated in Fig. II.1. The equations (91)-(93) are greatly simplified for the case of D_{2d} symmetry, for which the wave functions Ψ_ζ, Ψ_ξ, Ψ_η, Ψ_θ, and Ψ_ε transform like the orthogonal sets xy, yz, xz, $3z^2-r^2$, and x^2-y^2 respectively, where x, y, z are the coordinates of the central system of reference (see Fig. III.3). The application of the L_z and L_x operators upon these orthogonal sets results in[64]

$$L_z(xy)_\zeta = -2i(x^2 - y^2)_\varepsilon \tag{94-a}$$

$$L_x(xy)_\zeta = -L_x(yz)_\xi = i(xz)_\eta \tag{94-b}$$

From Eqs. (94-a) and (94-b), one sees that the L_z operator mixes the ground state Ψ_ζ with the Ψ_ε excited state only, and L_x mixes the ground state Ψ_ζ with the Ψ_η state only. Upon substitution of the ground state Ψ_0 and the excited states Ψ_n in Eqs. (91)-(93) by the corresponding states Ψ_ζ and Ψ_ξ, Ψ_η, Ψ_θ, and Ψ_ε states, the expressions for $g_{\parallel}$, $g_\perp$, and D are reduced to

$$g_{\parallel} = g_0 - 2\frac{\langle \Psi_\zeta | \lambda L_z | \Psi_\varepsilon \rangle \langle \Psi_\varepsilon | L_z | \Psi_\zeta \rangle}{E_3} \tag{95}$$

$$g_\perp = g_0 - 2\frac{\langle \Psi_\zeta | \lambda L_x | \Psi_\eta \rangle \langle \Psi_\eta | L_x | \Psi_\zeta \rangle}{E_1} \tag{96}$$

$$D = \frac{\langle \Psi_\xi | \lambda L_x | \Psi_\eta \rangle \langle \Psi_\eta | \lambda L_x | \Psi_\xi \rangle}{E_1} - \frac{\langle \Psi_\xi | \lambda L_z | \Psi_\epsilon \rangle \langle \Psi_\epsilon | \lambda L_z | \Psi_\xi \rangle}{E_3}$$

$$- \frac{3}{2} \rho \langle \Psi_\xi | L_z^2 - \frac{1}{3} L(L+1) | \Psi_\xi \rangle \qquad (97)$$

For both GaAs:Cr^{2+} and InP:Cr^{2+}, the energies E_1 and E_3 are indicated in Fig. II.1, and the d-electron spin-spin parameter ρ, according to Eq. (84), for the ^5D term state (L = 2, S = 2) is

$$\rho = \frac{2}{49} \mu_b^2 (7p_{1,2} - 8p_{3,4}) \quad , \qquad (98)$$

where $p_{1,2}$ and $p_{3,4}$ are defined as before, in Eq. (85). To simplify the notation in Eqs. (95)-(97), we define

$$\zeta_1 = \langle \Psi_\zeta | \lambda L_x | \Psi_\eta \rangle / i \qquad (99\text{-a})$$

$$S_1 = \langle \Psi_\eta | L_x | \Psi_\zeta \rangle / (-i) \qquad (99\text{-b})$$

$$\zeta_2 = \langle \Psi_\zeta | \lambda L_z | \Psi_\varepsilon \rangle / 2i \qquad (99\text{-c})$$

$$S_2 = \langle \Psi_\varepsilon | L_z | \Psi_\zeta \rangle / (-2i) \qquad (99\text{-d})$$

and Eqs. (95)-(97) can be written in the compact form

$$g_{\parallel} = g_0 - \frac{8\zeta_2 S_2}{E_3} \qquad (100)$$

$$g_{\perp} = g_0 - \frac{2\zeta_1 S_1}{E_1} \qquad (101)$$

$$D = \frac{|\zeta_1|^2}{E_1} - \frac{4|\zeta_2|^2}{E_3} - 3\rho \qquad (102)$$

$$a = \frac{36}{E_1^2 E_2}\left\{ \zeta_2^2 \zeta_1^2 + \rho^2 E_1^2 + 2\zeta_2 \zeta_1 \rho E_1 + \zeta_1^2 \rho E_2 \right\} \qquad (103)$$

It has been demonstrated[23] that second-order spin-orbit coupling between different LS terms provides an additional interaction with the ground state. Vallin and Watkins[23] have deduced the contribution to the D and $\underline{a}$ spin-Hamiltonian parameters due to the spin-orbit coupling of the ground state with the triplet excited states, for a d^4 configuration. Including these second-order spin-orbit coupling to the triplet states, one has[23]

$$D = |\zeta_1|^2 \left[\frac{1}{E_1} - \frac{5}{3E} \right] - 4|\zeta_2|^2 \left[\frac{1}{E_3} - \frac{5}{3E} \right] - 3\rho \qquad (104)$$

$$a = \frac{36}{E_1^2 E_2}\left\{ \zeta_2^2 \zeta_1^2 \left[1 + \frac{5}{3}\frac{(2E_1 + E_2)}{E} + \left(\frac{5E_1}{3E}\right)^2 \right] \right.$$

$$\left. + \rho^2 E_1^2 + 2\zeta_2 \zeta_1 \rho E_1 \left(\frac{1 + 5E_1}{E}\right) + \zeta_1^2 \rho E_2 \right\} \qquad (105)$$

where the energy E is the difference of the average energy of the triplet states and the ground-state energy. The spin-

spin interaction and the spin-orbit coupling to the triplet states make a very small contribution to the spin-Hamiltonian parameters D and $\underline{a}$. The order of magnitude of E_1, E_2, and E_3 is 10^2 to 10^3 cm^{-1}, whereas E is of the order of 10^4 cm^{-1}. The order of magnitude of the spin-spin parameter ρ is 10^{-1} cm^{-1}, and ζ_1 and ζ_2 are of the order of 10^2 cm^{-1}. Although the spin-spin and spin-orbit coupling to the triplet excited states result in a very small contribution to D and $\underline{a}$, we will include them in our calculations, so that more accurate estimates of the spin-Hamiltonian parameters can be made.

To obtain the expressions of $g_{||}$, $g_{\perp}$, D, and $\underline{a}$ for GaAs:Cr^{2+} and InP:Cr^{2+}, we calculate the integrals ζ_1, S_1, ζ_2, and S_2 (see Eq. 99) using the cluster wave functions Ψ_ζ, Ψ_ξ, Ψ_η, Ψ_θ, and Ψ_ε as expressed by Eqs. (10)-(14). For the matrix elements of the $\vec{L}$ operator between ligand wave functions, one has to express this operator in terms of each ligand's own coordinate system $x_i y_i z_i$. The position vector of an electron located at the i^{th} ligand is expressed by

$$\vec{r} = \vec{R}_i + \vec{r}_i$$

where $\vec{R}_i$ is the position vector of the i^{th} ligand and $\vec{r}_i$ is the position vector of the electron relative to the i^{th} nuclear position (see Fig. III.5). The j^{th} component of the angular momentum ($j \equiv x, y, z$) is then expressed in terms of the coordinate system centered at the i^{th} ligand:

$$L_j = [(\vec{R}_i + \vec{r}_i) \times \vec{p}_i]_j = [\vec{L}_i]_j - i(\vec{R}_i \times \vec{\nabla}_i)_j$$

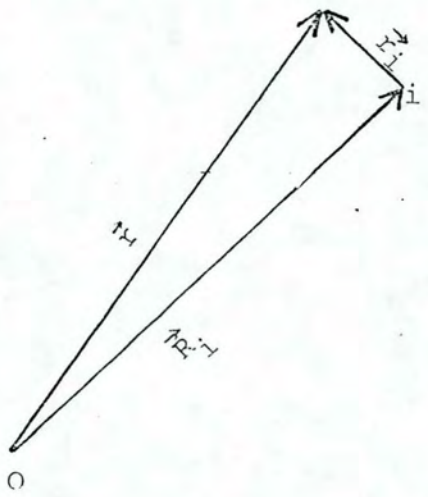

FIG.III.5

Position vector $\vec{r}$ of an electron located at the i^{th} ligand. $\vec{R}_i$ is the position vector of the i^{th} ligand and $\vec{r}_i$ is the position vector of the electron relative to the i^{th} nuclear position.

For tetrahedral symmetry defined by four ligands, and the coordinate systems as shown in Fig. III.3, we obtain the following expressions for the L_z operator, expressed in terms of operators defined relative to each of the ligand coordinate systems:

$$L_z(1) = \frac{L_{z1}}{\sqrt{3}} + \sqrt{\frac{2}{3}}\, L_{x1} - \sqrt{\frac{2}{3}}\, iR \frac{\partial}{\partial y_1}$$

$$L_z(2) = \frac{-L_{z2}}{\sqrt{3}} + \sqrt{\frac{2}{3}}\, L_{x2} - \sqrt{\frac{2}{3}}\, iR \frac{\partial}{\partial y_2}$$

$$L_z(3) = \frac{-L_{z3}}{\sqrt{3}} + \sqrt{\frac{2}{3}}\, L_{x3} - \sqrt{\frac{2}{3}}\, iR \frac{\partial}{\partial y_3}$$

$$L_z(4) = \frac{L_{z4}}{\sqrt{3}} + \sqrt{\frac{2}{3}}\, L_{x4} - \sqrt{\frac{2}{3}}\, iR \frac{\partial}{\partial y_4}$$

Using the cluster wave functions (Eqs. 10-14) and the equations above when the ligand wave functions are involved in the matrix elements (see Eq. 39), we obtain the expressions of ζ_1, S_1, ζ_2, and S_2 for GaAs:Cr^{2+} and InP:Cr^{2+}. Since the cluster wave functions are written in terms of the admixture coefficients $\lambda_{d,s}$, λ_{d,p_σ}, and λ_{d,p_π}, the expressions derived for ζ_1, S_1, ζ_2, and S_2 will also depend on these coefficients, and are given by

$$\zeta_1 = \frac{N_T^2}{4}{}_2 \{\zeta_{d,d} - [2(\lambda_{d,p_\pi}\langle\phi_{d_\xi}|\zeta^{(r)}|\chi_{p_\pi\xi}\rangle + \lambda_{d,p_\sigma}\langle\phi_{d_\xi}|\zeta^{(r)}|\chi_{p_\sigma\xi}\rangle + \lambda_{d,s}\langle\phi_{d_\xi}|\zeta^{(r)}|\chi_{s_\xi}\rangle)] + [(\sqrt{2}\,\lambda_{d,p_\pi}\lambda_{d,p_\sigma} - \lambda^2_{d,p_\pi}/2)\,\zeta_{p,p}]\} \quad (106\text{-a})$$

$$S_1 = N_T^2{}_2 \{1 - [2(\lambda_{d,p_\pi}\langle\phi_{d_\xi}|\chi_{p_\pi\xi}\rangle + \lambda_{d,p_\sigma}\langle\phi_{d_\xi}|\chi_{p_\sigma\xi}\rangle + \lambda_{d,s}\langle\phi_{d_\xi}|\chi_{s_\xi}\rangle)] + \sqrt{2}\,\lambda_{d,p_\pi}\lambda_{d,p_\sigma} - \lambda^2_{d,p_\pi}/2 - 2AR\,\lambda_{d,p_\pi}\lambda_{d,s}]\} \quad (106\text{-b})$$

$$\zeta_2 = \frac{N_E\,N_T}{4}{}_2 \{\zeta_{d,d} - [4\,\lambda_{d,p_\pi}\langle\phi_{d_\zeta}|\zeta^{(r)}|\chi_{p_\pi\zeta}\rangle + \lambda_{d,p_\sigma}\langle\phi_{d_\zeta}|\zeta^{(r)}|\chi_{p_\sigma\zeta}\rangle + \lambda_{d,s}\langle\phi_{d_\zeta}|\zeta^{(r)}|\chi_{s_\zeta}\rangle] + [(\lambda_{d,p_\pi}\lambda_{d,p_\sigma}/\sqrt{2} + \lambda^2_{d,p_\pi}/2)\,\zeta_{p,p}]\} \quad (107\text{-a})$$

$$S_2 = N_E\,N_T{}_2 \{1 - [4\,\lambda_{d,p_\pi}\langle\phi_{d_\zeta}|\chi_{p_\pi\zeta}\rangle + \lambda_{d,p_\sigma}\langle\phi_{d_\zeta}|\chi_{p_\sigma\zeta}\rangle + \lambda_{d,s}\langle\phi_{d_\zeta}|\chi_{s_\zeta}\rangle] + [\lambda_{d,p_\pi}\lambda_{d,p_\sigma}/\sqrt{2} + \lambda^2_{d,p_\pi}/2 - AR\lambda_{d,p_\pi}\lambda_{d,s}]\} \quad (107\text{-b})$$

where . (83) was used in order to express ζ_1 and ζ_2 in terms of the one-electron spin-orbit constant ζ. The symbols $\zeta_{d,d}$ and $\zeta_{p,p}$ are, respectively, the spin-orbit coupling constants associated with the d-electrons of Cr^{2+} and with the p-electrons of the ligands (4p electrons of As, in the case of GaAs:Cr^{2+}, and 3p electrons of P, in the case of InP:Cr^{2+}). The spin-orbit coupling constants $\zeta_{d,d}$ and $\zeta_{p,p}$ can be evaluated by means of the integral

$$\zeta_{\ell,\ell} = \int \mu_{n\ell}(r)\, \varsigma(r)\, \mu_{n\ell}(r)\, dr \tag{108}$$

where $\mu_{n\ell}(r)$ is r times the radial orbital (with quantum numbers n, ℓ) of the atom or ion concerned, and $\rho(r)$ is the r-dependent spin-orbit coupling operator:

$$\varsigma(r) = \frac{\mu_B^2}{a_0^3}\,\frac{1}{r}\,\frac{dV(r)}{dr} \tag{109}$$

In Eq. (109), the potential, V(r), experienced by an electron is given by

$$V(r) = \left[\frac{d^2\mu_{n\ell}(r)}{dr^2} \Big/ \mu_{n\ell}(r)\right] - \frac{\ell(\ell+1)}{r^2} + E_{n\ell} \tag{110}$$

where $E_{n\ell}$ is the orbital energy. Since $\rho(r)$, in Eq. (109), depends on $dV(r)/dr$, $E_{n\ell}$ in Eq. (110) effectively does not contribute to the spin-orbit coupling constant. The matrix elements such as $\langle \phi_{d_\zeta} | \rho(r) | \chi_{p_{\pi\zeta}} \rangle$, in Eqs. (100) and (107), are two-center integrals of the spin-orbit coupling operator (Eq. 109) between the Cr^{2+} wave functions (such as ϕ_{d_ζ}) and

the ligand's wave functions (such as $\chi_{p_{\pi\zeta}}$). In Eqs. (106-b) and (107-b), R is the distance of a ligand from the central ion, and A is the integral

$$A = \frac{1}{\sqrt{2}} \left\langle \chi_s \left| \frac{d}{dy} \right| \chi_{p_y} \right\rangle \tag{111}$$

The integral A originates from the action of the L operator on the ligand wave functions.

In arriving at the expressions (106)-(107) we have retained all the "local", "non-local", and "distant" terms. The local terms are defined as those elements which contain only the wave function of the central ion; the distant terms are the ones which contain only the wave functions of the ligands; and the non-local terms contain not only the wave functions of the central ion, but also those of the ligand ions. For the spin-spin interactions, only the local terms have been retained. Also, the ligand-ligand interaction terms arising from the spin-orbit effect, and the ligand-ligand overlaps, have been neglected.

The numerical values of the various integrals, such as ρ, A, $\zeta_{d,d}$, $\zeta_{p,p}$, and overlaps discussed in this section will be given in Chapter IV. The numerical values for $g_{\parallel}$, $g_{\perp}$, D, a, and the admixture coefficients $\lambda_{d,s}$, λ_{d,p_σ}, and λ_{d,p_π} for GaAs:Cr^{2+} and InP:Cr^{2+} will also be presented (and compared with the available experimental results) in the next chapter.

B.2 Energy splittings in GaAs:Fe^{2+}, GaP:Fe^{2+}, and InP:Fe^{2+}

For GaAs:Fe^{2+}, GaP:Fe^{2+}, and InP:Fe^{2+} semiconductors, the

photoluminescence spectra[28-32,34] were found to exhibit four well-resolved lines. To explain these lines, one has to consider the crystal field, spin-orbit, and spin-spin interactions. The ^5D free-electron level of $Fe^{2+}(3d^6)$ is split by the cubic crystal field into the levels $^5T_2$ and ^5E (see Fig. II.3). The ground state ^5E is not split by first-order of the spin-orbit interaction, as can be seen by direct application of the $\vec{L}$ operator on the angular parts of the Ψ_θ and Ψ_ε wave functions. The degenerate ground state ^5E splits under second-order of the spin-orbit interaction and first-order of the spin-spin interaction.[78] The degenerate states Ψ_ε and Ψ_θ are also mixed under these perturbations. Low and Weger[37,38] have calculated the energy level splittings of the ground state ^5E of the d^6 configuration in a cubic field, on the approximation that the wave functions are of pure d-character. We have modified Low and Weger's[37,38] results, by considering the cluster wave functions. This modification is reflected in the spin-oribt coupling parameter, which in our case is expressed by ζ_2 (see Eq. 99) instead of the pure d-electron spin-orbit coupling parameter. Table III.13 lists the wave functions and the energy splittings due to first-order spin-spin interaction and second-order spin-orbit interaction. The energies in Table III.13 are given in terms of the crystal field splitting parameter Δ, the spin-orbit coupling constant ζ_2, and the spin-spin parameter ρ. The energy values given in Table III.13 properly reduce to the values given by Low and Weger in the limit of pure d-electrons.

To obtain the energy splittings for GaAs:Fe^{2+}, GaP:Fe^{2+},

Table III.13

ENERGY LEVELS AND STATES FOR THE ORBITAL DOUBLET E WITH SPIN S=2. THE NOMENCLATURE $|\Psi_a, b\rangle$ REPRESENTS AN ORBITAL STATE Ψ_a AND A SPIN STATE b, 2^s AND 2^a STANDS FOR SYMMETRIC AND ANTI-SYMMETRIC COMBINATIONS OF THE $m_s=2$ AND $m_s=-2$ QUANTUM NUMBERS ($|2^s\rangle = \frac{1}{\sqrt{2}}\{|+2\rangle + |-2\rangle\}$, $|2^a\rangle = \frac{1}{\sqrt{2}}\{|+2\rangle - |-2\rangle\}$).

Energy Splittings	States
0	$\frac{1}{\sqrt{2}}\{|\Psi_\theta, 2^s\rangle - |\Psi_\epsilon, 0\rangle\}$
$-6(\rho+\frac{3_2^2}{\Delta})$	$\frac{\sqrt{3}}{2}|\Psi_\epsilon,+1\rangle - \frac{1}{2}|\Psi_\theta,-1\rangle$ $|\Psi_\theta, 2^a\rangle$ $-\frac{\sqrt{3}}{2}|\Psi_\epsilon,-1\rangle + \frac{1}{2}|\Psi_\theta,+1\rangle$
$-12(\rho+\frac{3_2^2}{\Delta})$	$\frac{1}{\sqrt{2}}\{|\Psi_\theta, 2^s\rangle + |\Psi_\epsilon, 0\rangle\}$ $\frac{1}{\sqrt{2}}\{|\Psi_\epsilon, 2^s\rangle - |\Psi_\theta, 0\rangle\}$
$-18(\rho+\frac{3_2^2}{\Delta})$	$-\frac{1}{2}|\Psi_\epsilon,-1\rangle - \frac{\sqrt{3}}{2}|\Psi_\theta,+1\rangle$ $|\Psi_\epsilon, 2^a\rangle$ $\frac{1}{2}|\Psi_\epsilon,+1\rangle + \frac{\sqrt{3}}{2}|\Psi_\theta,-1\rangle$
$-24(\rho+\frac{3_2^2}{\Delta})$	$\frac{1}{\sqrt{2}}\{|\Psi_\epsilon, 2^s\rangle + |\Psi_\theta, 0\rangle\}$

and InP:Fe^{2+}, we make use of expression (107-a) for ζ_2, with the atomic wave functions ϕ_d for Fe^{2+}, and χ_s, χ_{p_σ}, and χ_{p_π} for the wave functions of As and P. The spin-orbit interaction taken to first and second order splits the excited triplet state $^5T_2$ into three levels, with eigenvalues J' = 1, 2, 3 of an effective angular momentum operator J.[35-38,78] The energy levels, up to second order in the spin-orbit interaction, and the eigenfunctions of the d^6 configuration (in cubic symmetry) have been given by Low and Weger[37], in the case of pure d-electrons. Making use of the cluster wave functions (Ψ_ξ, Ψ_η, Ψ_ζ), the energy contribution of the $^5T_2$ state of the cluster with J' = 1 (see Fig. II.3), due to first- and second-order effects, the spin-orbit interaction is given by

$$\Delta E = -3\zeta_1 + \frac{18}{5}\,\frac{\zeta_2^2}{\Delta} \qquad (112)$$

where ζ_1 and ζ_2 are our derived expressions given by Eqs. (106-a) and (107-a), and Δ is the crystal field splitting. In the limit of pure d-electrons, Eq. (112) properly reduces to the value given by Low and Weger[37].

There is no allowed electric dipole transition from the excited state $^5T_2$ with J' = 2, 3 to the ground state ^5E. The allowed electric dipole transitions are the ones from the state $^5T_2$ with J' = 1 to the four lowest levels of ^5E, as indicated in Fig. II.3. This selection rule can be obtained from the direct product of the irreducible representations in the T_d group, of the irreducible representations of the involved eigenfunctions (see Fig. II.3) and the electric dipole moment

operator (T_2). The final result of these direct products must contain the totally symmetric representation A_1. For the electric dipole transitions, the energies for the transition between $^5T_2$ [level (6) in Fig. II.3] and the level ^5E [split states (4), (3), (2), and (1) in Fig. II.3] are

$$E(6\text{-}4) = \Delta - 3\zeta_1 + \frac{18}{5}\frac{\zeta_2^2}{\Delta} + K \qquad (113\text{-a})$$

$$E(6\text{-}3) = \Delta - 3\zeta_1 + \frac{18}{5}\frac{\zeta_2^2}{\Delta} + 2K \qquad (113\text{-b})$$

$$E(6\text{-}2) = \Delta - 3\zeta_1 + \frac{18}{5}\frac{\zeta_2^2}{\Delta} + 3K \qquad (113\text{-c})$$

$$E(6\text{-}1) = \Delta - 3\zeta_1 + \frac{18}{5}\frac{\zeta_2^2}{\Delta} + 4K \qquad (113\text{-d})$$

where K is the energy spacing between the ^5E split levels (see Table III.13):

$$K = 6\left(\rho + \frac{\zeta_2^2}{\Delta}\right) \qquad (114)$$

The equal spacing K of the energy levels were obtained because the effects up to second-order of the spin-orbit interaction were considered. If the spin-orbit coupling effects are taken to third-order, one obtains unequal spacings for the split ^5E levels.[32] Here, we will not consider this higher-order effect, which makes a contribution to K of about 1 cm^{-1}, as one can infer from the experimental results[28-32,34] for GaAs:Fe^{2+}, GaP:Fe^{2+}, and InP:Fe^{2+}, as compared to the values of about 15 cm^{-1} given by Eq. (114) for the same systems.

The evaluation of the energy transitions for GaAs:Fe^{2+}, GaP:Fe^{2+}, and InP:Fe^{2+}, using expressions (113) and (114), together with Eqs. (106-a) and (107-a) for ζ_1 and ζ_2, will be presented in Chapter IV.

C. Electronic transition moment

In the study of optical transitions, intensity is one of the physical quantities which is commonly measured. The intensity irradiated by an electric dipole moment can be expressed in terms of the probability per unit time, C_{mn}, for a transition to occur, from the state m to the state n[81]:

$$I = N_m h\nu_{mn} C_{mn} \quad . \tag{115}$$

N_m is the number of particles in the m state, and $h\nu_{mn}$ is the energy difference between states m and n. For emission, the transition probability C_{mn} is given by

$$C_{mn} = A_{mn} + \rho(\nu_{mn}) B_{mn} \quad , \tag{116}$$

where A_{mn} is the coefficient of spontaneous emission, $\rho(\nu_{mn})$ is the density of radiation[81,82], and B_{mn} is the coefficient of stimulated emission. The transition probability is proportional to the square of the dipole matrix element[82]:

$$A_{mn} = \frac{64\pi^4}{3c^3h} \nu_{mn}^3 |P_{mn}|^2 \tag{117-a}$$

$$B_{mn} = \frac{8\pi^3}{3h^2} |P_{mn}|^2$$

The dipole matrix elements, P_{mn}, are commonly referred to as

"electronic dipole transition moments", or simply as"transition moments". As one can see from Eqs. (115) to (117), the quantity to be calculated is the transition moment, as far as intensities are concerned.

The dipole moment operator is $e\vec{r}$, where $\vec{r}$ is the position vector of an electron, relative to the central coordinate system of the complex. The components of the transition moment, with $e \equiv 1$, are given by

$$P_x^{m,n} = \langle \Psi_n | x | \Psi_m \rangle \tag{118-a}$$

$$P_y^{m,n} = \langle \Psi_n | y | \Psi_m \rangle \tag{118-b}$$

$$P_z^{m,n} = \langle \Psi_n | z | \Psi_m \rangle \tag{118-c}$$

where the superscripts m,n correspond to the subscripts in Eq. (117). The x, y, and z coordinates can be expressed as r times a linear combination of spherical harmonics[64], Y_ℓ^m of order $\ell = 1$. The cluster wave functions, Ψ_m and Ψ_n, to be used in Eqs. (118-a) to (118-c), can be written as products of the radial wave functions and spherical harmonics. To evaluate the matrix elements $P_x^{m,n}$, $P_y^{m,n}$, and $P_z^{m,n}$, we make use of the addition of angular momenta, to express the product of two spherical harmonics in terms of Clebsh-Gordon coefficients and single spherical harmonics:

$$Y_{\ell_i}^{m_1}(\theta,\phi)\, Y_{\ell_2}^{m_2}(\theta,\phi) = \sum_{\ell} \sqrt{\frac{(2\ell_1+1)(2\ell_2+1)}{4\pi(2\ell+1)}} \langle \ell_1 \ell_2 00 | \ell_1 \ell_2 \ell 0 \rangle \cdot$$

$$\langle \ell_1 \ell_2 m_1 m_2 | \ell_1 \ell_2 \ell, m_1+m_2 \rangle\, Y_\ell^{m_1+m_2}(\theta,\phi) \tag{119}$$

The index ℓ, under the summation sign, spans the values $\ell = (\ell_1 + \ell_2), (\ell_1 + \ell_2 - 1), \ldots, (\ell_1 - \ell_2)$. Table III.14 lists the product of the spherical harmonics needed for the calculations of $P_x^{m,n}$, $P_y^{m,n}$, and $P_z^{m,n}$, when the orbitals Ψ_m and Ψ_n are substituted for by the cluster wave functions Ψ_ε, Ψ_θ, Ψ_ξ, Ψ_η, and Ψ_ζ (Eqs. 10-14 or 52-56). Table III.14 was obtained using Eq. (119) and the Clebsh-Gordon coefficients given by Rotenberg et al.[83].

When we substitute Ψ_m and Ψ_n in Eqs. (118-a)-(118-c), the transition moment matrix elements contain one-center, two-center, and three-center integrals. The one-center integrals are the ones in which the central ion atomic orbitals are taken (ϕ_m and ϕ_n). The two-center integrals are the ones in which the central ion atomic orbital is taken for one state, and the ligand atomic orbitals (χ_n) are taken for the other state, so that the matrix element is of the type $\langle \chi_n | x | \phi_m \rangle$. Also, two-center integrals arise when the ligand atomic orbitals are taken for both states, excluding the matrix elements of different ligands. Three-center integrals arise when the ligand atomic orbitals are taken for both states m and n, and different ligands are considered. We will neglect the three-center integrals, under the assumption that they are small compared to the two-center integrals.

In order to solve two-center integrals, we perform rotations on the central-coordinate system, transforming it into a system of coordinates which is

Table III.14

PRODUCT OF TWO SPHERICAL HARMONICS $Y_{\ell_1}^{m_1} Y_{\ell_2}^{m_2} = \sum_{\ell} C_{\ell}^{m_1+m_2} \cdot \mathcal{Y}_{\ell}^{m_1+m_2}$, WHERE $\mathcal{Y}_{\ell}^{m_1+m_2} = \frac{1}{\sqrt{4\pi}} Y_{\ell}^{m_1+m_2}$, AND THE ANGULAR DEPENDENCE (θ,ϕ) IS IMPLIED FOR THE SPHERICAL HARMONICS.

$Y_{\ell_1}^{m_1}$ \ $Y_{\ell_2}^{m_2}$	Y_1^1	Y_1^0	Y_1^1
Y_2^2	$\frac{3}{\sqrt{7}}\mathcal{Y}_3^3$	$\sqrt{\frac{3}{7}}\mathcal{Y}_3^2$	$\sqrt{\frac{3}{35}}\mathcal{Y}_3^1 - \sqrt{\frac{6}{5}}\mathcal{Y}_1^1$
Y_2^1	$\sqrt{\frac{6}{7}}\mathcal{Y}_3^2$	$\sqrt{\frac{3}{5}}\mathcal{Y}_1^1 + 2\sqrt{\frac{6}{35}}\mathcal{Y}_3^1$	$-\left\{\sqrt{\frac{3}{5}}\mathcal{Y}_1^0 \frac{-3}{\sqrt{35}}\mathcal{Y}_3^0\right\}$
Y_2^0	$-\frac{1}{5}\mathcal{Y}_1^1 + 3\sqrt{\frac{2}{35}}\mathcal{Y}_3^1$	$\frac{2}{\sqrt{5}}\mathcal{Y}_1^0 + 3\sqrt{\frac{3}{35}}\mathcal{Y}_3^0$	$\frac{-1}{\sqrt{5}}\mathcal{Y}_1^{-1} + 3\sqrt{\frac{2}{35}}\mathcal{Y}_3^{-1}$
Y_2^{-1}	$-\left\{\sqrt{\frac{3}{5}}\mathcal{Y}_1^0 - \frac{3}{35}\mathcal{Y}_3^0\right\}$	$\sqrt{\frac{3}{5}}\mathcal{Y}_1^{-1} + 2\sqrt{\frac{6}{35}}\mathcal{Y}_3^{-1}$	$\sqrt{\frac{6}{7}}\mathcal{Y}_3^{-2}$
Y_2^{-2}	$\sqrt{\frac{3}{35}}\mathcal{Y}_3^{-1} - \sqrt{\frac{6}{5}}\mathcal{Y}_1^{-1}$	$\sqrt{\frac{3}{7}}\mathcal{Y}_3^{-2}$	$\frac{3}{\sqrt{7}}\mathcal{Y}_3^{-3}$
Y_1^1	$\sqrt{\frac{6}{5}}\mathcal{Y}_2^2$	$\sqrt{\frac{3}{5}}\mathcal{Y}_2^1$	$-\mathcal{Y}_0^0 + \frac{1}{\sqrt{5}}\mathcal{Y}_2^0$
Y_1^0	$\sqrt{\frac{3}{5}}\mathcal{Y}_2^1$	$\mathcal{Y}_0^0 + \frac{2}{\sqrt{5}}\mathcal{Y}_2^0$	$\sqrt{\frac{3}{5}}\mathcal{Y}_2^{-1}$
Y_1^{-1}	$-\mathcal{Y}_0^0 + \frac{1}{\sqrt{5}}\mathcal{Y}_2^0$	$\sqrt{\frac{3}{5}}\mathcal{Y}_2^{-1}$	$\sqrt{\frac{6}{5}}\mathcal{Y}_2^{-2}$

z-colinear with and parallel to the ligand's system of reference. The spherical harmonics (in the x y z system) is then expressed in terms of rotation matrix elements and spherical harmonics which are functions of the rotated coordinates (x'y'z'), as explained earlier in this chapter. Equation (22) expresses the transformation of a spherical harmonic $Y_\ell^m(\theta,\phi)$ into functions of the rotated frame of angular coordinates θ' and ϕ'. The calculation of $P_x^{m,n}$, $P_y^{m,n}$, and $P_z^{m,n}$, using cluster wave functions, involves spherical harmonics with ℓ = 1, 2, 3 (see Table III.14). To rotate these spherical harmonics, we use the rotation matrices for ℓ = 1, 2, 3 (see Tables III.4 to III.6).

To calculate the transition moments, one has to use the wave functions Ψ_m and Ψ_n for the states m and n respectively. We will consider transitions from the ground state m to the excited states n of GaAs:Cr^{2+}. Fig. II.1 shows the energy diagram for these systems, with the ground state described by the cluster wave function Ψ_ζ and the excited states by Ψ_ξ, Ψ_η, Ψ_θ, and Ψ_ε. When we calculate $P_x^{m,n}$, $P_y^{m,n}$, and $P_z^{m,n}$ using the cluster wave functions (Eqs. 52-56), we observe that the one-center integrals, coming from the d-wave functions of Cr^{2+}, are vanishing. More specifically, these matrix elements are

$$\left\langle \phi_{d_\xi} | \vec{r} | \phi_{d_\zeta} \right\rangle = 0$$

$$\left\langle \phi_{d_\eta} | \vec{r} | \phi_{d_\zeta} \right\rangle = 0$$

$$\left\langle \phi_{d_\theta} | \vec{r} | \phi_{d_\zeta} \right\rangle = 0$$

Table III.15

DIPOLE TRANSITION MOMENTS BETWEEN THE GROUND STATE m= ζ AND THE EXCITED STATES n= ξ, η, θ and ϵ, FOR SYSTEMS WITH LOCAL TETRAGONAL SYMMETRY (SEE FIG.II.1).

n \ m=ζ	$P_x^{m,n}$	$P_y^{m,n}$	$P_z^{m,n}$
ξ	0	$P_y^{\zeta,\xi}$	0
η	$P_x^{\zeta,\eta}$	0	0
θ	0	0	$P_z^{\zeta,\theta}$
ϵ	0	0	0

$$\left\langle \phi_{d_\varepsilon} | \vec{r} | \phi_{d_\zeta} \right\rangle = 0$$

In other words, dipole transitions in these systems would not be observed if only pure d-electrons were involved in such transitions. The contribution to the dipole transition moments comes from the two-center integrals of the type

$$\left\langle \mathcal{F}(r,\theta',\phi') | \chi(R, \textcircled{H}, \Phi) \right\rangle \quad ,$$

where $\mathcal{F}$ is a function of the central ion's coordinates (r,θ',ϕ'), which are parallel to the ligand's coordinate system $(R, \textcircled{H}, \Phi)$. Table III.15 lists the dipole transition moments between the states $m = \zeta$ and $n = \xi$, η, θ, and ε. The x, y, and z components of $P^{m,n}$, listed in Table III.15, with the notation $s = \sin\beta'$ and $t = \cos\beta'$ (where β' is as shown in Fig. III.4), are given by

$$P_x^{\xi,\eta} = P_y^{\eta,\xi} = N_\eta N_\xi t \{ \Lambda_{d,s} [-4 \sqrt{\tfrac{3}{5}} s^2 I_{10} + \sqrt{\tfrac{36}{35}} s^2 I_{30}]$$

$$+ \Lambda_{d,p_\sigma} [-4 \sqrt{\tfrac{3}{5}} s^2 I_{11} + \sqrt{\tfrac{36}{35}} s^2 I_{31}]$$

$$+ \Lambda_{d,p_\pi} [\tfrac{4}{\sqrt{5}} (s^2 - t^2) I'_{11} + \sqrt{\tfrac{2}{35}} (2 + s^2(-19+30s^2)) I'_{31}]$$

$$+ \Lambda^2_{d,s} \sqrt{3}\, s^4 R_{10} + \Lambda^2_{d,p_\sigma} \sqrt{3}\, s^4 (R'_{10} + \tfrac{2}{\sqrt{5}} R_{12})$$

$$+ \Lambda^2_{d,p_\pi} \frac{2}{\sqrt{3}} s^2(1-2s^2)\left[R'_{10} - \frac{1}{\sqrt{5}} R_{12}\right]$$

$$+ \Lambda_{d,s}\, \Lambda_{d,p_\sigma} 2\sqrt{3}\, s^4\, R_{11} + \Lambda_{d,s}\, \Lambda_{d,p_\pi} 4s^2t^2 R'_{11}$$

$$+ \Lambda_{d,p_\sigma}\, \Lambda_{d,p_\pi} 4\cdot\sqrt{\frac{3}{5}}\, s^2t^2 R'_{12}\ \Big\} \qquad (120)$$

$$P_z^{\zeta,\theta} = N_\theta N_\zeta ts^2\Big\{\Lambda_{d,s}\left[\frac{-4}{\sqrt{5}} I_{10} - 2\sqrt{\frac{3}{35}}\,(8-15s^2) I_{30}\right]$$

$$+ \Lambda_{d,p_\sigma}\left[\frac{-4}{\sqrt{5}} I_{11} - 2\sqrt{\frac{3}{35}}\,(8-15s^2)\, I_{31}\right]$$

$$+ \Lambda_{d,p_\pi}\left[\frac{8}{\sqrt{15}} I'_{11} - \sqrt{\frac{3}{70}}\,(-32+45s^2)\, I'_{31}\right]$$

$$+ \Lambda^2_{d,s}(3t^2-1) R_{10} + \Lambda^2_{d,p_\sigma}(3t^2-1)\left[R'_{10} + \frac{2}{\sqrt{5}} R_{12}\right]$$

$$+ \Lambda^2_{d,p_\pi}(-4t^2)\left[R'_{10} - \frac{1}{\sqrt{5}} R_{12}\right] + \Lambda_{d,s}\, \Lambda_{d,p_\sigma} 2(3t^2-1) R_{11}$$

$$+ \Lambda_{d,s}\, \Lambda_{d,p_\pi} \frac{4}{\sqrt{3}}(3s^2-1) R'_{11} + \Lambda_{d,p_\sigma}\, \Lambda_{d,p_\pi} \frac{4}{\sqrt{5}}(3s^2-1) R'_{12} \qquad (121)$$

where the various integrals $I_{\ell\ell'}$, $I'_{\ell\ell'}$, $R_{\ell\ell'}$, and $R'_{\ell\ell'}$ are

$$I_{10} = \left\langle r R_d(r)\, Y_1^0(\theta',\phi') \;\; R_s(R)\, Y_0^0(\Theta,\Phi) \right\rangle \tag{122-a}$$

$$I_{11} = \left\langle r R_d(r)\, Y_1^1(\theta',\phi') \;\; R_p(R)\, Y_1^0(\Theta,\Phi) \right\rangle \tag{122-b}$$

$$I_{30} = \left\langle r R_d(r)\, Y_3^0(\theta',\phi') \;\; R_s(R)\, Y_0^0(\Theta,\Phi) \right\rangle \tag{122-c}$$

$$I_{31} = \left\langle r R_d(r)\, Y_3^0(\theta',\phi') \;\; R_p(R)\, Y_1^0(\Theta,\Phi) \right\rangle \tag{122-d}$$

$$I'_{11} = \left\langle r R_d(r)\, Y_1^1(\theta',\phi') \;\; R_p(R)\, Y_1^1(\Theta,\Phi) \right\rangle \tag{122-e}$$

$$I'_{31} = \left\langle r R_d(r)\, Y_3^1(\theta',\phi') \;\; R_p(R)\, Y_1^1(\Theta,\Phi) \right\rangle \tag{122-f}$$

$$R_{10} = \left\langle r Y_1^0(\theta',\phi') \;\; R_s^2(R)\, Y_0^0(\Theta,\Phi) \right\rangle \tag{122-g}$$

$$R'_{10} = \left\langle r Y_1^1(\theta',\phi') \;\; R_p^2(R)\, Y_0^0(\Theta,\Phi) \right\rangle \tag{122-h}$$

$$R_{12} = \left\langle r Y_1^0(\theta',\phi') \;\; R_p^2(R)\, Y_2^0(\Theta,\Phi) \right\rangle \tag{122-i}$$

$$R_{11} = \left\langle r Y_1^0(\theta',\phi') \;\; R_s(R)\, R_p(R)\, Y_1^0(\Theta,\Phi) \right\rangle \tag{122-j}$$

$$R'_{11} = \left\langle r Y_1^1(\theta',\phi') \;\; R_s(R)\, R_p(R)\, Y_1^1(\Theta,\Phi) \right\rangle \tag{122-k}$$

$$R'_{12} = \left\langle r Y_1^1(\theta',\phi') \;\; R_p^2(R)\, Y_2^1(\Theta,\Phi) \right\rangle \tag{122-l}$$

Expressions (120) and (121) were deduced using the cluster wave functions (52)-(56) which are appropriate for a tetragonal local symmetry (or a tetrahedral symmetry, for which $\cos\beta' = 1/\sqrt{3}$ and $\sin\beta' = \sqrt{2}/\sqrt{3}$). The numerical values appearing in Eqs. (120) and (121) originated from the rotation of the central ion wave functions and from the Clebtsh-Gordon coefficients in the process of combining two spherical harmonics. The matrix elements defined in Eqs. (122-a) to (122-l) are written in terms of integrals involving radial atomic functions and spherical harmonics. $R_d(r)$ is the radial wave function of the central ion [in particular, we will be concerned with the $Cr^{2+}(3d^4)$ wave function]. As was mentioned early in this chapter, the radial atomic wave functions can be expressed in terms of Slater-type orbitals (see Eq. 8), obtained by self-consistent calculations[66,67]. One notices that the matrix elements, Eqs. (122-a) to (122-l), are of the form of overlap integrals, which one can evaluate using the α-function technique[60] and appropriate wave functions. The results for dipole transitions for $GaAs:Cr^{2+}$ will be presented in the following chapter, along with calculations of pertinent physical parameters using the theory outlined in this chapter.

IV. CALCULATION AND COMPARISON WITH EXPERIMENTS

This chapter presents the results of calculations based on the theory previously described for GaAs:Cr^{2+}, GaAs:Cr^{3+}, GaAs:Fe^{2+}, InP:Cr^{2+}, InP:Fe^{2+}, and GaP:Fe^{2+}. The values of overlap integrals, as well as spin-spin and spin-orbit coupling constants for the materials mentioned above, are also presented. An estimate for Jahn-Teller distortion is given for GaAs:Cr^{2+}, and the values of the spin-Hamiltonian parameters $g_{\parallel}$, $g_{\perp}$, D, and $\underline{a}$ for GaAs:Cr^{2+} and InP:Cr^{2+} are obtained and compared with experimental results. Estimates of intensity ratios for GaAs:Cr^{2+} are discussed in conjunction with experimentally determined values of the Jahn-Teller energy. The best values obtained for the admixture coefficients ($\lambda_{d,s}$, λ_{d,p_σ}, and λ_{d,p_π}), and consequently the charge transfers, of the cluster wave functions of the GaAs:Cr^{2+}, GaAs:Fe^{2+}, InP:Cr^{2+}, InP:Fe^{2+}, and GaP:Fe^{2+} semiconductors are also presented.

A. GaAs:Cr^{2+} and GaAs:Cr^{3+} energies

As mentioned in Chapter II, Hemstreet and Dimmock[39,40] have recently calculated electronic energy levels for GaAs doped with Cr^{3+} and Cr^{2+}, using a modification of the free-ion one-electron orbitals of t_2 and e symmetry. The resultant wave function normalization constants obtained in this way were described in terms of the parameters R_{ee}, R_{tt}, and R_{et} ($= \sqrt{R_{ee}R_{tt}}$), deduced from X_α calculations[40,42]. We have obtained the electronic energy levels for these two systems using the matrix elements listed in Tables III.10 and III.11 for d^3(GaAs:Cr^{2+}) and d^4(GaAs:Cr^{2+}) electrons in order to compare the results from

their calculations and the extended theory presented here.

To repeat the calculations done by Hemstreet and Dimmock[39,40], we have used the same parameters R_{ee}, R_{tt}, and R_{et}, to relate the ten independent integrals (a, b, . . ., j) [refer to Chapter III, Section A] to the free-ion Racah parameters A, B, and C, as follows:

$$a = R_{tt}^2 \ (A + 4B + 3C) \tag{123-a}$$

$$b = R_{tt}^2 \ (A - 2B + C) \tag{123-b}$$

$$c = R_{et}^2 \ (2\sqrt{3}\ B) \tag{123-c}$$

$$d = R_{et}^2 \ (A - 2B + C) \tag{123-d}$$

$$e = R_{ee}^2 \ (A + 4B + 3C) \tag{123-e}$$

$$f = R_{ee}^2 \ (4B + C) \tag{123-f}$$

$$g = R_{et}^2 \ (B + C) \tag{123-g}$$

$$h = R_{et}^2 \ (\sqrt{3}\ B) \tag{123-h}$$

$$i = R_{et}R_{tt} \ (\sqrt{3}\ B) \tag{123-i}$$

$$j = R_{tt}^2 \ (3B + C) \tag{123-j}$$

The values we have used for R_{ee}, R_{tt}, R_{et}, A, B, C, and the crystal field parameter Δ are the same as the ones used by Hemstreet and Dimmock, for GaAs:Cr^{2+} and GaAs:Cr^{3+}, and are listed in Table IV.1. To solve for the eigenvalues in both cases, we diagonalize a 20 x 20 and a 43 x 43 matrix (see Tables III.10 and III.11).

TABLE IV.1

$R_{ee}, R_{tt}, R_{et}, A, B, C, \Delta$ PARAMETERS USED IN ENERGY CALCULATIONS FOR $GaAs:Cr^{2+}$ and $GaAs:Cr^{3+}$

Parameter	$GaAs:Cr^{3+}$	$GaAs:Cr^{2+}$
R_{ee}	0.63	0.63
R_{tt}	0.21	0.21
R_{et}	0.36	0.36
A	-0.09 eV	-0.09 eV
B	0.098 eV	0.098 eV
C	0.312 eV	0.312 eV
Δ	0.5 eV	0.27 eV

The energy levels obtained for GaAs:Cr^{2+} are shown in Fig. IV.1, and for GaAs:Cr^{3+}, in Fig. IV.2. The results of our calculations are compared, side by side, with those of Hemstreet and Dimmock in Figs. IV.1 and IV.2. Although there is general agreement between the two, as can be observed, there are some minor differences for GaAs:Cr^{2+}, which are these:

(i) their two $^1T_1$ levels of energies 0.74 and 0.84 eV have energies 0.80 and 1.02 eV by our calculations;

(ii) the level designated $^5T_1$ by Hemstreet and Dimmock should have been $^3T_1$;

(iii) our calculations show that the ^1E level, with energy 1.45 eV, and $^3T_1$, with energy 1.33 eV, originate from the configuration e^2t^2 instead of the configuration t^4 assigned by them. Our results for GaAs:Cr^{3+} (see Fig. IV.2) are in good agreement with those of Hemstreet and Dimmock, except that their $^4T_1$ level at 0.7 eV and $^2T_2$, at 0.95 eV, should both be $^2T_1$.

The value obtained for the energy difference between states ^5E and $^5T_2$ of GaAs:Cr^{2+} (see Fig. IV.1) is 0.65 eV. The present calculations do not include the Jahn-Teller and spin-orbit interactions, which are expected to increase the energy difference between the ^5E and $^5T_2$ states. This value of the $^5T_2$-^5E transition energy, when coupled with the Jahn-Teller energy splittings determined by Krebs and Stauss[18] (E_{JT} = 0.188 eV), is in good agreement with the 0.84 eV photoluminescence peak[2,4] observed for Cr-doped GaAs.

B. Estimate of the Jahn-Teller distortion for GaAs:Cr^{2+}

Krebs and Stauss[18] have determined the value of the Jahn-

FIG.IV.1 Shows the energy levels of GaAs:Cr^{2+} ; (a) calculations by Hemstreet and Dimmock (ref.40) and (b) present calculations employing d^4 matrices from Table III.11. The values of the parameters A, B, C, Δ, R_{ee}, R_{tt} and R_{et} in both cases are kept the same as in Ref. 40.

FIG.IV.1

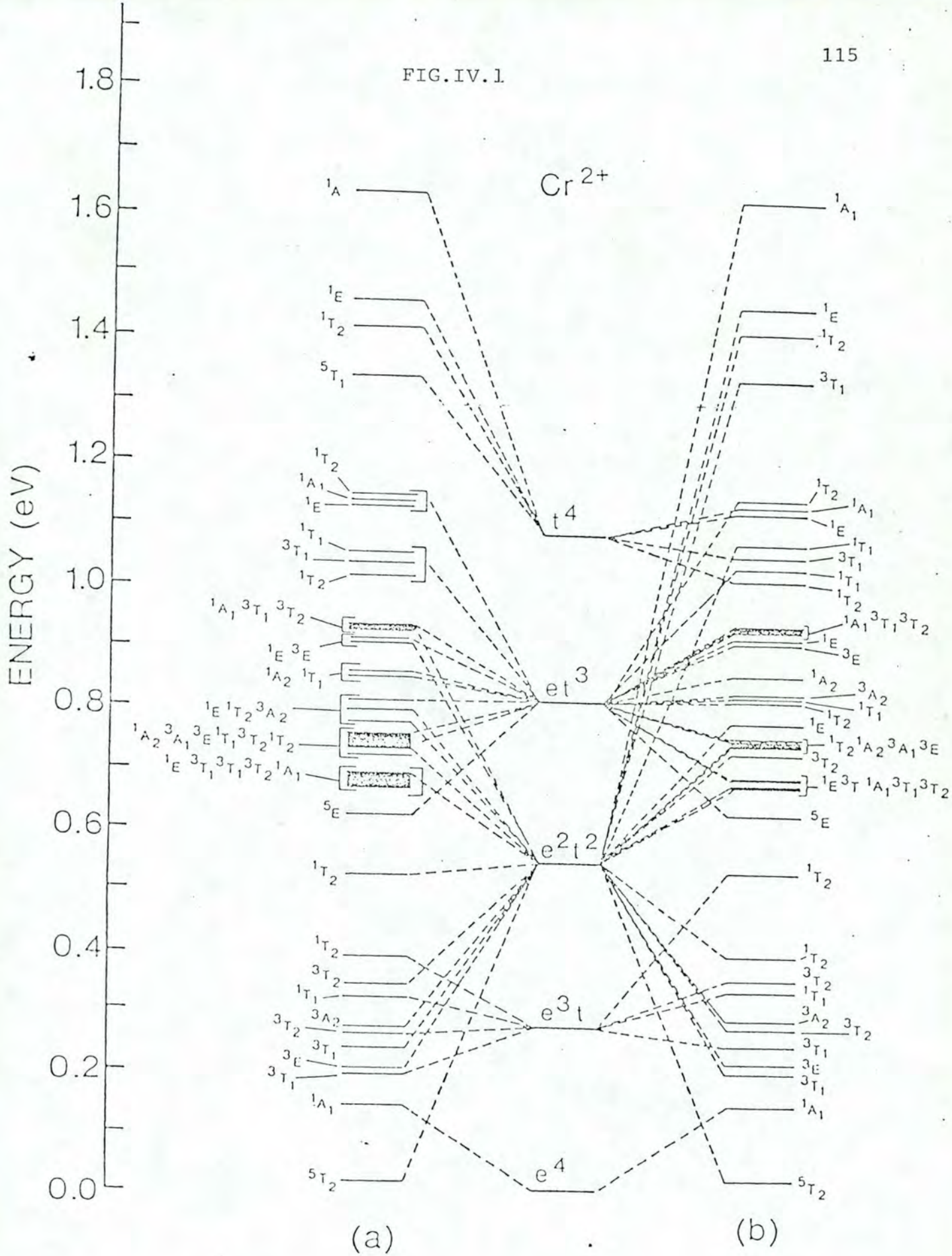

FIG.IV.2 Energy levels of GaAs:Cr^{3+} ;
(a) Hemstreet and Dimmock's calculations (Ref.40) and
(b) present calculations using d^3 matrices from Table III.10. The values of the parameters A, B, C, Δ, R_{ee}, R_{tt} and R_{et} are those of Ref.40.

FIG.IV.2

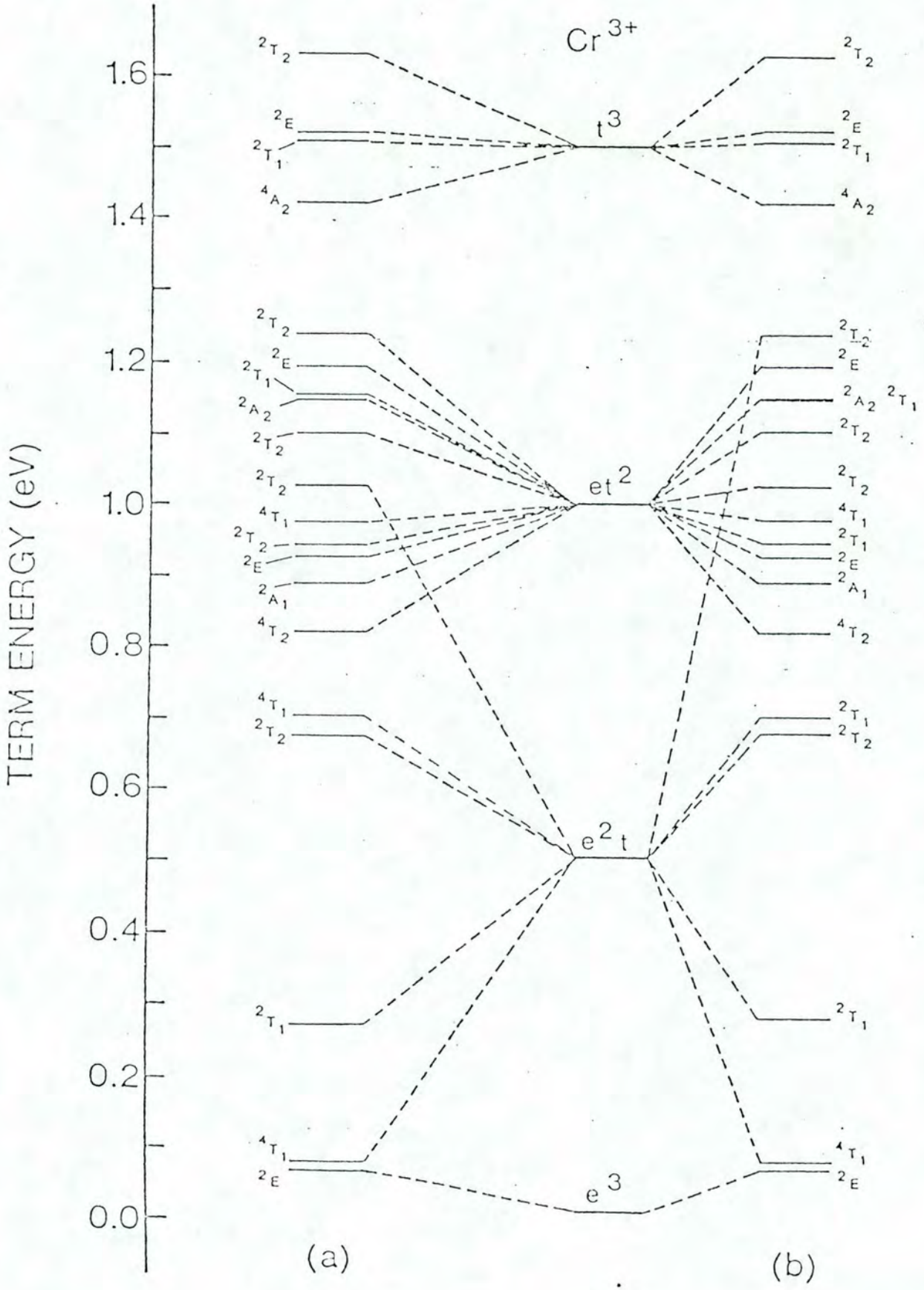
Cr 3+
t 3
et 2
e 2 t
e 3
(a)
(b)
TERM ENERGY (eV)
1.6
1.4
1.2
1.0
0.8
0.6
0.4
0.2
0.0
2T2
2E
2T1
4A2
2A2
4T1
2A1
4T2

Teller distortion for GaAs:Cr^{2+} to be E_{JT} = 0.188 eV, and the value of the coupling coefficient V_1 to be -0.85 eV. These values give a value of $\mathcal{Q}_\theta$ = -0.44 Å for the nuclear displacement (see Appendix I). For a fourfold tetrahedral coordination, the vibrational mode $\mathcal{Q}_\theta$ is related to the tetragonal strain e_θ as derived by Ham[84]:

$$\mathcal{Q}_\theta = \left(\frac{2\sqrt{2}}{3}\right) R\, e_\theta \tag{124}$$

where R is the nearest-neighbor distance, and the tetragonal strain e_θ is related to the strains in the x, y, and z directions as[84]

$$e_{xx} = e_{yy} = -\frac{1}{3} e_\theta \tag{125-a}$$

$$e_{zz} = \frac{2}{3} e_\theta \tag{125-b}$$

With the value of $\mathcal{Q}_\theta$ = -0.44 Å and the nearest-neighbor distance R = 2.43 Å for GaAs, Eqs. (125) and (125) give us the values of $e_{xx} = e_{yy}$ = 0.064 and e_{zz} = -0.128. As one can see from the sign of e_{zz}, this tetragonal distortion corresponds to a compression along the z-axis. The angle β' (see Fig. III.4) for the distorted tetrahedron is given by

$$\cos\beta' = \frac{1}{2} \frac{a(1+ e_{zz})}{R} \tag{126}$$

where a is the length of the sides of the undistorted cube [$a = (2/\sqrt{3})R$]. The value of e_{zz} = -0.128 and Eq. (126) give us an estimate of the angle β':

$$\cos\beta' = 0.872/\sqrt{3} \qquad (127\text{-a})$$

$$\sin\beta' = 0.864 \qquad (127\text{-b})$$

From the estimate of the angle β' given by (127-a) and (127-b) for GaAs:Cr^{2+}, we can see that this distortion does not significantly affect the wave functions (see Eqs. 10-14 and 52-56), and the main effect of the Jahn-Teller distortion is the splitting of the energy levels.

C. Overlap integrals

Using the α-function technique[60,72-75], a Slater-type orbital (STO) centered at a ligand site, with coordinates R, (H), Φ, displaced by a distance a from the origin of the central ion's coordinate system, with coordinates r, θ, ϕ (see Fig. IV.3), may be expanded as

$$R^{N-1}e^{-\eta R}Y_L^M(\text{(H)},\Phi) = \sum_{\ell} \frac{1}{r}\,\alpha_{\ell}(N\eta LM/ar)\,Y_{\ell}^{M}(\theta,\phi)$$

Sharma[60] derived a closed form for $\alpha_l(N\ LM/ar)$ and obtained the following expression for a two-center overlap integral between (unnormalized) STOs:

$$\langle r^{N'-1}e^{-\eta' r}Y_{L'}^{M'}(\theta,\phi) \mid R^{N-1}e^{-\eta R}Y_L^M(\Theta,\Phi)\rangle = \delta_{M',M}\,a^{N+N'+1}\cdot$$

$$\sum_{k'=0}^{N+L'}\Big[\, e^{-\eta a}\Big(-\frac{n!}{[a(\eta'+\eta)]^{n+1}} + (-1)^{k'}g_n[a(\eta'-\eta)]\sum_{k=0}^{k_{max}}\Big(\frac{1}{\eta a}\Big)^{k+1}F_k(NL'LM)$$

$$-e^{-\eta' a}(-1)^{L+N-k'}h_n[a(\eta'+\eta)]\sum_{k=0}^{k_{max}}\Big(\frac{-1}{\eta a}\Big)^{k+1}F_{k'k}(NL'LM)\Big] \qquad (128)$$

where

$$n=N'-L'+k'$$

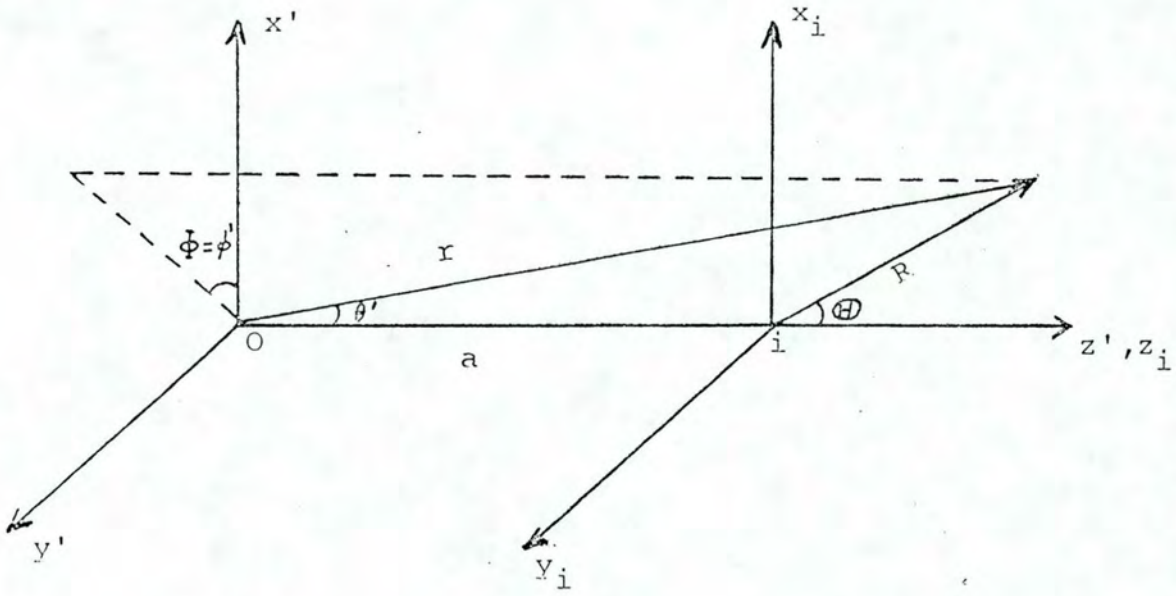

FIG. IV.3

Coordinate systems used for expansion of a wave function centered at i , in terms of a set of radial functions α(NLM/a,r) and spherical harmonics centered at O , which is at a distance a along the common z-axis.

where g_n, h_n, and $F_{k'k}$ are listed in Appendix II.

With Sharma's[60] expression for overlap between STO (Eq. 128) and Clementi's[66] wave functions (which are given in terms of expansion of STO) for Cr^{2+}, Fe^{2+}, As, and P, we obtained the overlap integrals $S_{d,s}$, S_{d,p_σ}, and S_{d,p_π} (see Eqs. 8 and 38) for GaAs:Cr^{2+}, GaAs:Fe^{2+}, InP:Cr^{2+}, InP:Fe^{2+}, and GaP:Fe^{2+}. The overlap integrals which are listed in Table IV.2 will be used in the following sections in the calculations of several physical parameters, such as $g_{\parallel}$, $g_{\perp}$, D, $\underline{a}$, and spin-orbit splitting energies.

The integrals $I_{\ell\ell'}$, $I'_{\ell\ell'}$, $R_{\ell\ell'}$, and $R'_{\ell\ell'}$, used in the calculations of dipole transition moments, as defined in Eqs. (122-a) to (122-l), are also of the form of two-center overlap integrals. We have evaluated these integrals for GaAs:Cr^{2+}, using Eq. (128) and Clementi's[60] wave functions for Cr^{2+} and As, and the values obtained are listed in Table IV.3.

D. Calculation of spin-spin and spin-orbit constants

In order to evaluate the spin-Hamiltonian parameters $g_{\parallel}$, $g_{\perp}$, D, and $\underline{a}$ (Eqs. 100-105), and the spin-orbit and spin-spin energy splittings (Eq. 113), we must first evaluate the various integrals involved in the expressions of the physical parameters mentioned above. To calculate the spin-orbit coupling constants for GaAs:Cr^{2+}, GaAs:Fe^{2+}, InP:Cr^{2+}, InP:Fe^{2+}, and GaP:Fe^{2+}, we have used Eq. (108) and Clementi's[66] wave functions for Cr^{2+}, As, and P. Also, the integral A (Eq. 111) was calculated using Clement's wave functions for As and P. The spin-spin parameter

Table IV.2

OVERLAP INTEGRALS (S_{d,p_π}, $S_{d,s}$, S_{d,p_σ}) for GaAs:Cr^{2+}, GaAs:Fe^{2+}, InP:Cr^{2+}, InP:Fe^{2+} and GaP:Fe^{2+}.

Material	S_{d,p_π}	$S_{d,s}$	S_{d,p_σ}
GaAs:Cr^{2+}	0.06181	0.06857	-0.08488
GaAs:Fe^{2+}	0.04802	0.05358	-0.06899
InP:Cr^{2+}	0.05000	0.06021	-0.07976
InP:Fe^{2+}	0.03756	0.04522	-0.06342
GaP:Fe^{2+}	0.04944	0.05711	-0.07288

Table IV.3

$I_{\ell\ell'}$, $I'_{\ell\ell'}$, $R_{\ell\ell'}$, $R'_{\ell\ell'}$ (see Eqs.122) for GaAs:Cr^{2+}

Type of Integral	ℓ \ ℓ'	0	1	2
$I_{\ell\ell'}$	1	0.1518	-0.2249	—
	3	0.06852	-0.05622	—
$I'_{\ell\ell'}$	1	—	0.08842	—
	3	—	0.08346	—
$R_{\ell\ell'}$	1	8.0076	2.1573	0
$R'_{\ell\ell'}$	1	8.0076	2.1573	0

ρ was calculated for Cr^{2+} and Fe^{2+} using expression (98) and Clementi's wave functions. The results of these integrals are listed in Table IV.4, where our results are compared with values from other sources whenever they were available. The two-center spin-orbit matrix elements, of the type $\langle \Phi_d | \zeta(r) | \chi \rangle$, (see Eqs. 106 and 107), are about two orders of magnitude lower than the relevant one-center spin-orbit matrix elements and therefore have not been listed. Our calculated values of $\zeta_{d,d'}$ $\zeta_{p,p'}$ and ρ are in reasonably good agreement with the published results, as one can see from Table IV.4.

E. Spin-Hamiltonian parameters $g_{\parallel}$, $g_{\perp}$, D, and a, for $GaAs:Cr^{2+}$ and $InP:Cr^{2+}$

The expressions (100)-(107), for the spin-Hamiltonian parameters, are appropriate for tetragonal symmetry. They depend on the various one- and two-center matrix elements, such as $\zeta_{d,d'}$ $\zeta_{p,p'}$ A, ρ, and overlap integrals. We have used our calculated values of these integrals, which were presented in the preceding section, in order to obtain values for $g_{\parallel}$, $g_{\perp}$, D, and $\underline{a}$ for $GaAs:Cr^{2+}$ and $InP:Cr^{2+}$. As for the energy values (Fig. II.1), we have taken $E_1 = 4500\ cm^{-1}$, $E_2 = 7300\ cm^{-1}$, and $E_3 = 9700\ cm^{-1}$ for $GaAs:Cr^{2+}$, as deduced by Krebs and Stauss[18]; and the average energy E of the triplet states relative to the ground state has been estimated[23] to be on the order of 20,000 cm^{-1}. For $InP:Cr^{2+}$, the energy values are not available, and we have used the values $E_1 = 1200\ cm^{-1}$, $E_2 = 2200\ cm^{-1}$, and $E_3 = 5800\ cm^{-1}$, which we obtained by fitting the experimental values[33] for $g_{\parallel}$, $g_{\perp}$, D, and $\underline{a}$, and are consistent with an

Table IV.4

SPIN-ORBIT AND SPIN-SPIN PARAMETERS.

ION	$\zeta_{d,d}(cm^{-1})$ *	$\zeta_{d,d}(cm^{-1})$ [Ref.]	$\rho(cm^{-1})$ *	$\rho(cm^{-1})$ [Ref.]
Cr^{2+}	303.415	236 [78]	0.128	0.12 [78]
Fe^{2+}	503	456 [78], 412 [34]	1.047	1.04 [78]

	$\zeta_{p,p}(cm^{-1})$ *	$\zeta_{p,p}(cm^{-1})$ [Ref.]	$A(A^{-1})$ *
As	1256.253	1273.33 [85]	1.733
P	252.623	244.67 [85]	1.858

* This work

energy splitting Δ on the order of 3000 cm^{-1} found for similar semiconductors[30-35].

The evaluation of the spin-Hamiltonian parameters, according to Eqs. (100)-(107), requires the use of the values of $\lambda_{d,s}$, λ_{d,p_σ}, and λ_{d,p_π}. Since they are unknown, we follow the procedure of determining them from the available experimental data. To this end, we vary $\lambda_{d,s}$, λ_{d,p_σ}, and λ_{d,p_π}, and obtain $g_{\parallel}$, $g_{\perp}$, D, and $\underline{a}$ from Eqs. (100)-(107). Fig. IV.4 illustrates the variation of the spin-Hamiltonian parameters as a function of $\lambda_{d,s}$, λ_{d,p_σ}, and λ_{d,p_π} values, for GaAs:Cr^{2+}. The dotted lines (in Fig. IV.4) have been drawn to mark the experimental values. The value of |D| increases monotonically with λ_{d,p_π}, while $g_{\parallel}$ and $g_{\perp}$ increase if $\lambda_{d,p_\sigma} < 0.3$ and decrease if $\lambda_{d,s} > 0.3$ (see Fig. IV.4). Also, when $\lambda_{d,s}$ increases, the value of |D| decreases, whereas the values of $g_{\parallel}$ and $g_{\perp}$ increase. The values of $\underline{a}$ are not significantly altered by the variations of $\lambda_{d,s}$, λ_{d,p_σ}, and λ_{d,p_π}. The set of values of the admixture coefficients, for GaAs:Cr^{2+}, which explains best the experimental data for the spin-Hamiltonian parameters lies close to $\lambda_{d,s} = 0.6$, $\lambda_{d,p_\sigma} = 0.8$, and $\lambda_{d,p_\pi} = 0.08$, which correspond to the calculated values $g_{\parallel} = 1.975$, $g_{\perp} = 1.995$, $D = -1.865\ cm^{-1}$, $a = 0.0043\ cm^{-1}$ (the experimental values[18] are $g_{\parallel} = 1.974 \pm 0.003$, $g_{\perp} = 1.997 \pm 0.002$, $D = -1.860 \pm 0.0016$, and $a = 0.031 \pm 0.013$). The values of λs as deduced above would appear to be too large. In an attempt to search for a better set, we have selected other values of the admixing parameters, viz., $\lambda_{d,s} = 0.369$, $\lambda_{d,p_\sigma} = 0.509$, and $\lambda_{d,p_\pi} = 0.045$ (see Table IV.5), with only a fair agreement with the experimental data. This new set yields the

FIG. IV.4 Shows the variations of the spin-Hamiltonian parameters $D, g_{\parallel}, g_{\perp}$, and $\underline{a}$, for GaAs:Cr^{2+}, with the admixture coefficients $\lambda_{d,s}$, λ_{d,p_σ} and λ_{d,p_π}. Only the curves for $\lambda_{d,s}$=0.4, 0.6 and 0.8 are shown for representative purposes. The curves marked I, II, III and IV correspond to the values of λ_{d,p_π} equal to 0.0, 0.04, 0.08 and 0.1, respectively. The dashed lines represent the experimental values (Ref. 18) of the spin-Hamiltonian parameters.

FIG. IV.4

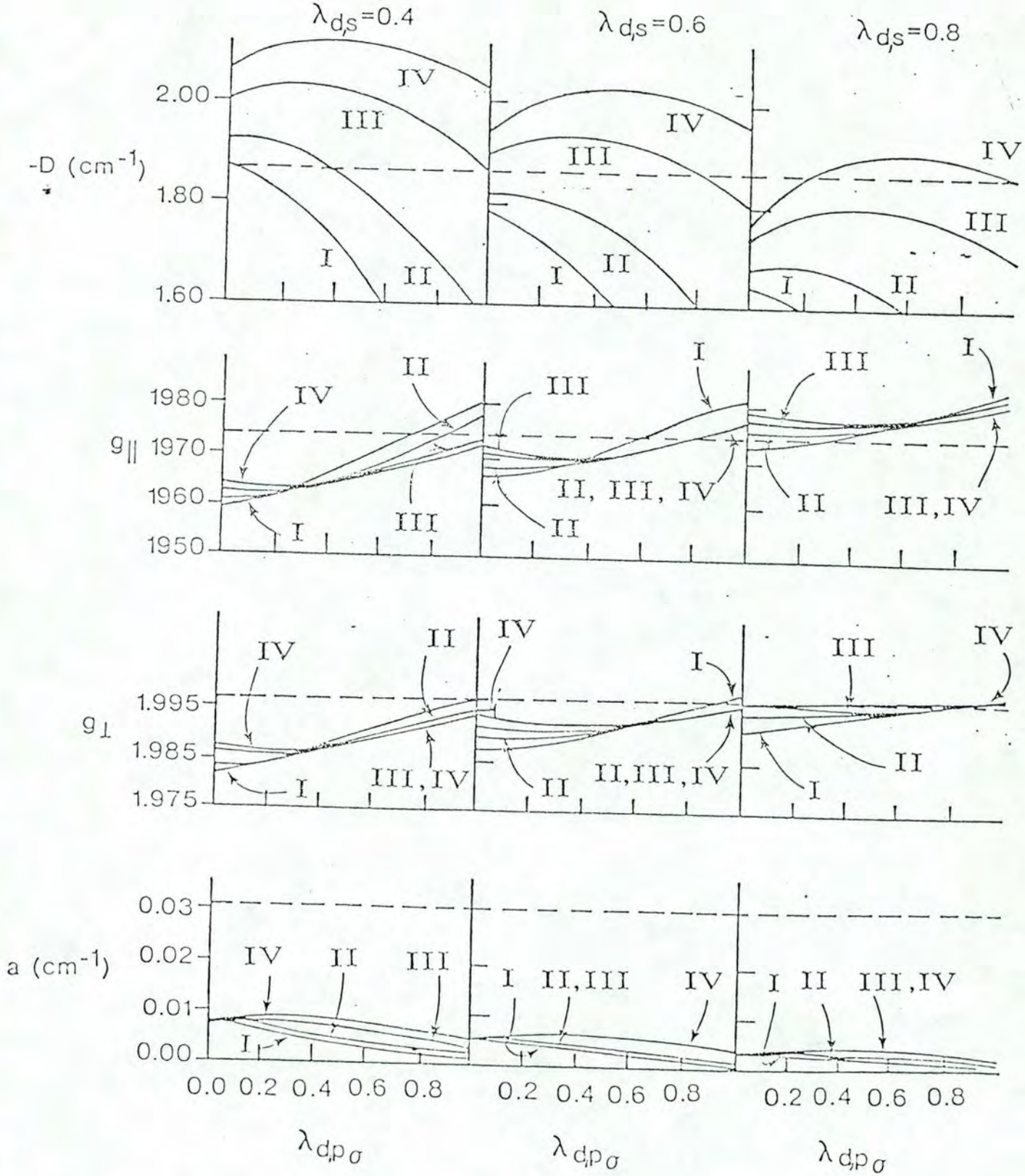
λd,s=0.4
λd,s=0.6
λd,s=0.8
-D (cm-1)
2.00
1.80
1.60
IV
III
II
I
g||
1980
1970
1960
1950
g⊥
1.995
1.985
1.975
a (cm-1)
0.03
0.02
0.01
0.00
III,IV
II,III,IV
0.0 0.2 0.4 0.6 0.8
0.2 0.4 0.6 0.8
λd,pσ

TABLE IV.5

SPIN-HAMILTONIAN PARAMETER($g_{\parallel}$, $g_{\perp}$, D and a) and ADMIXTURE COEFFICIENTS(λ_{ds}, λ_{dp_σ}, and λ_{dp_π}) for GaAs:Cr^{2+} and InP:Cr^{2+}

Material	Admixture Coefficients			Spin-Hamiltonian Parameters			
	λ_{ds}	λ_{dp_σ}	λ_{dp_π}	$g_{\parallel}$	$g_{\perp}$	D(cm^{-1})	a (cm^{-1})
GaAs:Cr^{2+}	0.6	0.8	0.08	1.975	1.995	-1.865	0.0043
	0	0.9	0.07	1.968	1.990	-1.879	0.005
	0.369	0.509	0.045	1.966	1.988	-1.860	0.01
	Experiment [18]			1.974(3),	1.997(2),	-1.860(16),	0.031(13)
	λ_{ds}	λ_{dp_σ}	λ_{dp_π}	$g_{\parallel}$	$g_{\perp}$	D(cm^{-1})	a (cm^{-1})
InP:cr^{2+}	0.45	0.47	0.45	1.981	2.010	-0.979	0.089
	Experiment [33]			1.981	2.010	-0.967	0.089

calculated values $g_{\parallel} = 1.966$, $g_{\perp} = 1.988$, $D = -1.860$, and $a = 0.01$, which are not in as good agreement with the experimental values as those from the previous set (see Table IV.5). The new set still gives a high value of λ_{d,p_σ}. It seems that with the experimental data at hand, it is hard to obtain acceptable values of the admixing parameters, although Krebs[86] claims that for the present system, the values of λs are, indeed, high.

The same procedure, described above for GaAs:Cr^{2+}, was followed to interpret $g_{\parallel}$, $g_{\perp}$, D, and $\underline{a}$ of InP:Cr^{2+}. The set of values of λs for InP:Cr^{2+} which best explain the experimental data for the spin-Hamiltonian parameters (see Table IV.5) are $\lambda_{d,s} = 0.45$, $\lambda_{d,p_\sigma} = 0.47$, and $\lambda_{d,p_\pi} = 0.45$, which give the calculated values $g_{\parallel} = 1.981$, $g_{\perp} = 2.010$, $D = -0.979\ cm^{-1}$, $a = 0.089\ cm^{-1}$ (the experimental values[33] are $g_{\parallel} = 1.981$, $g_{\perp} = 2.010$, $D = -0.967\ cm^{-1}$, and $a = 0.089\ cm^{-1}$). One notices that high values of $\lambda_{d,s}$ and λ_{d,p_π}, comparable to the value of λ_{d,p_σ}, were required to explain the fact that $g_{\perp}$, for InP:Cr^{2+}, is greater than g_0 (= 2.0023).

The best set of λs for GaAs:Cr^{2+} and InP:Cr^{2+} which explains the experimental data[18,33] may be used, in a first-order approximation (see Eq. 46), to deduce the charge transfer covalencies (see Table IV.6). The calculated values of the charge transfer covalencies turn out to be $\gamma_{ds} = 0.522$, $\gamma_{dp_\sigma} = 0.8988$, and $\gamma_{dp_\pi} = 0.0217$ for GaAs:Cr^{2+}, and $\gamma_{ds} = 0.38$, $\gamma_{dp_\sigma} = 0.56$, and $\gamma_{dp_\pi} = 0.40$ for InP:Cr^{2+}. As mentioned before, the experimental data we have used for GaAs:Cr^{2+} and which give rise to our rather large admixture coefficients are those of Krebs and Stauss[18], who deduce E_1, E_2, and E_3 from uniaxial stress measurements.

TABLE IV.6

ADMIXTURE COEFFICIENTS (λ'_s) and CHARGE TRANSFER COVALENCIES (γ'_s) WHICH BEST EXPLAIN THE EXPERIMENTAL DATA FOR GaAs:Cr^{2+} and InP:Cr^{2+}

Material	λ_{ds}	$\lambda_{dp\sigma}$	$\lambda_{dp\pi}$	γ_{ds}	$\gamma_{dp\sigma}$	$\gamma_{dp\pi}$
GaAS:Cr^{2+}	0.6	0.8	0.08	0.522	0.8988	0.0217
InP:Cr^{2+}	0.45	0.47	0.45	0.38	0.56	0.40

They estimate $E_1 = 3E_{JT}$ ($^5T_2$) by using their measured Jahn-Teller coefficient $V_E = -0.85$ eV/Å. Then they obtain E_2 and E_3 by employing the model calculations of Vallin et al.[21], in which E_2 is given by the peak of the ^5E-$^5T_2$ optical transition at 7300 cm^{-1}, and E_3 is related to E_1 and the zero-phonon line at 6760 cm^{-1}. Hennel et al.[25], on the other hand, have observed a new set of zero-phonon lines around 6620 cm^{-1} which they have identified as due to the isolated Cr^{2+} center in GaAs. Accounting for this observation, and based on their detailed optical absorption measurements at low temperatures with different amounts of n and p doping in samples, Hennel et al.[25] have concluded that $E_{JT}(^5T_2) \leq 660$ cm^{-1}; consequently, $E_1 \leq 2000$ cm^{-1}, $E_3 - E_2 \cong 320$ cm^{-1}, $E_2 \cong 6620$ cm^{-1}, and hence $E_3 \cong 6940$ cm^{-1}. Clearly, the E_i values deduced by Hennel et al. are considerably lower than the values given by Krebs and Stauss[18]. The reduction factors for E_1, E_2, and E_3 are 0.44, 0.91, and 0.71, respectively. If the energy values are, indeed, reduced, it is obvious from Eqs. (100)-(105) that the resulting admixture coefficients in our model would also be reduced. This fact alone, however, is not sufficient to resolve which of the two experimental assignments is indeed correct.

F. Estimate of intensity ratios

In Section C of Chapter III we discussed the dipole transition moments appropriate to systems with local tetragonal symmetry. We have predicted that if the admixture coefficients $\lambda_{d,s}$, λ_{d,p_σ}, and λ_{d,p_π} are non-zero, then electric dipole transitions may occur between the excited levels η, ξ, and θ,

and the ground state ζ (see Fig. II.1). In Section C of the present chapter, the values of the integrals $I_{\ell\ell'}$, $I'_{\ell\ell'}$, $R_{\ell\ell'}$, and $R'_{\ell\ell'}$ (needed for the transition-moment calculations) were given for GaAs:Cr^{2+}. With those values of the integrals mentioned above, and the set of admixture coefficients $\lambda_{d,s} = 0.6$, $\lambda_{d,p_\sigma} = 0.8$, and $\lambda_{d,p_\pi} = 0.08$ (see preceding section), we obtain the following values for dipole transition moments for GaAs:Cr^{2+}:

$$P_x^{\eta,\zeta} = P_y^{\xi,\zeta} = 1.626\ a_0$$

$$P_z^{\theta,\zeta} = 0.075\ a_0$$

With the values above of $P_x^{\eta,\zeta}$, $P_y^{\xi,\zeta}$, and $P_z^{\theta,\zeta}$, we calculate the ratio of the two allowed transitions (with energy separations E_1 and E_2 as shown in Fig. II.1) for the different values of energies E_1 and E_2 as given by Krebs and Stauss[18] and by Hennel et al.[25]. Table IV.7 summarizes these results. Our predicted values could not be compared with experimental values of relative intensities, because of the lack of experimental data. However, we can say that the predicted value for relative intensity using the E_1 and E_2 values of Krebs and Stauss[18] are much too high (135.1). The predicted value for the intensity ratio (7.45) using Hennel's values for E_1 and E_2 seems more likely.

G. Spin-orbit and spin-spin splittings of energy levels of InP:Fe^{2+}, GaP:Fe^{2+}, and GaAs:Fe^{2+}

In order to evaluate the spin-orbit and spin-spin splitting

Table IV.7

INTENSITY RATIOS FOR GaAs:Cr^{2+}. I_1 AND I_2 STAND FOR INTENSITIES RADIATED DUE TO A TRANSITION BETWEEN THE STATES (ξ,η) AND ζ WITH ENERGY SEPARATION E_1 (SEE Fig.II.1), AND BETWEEN THE STATES θ AND ζ WITH ENERGY SEPARATION E_2, RESPECTIVELY.

Calculated I_1/I_2	$E_1(cm^{-1})$, Ref.		$E_2(cm^{-1})$, Ref
135.1	4500	18	7300 18
7.45	1980	25	6619 25

energies, we use the spin-orbit and spin-spin coupling parameters presented in Section D. According to Eqs. (113) and (114), the evaluation of these splitting energies also requires the values of the admixture coefficients $\lambda_{d,s}$, λ_{d,p_σ}, and λ_{d,p_π} through expressions (106-a) and (107-a) for ζ_1 and ζ_2, respectively. These energy splittings are also a function of the crystal field parameter Δ. Since the admixture coefficients are unknown for InP:Fe^{2+}, GaP:Fe^{2+}, and GaAs:Fe^{2+}, we determine them from the available experimental data, which give the values of the crystal field splitting parameter Δ and the energies of the four allowed transitions from the $^5T_2$ state to the ground state ^5E (see Fig. II.3), namely, E(6-1), E(6-2), E(6-3), and E(6-4). The four lines observed experimentally give the energy spacings K and E(6-5) [not an allowed transition], where K and E(6-5) are shown in Fig. II.3. We have, then, the values of Δ, E(6-5), and K, deduced from available experimental data, from which the three unknown admixture coefficients must be determined. To this end, we vary $\lambda_{d,s}$, λ_{d,p_σ}, and λ_{d,p_π}, and select the sets of admixture coefficients consistent with the experimental results. Table IV.8 lists the selected sets of λs obtained in this way for InP:Fe^{2+}, GaP:Fe^{2+}, and GaAs:Fe^{2+}. Also, calculated values of the energy separations K and E(6-5) are listed for the case where overlap only (no charge transfer) is considered and for the case where neither charge transfer nor overlap is taken into account. In the latter case, the expressions given in Eqs. (113) and (114) reduce to those derived by Low and Weger.[37]

One notices that the energy splittings E(6-5) and K in

Table IV.8

ENERGY SEPARATIONS Δ, E(6-5), K AND ADMIXTURE COEFFICIENTS FOR $InP:Fe^{2+}$, $GaP:Fe^{2+}$ and $GaAs:Fe^{2+}$

Material	$\lambda_{d,s}$	λ_{d,p_σ}	λ_{d,p_π}	E(6-5)(cm^{-1})	K(cm^{-1})	Δ(cm^{-1})	
$InP:Fe^{2+}$	0.1	0.6	-0.4	2789	15.2	3040	*
	0.05	-0.07	0.04	2720.5	28.9	3040	**
	0.0	0.0	0.0	2723.3	28.4	3040	***
	—	—	—	2789	14±4	3040	Exp.[34]
$GaP:Fe^{2+}$	0.0	0.0	-0.4	3293.2	13.77	3559.4	*
	0.07	-0.08	0.05	3229.2	25.98	3559.4	**
	0.0	0.0	0.0	3232.2	25.9	3559.4	***
	—	—	—	3290.3	13±3	3559.4	Exp.[32]
$GaAs:Fe^{2+}$	0.1	0.5	-0.3	2949.6	11.1	2995	*
	0.06	-0.08	0.05	2663	29.4	2995	**
	0.0	0.0	0.0	2664.8	29.2	2995	***
	—	—	—	2950	13±4	2995	Exp.[30]

* This work: Overlap and Charge Transfer

** This work: Overlap only

*** This work: No Overlap and no Charge Transfer

Table IV.8 for the case when overlap and charge transfers are neglected, are much different from the experimental values. If overlap only is considered, neglecting charge transfer, the results do not improve. This implies that charge transfer effects are necessary to the explanation of the experimental data. For $InP:Fe^{2+}$, the set of admixture coefficients which is consistent with the experimental data is approximately $\lambda_{d,s} = 0.1$, $\lambda_{d,p_\sigma} = 0.6$, and $\lambda_{d,p_\pi} = -0.4$. For $GaAs:Fe^{2+}$, the best set is the one with values near $\lambda_{d,s} = 0.1$, $\lambda_{d,p_\sigma} = 0.5$, and $\lambda_{d,p_\pi} = -0.3$. For $GaAs:Fe^{2+}$, the set which is consistent with the experimental data is in the neighborhood of $\lambda_{d,s} = 0$, $\lambda_{d,p_\sigma} = 0$, and $\lambda_{d,p_\pi} = -0.4$. The small values of $\lambda_{d,s}$ and λ_{d,p_σ} for $GaP:Fe^{2+}$ are consistent with the fact that the energy spacing K, which depends on ζ_2^2/Δ, is of the same magnitude for all three compounds, whereas Δ is larger for Fe^{2+}-doped GaP. In other words, if Δ is larger, ζ_2 must also be larger if K remains the same. A larger value of ζ_2 for $GaP:Fe^{2+}$ is consistent if this system is less highly covalent than $InP:Fe^{2+}$ and $GaAs:Fe^{2+}$.

The calculated values of the energies of the allowed transitions, E(6-4), E(6-3), E(6-2), and E(6-1), with the values of the admixture coefficients obtained as described above for $InP:Fe^{2+}$, $GaAs:Fe^{2+}$, and $GaP:Fe^{2+}$, are listed in Table IV.9, along with the experimental values. Table IV.10 lists the obtained admixture coefficients, along with the calculated values of the corresponding charge transfers.

We have not considered Jahn-Teller distortions in the calculations of the spin-orbit and spin-spin splitting energies for $InP:Fe^{2+}$, $GaP:Fe^{2+}$, and $GaAs:Fe^{2+}$. These materials are

Table IV.9

CALCULATED VALUES OF ENERGIES OF THE ALLOWED TRANSITIONS, CONSIDERING OVERLAPS AND CHARGE TRANSFERS FOR $InP:Fe^{2+}$, $GaP:Fe^{2+}$ and $GaAs:Fe^{2+}$, AND COMPARISON WITH EXPERIMENTAL RESULTS.

Material	E(6-4) (cm^{-1})	E(6-3) (cm^{-1})	E(6-2) (cm^{-1})	E(6-1) (cm^{-1})
$InP:Fe^{2+}$ ($\lambda_{ds}=0.1$ $\lambda_{dp\sigma}=0.6$ $\lambda_{dp\pi}=-0.4$)	2804.2	2819.4	2834.6	2849.8
Exp.[34]	2802	2820	2830	2845
$GaP:Fe^{2+}$ ($\lambda_{ds}=0.0$ $\lambda_{dp\sigma}=0.0$ $\lambda_{dp\pi}=-0.4$)	3306.97	3320.74	3334.51	3348.28
Exp.[32]	3303.6	3319.6	3330.7	3343.5
$GaAs:Fe^{2+}$ ($\lambda_{ds}=0.1$ $\lambda_{dp\sigma}=0.5$ $\lambda_{dp\pi}=-0.3$)	2960.7	2971.8	2982.9	2994
Exp.[30]	2962	2979	2988	3002

Table IV.10

ADMIXTURE COEFFICIENTS AND CHARGE TRANSFERS, OBTAINED FROM EXPERIMENTAL DATA OF $InP:Fe^{2+}$, $GaAs:Fe^{2+}$ and $GaP:Fe^{2+}$.

Material	$\lambda_{d,s}$	λ_{d,p_σ}	λ_{d,p_π}	$\gamma_{d,s}$	γ_{d,p_σ}	γ_{d,p_π}
$InP:Fe^{2+}$	0.1	0.6	-0.4	0.05	0.7	-0.43
$GaP:Fe^{2+}$	0.0	0.0	-0.4	-0.07	0.08	-0.44
$GaAs:Fe^{2+}$	0.1	0.5	-0.3	0.04	0.58	-0.34

expected to undergo a Jahn-Teller distortion, but there is no experimental evidence, at this moment, that such distortions indeed occur for Fe^{2+}-doped InP, GaP, and GaAs. West et al.[32] estimated the value of the Jahn-Teller energy for the ^5E level of GaP:Fe^{2+} as $E_{JT} = 0.0024\ cm^{-1}$, confirming that the Jahn-Teller effect is small. If the Jahn-Teller effect on the ^5E levels of Fe^{2+}-doped InP, GaP, and GaAs is indeed small, the reduction of the energy separation K observed experimentally, from the corresponding free-ion values, is due mainly to covalency effects.

V. DISCUSSION AND CONCLUSION

The present work has been concerned with the electronic structure of chromium- and iron-doped GaAs, InP, and GaP materials. A generalized treatment of the electron-electron interaction matrices has been presented, and the result of its application to GaAs:Cr^{2+} and GaAs:Cr^{3+} systems is compared with the experimental results and the previous estimates by Hemstreet and Dimmock[40]. Calculations of intensity ratios for two electric dipole transitions in GaAs:Cr^{2+} have been performed, including the Jahn-Teller splitting energies. Also, the Jahn-Teller distortion has been estimated for the system mentioned above. The spin-Hamiltonian parameters $g_{\parallel}$, $g_{\perp}$, D, and $\underline{a}$ have been calculated for GaAs:Cr^{2+} and InP:Cr^{2+}, and compared with experimental results. For the GaAs:Fe^{2+}, InP:Fe^{2+}, and GaP:Fe^{2+} systems, we have calculated the energies of the transitions from the excited state $^5T_2$ to the ground state ^5E, the levels being split by spin-spin and spin-orbit interactions. We now discuss the important points pertinent to the physical quantities calculated for the various systems mentioned above.

Sharma and Sundaram[43] have derived, using group-theoretical techniques, general matrices for the d-electron interaction matrices appropriate to d-electron transition-metal ions in solids and complexes. Their generalized electron-electron interaction matrices eliminate the defects present in the previous treatments[44,46] based on the approximation that the d-electrons in the transition-metal ions contain pure d-orbitals.

Sharma and Sundaram have shown that their generalized treatment is very useful. They have deduced for the first time the values of the d-electron Coulomb and exchange integrals for $MgF_2:Co^{2+}$ and $MgF_2:Mn^{2+}$ using the generalized treatment in conjunction with detailed experimental optical data. Their theory is very significant, since it is able to give correct group-theoretical assignments to the observed energy levels of the impurity in solids, predict the values of the Coulomb and exchange interactions, which it is otherwise not possible to know from any other source, and remove the accidental degeneracy inherent in the free-atom type B, C, Δ, theory.

The generalized d-electron interaction matrices have been checked and compared with existing results by Sharma, Viccaro, and Sundaram[41]. In Section III.A the explicit expressions of the new matrix elements were given (Tables III.9-12) for the irreducible representations of the cubic crystal field, and were used in Section IV.A to check the approximate calculations of Hemstreet and Dimmock[40], who deduced the electronic energy levels of $GaAs:Cr^{2+}$ and $GaAs:Cr^{3+}$.

Hemstreet and Dimmock have calculated crystal-field term states for Cr^{2+} and Cr^{3+} in GaAs, for which they modified the standard electron-electron interaction matrix elements by introducing the parameters R_{ee}, R_{tt}, and R_{et} $(= \sqrt{R_{ee}R_{tt}})$, deduced from X_α calculations.[40,42] We have obtained the electronic energy levels for these two systems, using the generalized matrix elements listed in Tables III.10 and III.11 for $d^3(Cr^{3+})$ and $d^4(Cr^{2+})$ electrons, in order to compare them with the results from their calculations[40]. The comparison

has been presented in Figs. IV.1 and IV.2. We have found that although there is general agreement between the two, Hemstreet and Dimmock's results differ from ours. The notable differences are these (See Figs. IV.1 and IV.2): (i) their two $^1T_1$ levels of GaAs:Cr^{2+} with energies 0.74 and 0.84 eV should have energies 0.80 and 1.02 eV, as given by our calculations; (ii) the level $^5T_1$ assigned by Hemstreet and Dimmock in GaAs:Cr^{2+} should have been $^3T_1$; (iii) the ^1E level with energy 1.45 eV, and $^3T_1$ with energy 1.33 eV, in GaAs:Cr^{2+} originate from the configuration e^2t^2, instead of the configuration t^4 obtained by Hemstreet and Dimmock; (iv) for GaAs:Cr^{3+}, the levels $^4T_1$ at 0.7 eV and $^2T_2$ at 0.95 eV assigned in Ref. 40 should both be $^2T_1$. These differences are suspected to be due to some errors in the expressions for the d-electron interaction matrix elements in Ref. 40. The matrices of Hemstreet and Dimmock have not been published, and consequently we were unable to compare theirs with the ones used in Section IV.A. The obtained value of the energy of the ^5E-$^5T_2$ transition for GaAs:Cr^{2+} is 0.65 eV (see Fig. IV.1), in good agreement with the experimental value[18], 0.68 eV.

In order to investigate the electronic structure of transition-metal ions in III-V compounds, we have used the cluster approach with symmetry adopted electronic wave functions which include the impurity and the surrounding atoms. We have used the best available wave functions, obtained by self-consistent calculations[66], for the atomic orbitals of the impurity ions and ligands of the magnetic ions in GaAs:Cr^{2+}, InP:Cr^{2+}, InP:Fe^{2+}, GaAs:Fe^{2+}, and GaP:Fe^{2+}. For these systems, the

magnetic ions Cr^{2+} and Fe^{2+} are substitutional at the Ga site in GaAs and GaP, and at the In site in InP, and possess a local tetrahedral symmetry (in the absence of the Jahn-Teller effect). The effect of the environment has been accounted for by subjecting the cluster to the cubic crystal field and by incorporating the effects of the Jahn-Teller distortion present in these systems.

For GaAs:Cr^{2+}, the impurity states undergo a strong Jahn-Teller distortion[18], changing the symmetry of the Cr^{2+} site from tetrahedral (T_d) to tetragonal (D_{2d}). The ground state $^5T_2$ (in T_d) symmetry) splits into $^5B_2$ and ^5E (in D_{2d} symmetry), as shown in Fig. II.1, and the excited state ^5E (in T_d symmetry) splits into $^5A_1$ and $^5B_1$ (in D_{2d} symmetry). We have estimated, in Section IV.B, values of the distortion of the ligand ions due to the Jahn-Teller effect in this system, relative to the experimental values of the Jahn-Teller energies given by Krebs and Stauss[18]. We found that the angle β' (see Fig. III.4) is such that $\cos\beta' = 0.87/\sqrt{3}$, as compared to the values of the undistorted tetrahedron, for which $\cos\beta' = 1/\sqrt{3}$. We have also performed intensity calculations (Sec. IV.F) for electric-dipole transitions in GaAs:Cr^{2+}, between the levels split by the Jahn-Teller effect on the $^5T_2$ and ^5E levels. We have found that the transitions between the ground state ζ and the excited states ξ, η, and θ (see Fig. II.1) are possible because of the presence of significant overlap and charge transfer covalencies in this system. Thus, these intensity calculations have revealed one more aspect of the importance of overlap and charge transfer effects, since for the pure d-electrons

the transitions above would be completely absent. We predicted the intensity ratio relative to the transition with energy E_1 and the transition with energy E_2 (see Fig. II.1). With the values of E_1 and E_2 given by Krebs and Stauss[18] (see Table IV.7), we calculated the intensity ratio to be 135.1, whereas with the values of E_1 and E_2 of Hennel et al.[25] we predicted a value of 7.45. This implies that an experimental determination of the transition intensities could indicate which assignment is correct.

In order to understand the electronic structure of GaAs:Cr^{2+} and InP:Cr^{2+}, we have first deduced the expressions for the spin-Hamiltonian parameters (eqs. 100-107), taking into account overlap and charge transfer effects and the crystal fields present in the solid. The expressions for $g_{\parallel}$, $g_{\perp}$, and D were deduced by considering the perturbations on the ground state of the Zeeman and spin-orbit interactions in the second order and the spin-spin interaction in the first order. For the cubic field parameter a, fourth-order effects of the spin-orbit interaction and second-order effects of the spin-spin interaction were considered. The cubic crystal field and the Jahn-Teller splitting energies were accounted for in the energy separations between the ground and excited states, which were mixed by the spin-orbit and spin-spin interactions. Our expressions for the spin-Hamiltonian parameters contain explicitly the overlap and charge transfer contributions. The local, non-local, and distant contributions to the spin-orbit coupling constants have been retained in our expressions. The local terms arise when the central-ion wave functions alone

are involved in the matrix elements; the non-local are the terms which involve the atomic wave functions of the ligands as well as the central ion's; and the distant terms involve the ligands' wave functions alone. The two-center integrals, such as the non-local spin-orbit term and overlap integrals, have been accurately evaluated using Sharma's[50] formula for the expansion of Slater-type orbitals from one center onto another (see Sec. IV.C). Our calculated values of the local, non-local, and distant terms of the spin-orbit constants, in Section IV.D, using accurate atomic wave functions obtained by self-consistent methods[66], have shown the relative importance of these terms. As is clear from Table IV.4 and eqs. (106) and (107), the local and distant terms are the dominant contributors to the spin-order coupling constant. The non-local term of the spin-orbit coupling constant is two orders of magnitude lower than the others.

The values of overlap and charge transfer in our cluster treatment of GaAs:Cr^{2+} and InP:Cr^{2+} have been obtained in Section IV.E by calculations involving the spin-Hamiltonian parameters $g_{\parallel}$, $g_{\perp}$, D, and $\underline{a}$, as a function of the admixture coefficients $\lambda_{d,s}$, λ_{d,p_σ}, and λ_{d,p_π}. The values of the admixture coefficients were obtained for GaAs:Cr^{2+} and InP:Cr^{2+} and are listed in Table IV.5, where the calculated values of the spin-Hamiltonian parameters are also compared with the experimental values. For InP:Cr^{2+}, the calculated values $g_{\parallel} = 1.981$, $g_{\perp} = 2.010$, $D = -0.979\ cm^{-1}$, and $a = 0.089\ cm^{-1}$ obtained with the set of admixture coefficients $\lambda_{d,s} = 0.45$, $\lambda_{d,p_\sigma} = 0.47$, $\lambda_{d,p_\pi} = 0.45$ are in good agreement with the

experimental values[33] $g_{\parallel} = 1.981$, $g_{\perp} = 2.010$, $D = -0.967\ cm^{-1}$, and $a = 0.089\ cm^{-1}$. For GaAs:Cr^{2+} our calculations result in $g_{\parallel} = 1.975$, $g_{\perp} = 1.995$, and $D = -1.865\ cm^{-1}$ with $\lambda_{d,s} = 0.6$, $\lambda_{d,p_{\pi}} = 0.08$, and $\lambda_{d,p_{\sigma}} = 0.8$, compared to the experimental values[18] $g_{\parallel} = 1.974$, $g_{\perp} = 1.997$, and $D = -1.860\ cm^{-1}$. The cubic field parameter was explained only in sign, and its calculated value $a = 0.0043\ cm^{-1}$ is an order of magnitude too low, compared to the experimental[18] value $a = 0.031$. The values of covalencies for GaAs:Cr^{2+} were obtained by using the values of the Jahn-Teller splittings given by Krebs and Stauss[18]. These values of splitting energies have recently been criticized by Hennel et al.[25], in view of new estimates from optical absorption measurements. In future work, it would be interesting to examine whether the new values can explain the experimental data, including the magnitude of the spin-Hamiltonian parameter a.

Vallin and Watkins[23] have interpreted the spin-Hamiltonian parameters $g_{\parallel}$, $g_{\perp}$, D, and a for Cr^{2+} in II-VI compounds (ZnS, ZnSe, ZnTe, and CdTe) in the framework of the ligand field theory. Although the compounds are different from the semiconductors with which we have been concerned, it is interesting to compare our results with those of Vallin and Watkins. It must be noted that they have completely neglected the s-orbitals of the ligands, and as far as the formalism is concerned, they have not included the non-local terms in the expressions of the spin-Hamiltonian parameters. Also, they have restricted themselves to a single parameter approximation to estimate the admixture coefficients, assuming the same charge transfer

for all the compounds. In our treatment, we have taken into account the s-orbitals of the ligands and have also calculated exactly the overlap integrals. Also, we did not restrict ourselves to a single parameter approximation in order to determine the admixture coefficients. Our results for Cr^{2+}-doped GaAs and InP show that the s-orbitals of the ligands contribute significantly to the covalency effects on the spin-Hamiltonian parameters, and consequently, these orbitals should not be neglected. We have obtained the values of λ_{d,p_π} = 0.08, $\lambda_{d,s}$ = 0.6, and λ_{d,p_σ} = 0.8 for GaAs:Cr^{2+} and λ_{d,p_π} = 0.45, $\lambda_{d,s}$ = 0.45, and λ_{d,p_σ} = 0.47 for InP:Cr^{2+}. The values of admixture coefficients obtained by Vallin and Watkins for Cr^{2+} in II-VI compounds are λ_{d,p_π} = -0.248 and λ_{d,p_σ} = 0.274 ($\lambda_{d,s}$ was assumed to be zero). Although one is not justified in making rigorous comparisons among the results above (because of the approximations assumed by Vallin and Watkins), one notes that the covalency effects are also significant for Cr^{2+} in II-VI compounds. Further comparison indicates that Cr^{2+} in III-V systems is more strongly covalently bonded than in II-VI systems.

In order to keep the problem calculationally tractable, in our theoretical treatment of the spin-Hamiltonian parameters of GaAs:Cr^{2+} and InP:Cr^{2+} we have neglected the direct effect of the Jahn-Teller distortion on the cluster wave functions. This is justifiable, since the direct effect of this distortion on the wave functions is very small. However, the indirect effect on the wave functions has been appropriately taken into account by use of the Jahn-Teller splitting of the energy

levels, as shown in Fig. II.1. For future improvement, however, one should use the wave functions, like the ones we have derived in Chapter III, compatible with the distorted geometry of the cluster.

For the GaAs:Fe^{2+}, GaP:Fe^{2+}, and InP:Fe^{2+} systems, we have also adopted the cluster wave functions, taking into account the crystal fields and the spin-orbit and spin-spin interactions. We deduced, in Section III.B.2, the expressions of energy splittings due to the spin-orbit and spin-spin interactions, including the effects of overlap and charge transfer (eqs. 113-a to 114). Figure II.3 shows the energy diagram for these systems, as well as the allowed electric dipole transitions. We have considered perturbations up to second-order due to the spin-orbit interaction on the ground state ^5E and the excited state $^5T_2$, and also first-order perturbation due to spin-spin interaction on the ground state.

Our calculations, including overlap and charge transfer, have explained the four lines observed experimentally[30,32,34] for Fe^{2+}-doped GaAs, GaP, and InP, as it is clear from Table IV.9. For InP:Fe^{2+}, we obtained the transition energies (see Fig. II.3) E(6-1) = 2849.8 cm^{-1}, E(6-2) = 2834.6 cm^{-1}, E(6-3) = 2819.4 cm^{-1}, E(6-4) = 2804.2 cm^{-1}, compared to the experimental values[34] E(6-1) = 2845 cm^{-1}, E(6-2) = 2830 cm^{-1}, E(6-3) = 2820 cm^{-1}, E(6-4) = 2802 cm^{-1}. For GaP:Fe^{2+}, our calculated values are E(6-1) = 3348.28 cm^{-1}, E(6-2) = 3334.51 cm^{-1}, E(6-3) = 3320.74 cm^{-1}, E(6-4) = 3306.97 cm^{-1}, compared to the experimental values[32] E(6-1) = 3343.5 cm^{-1}, E(6-2) = 3330.7 cm^{-1}, E(6-3) = 3319.6 cm^{-1}, E(6-4) = 3303.6 cm^{-1}. For

GaAs:Fe^{2+}, we obtained E(6-1) = 2994 cm^{-1}, E(6-2) = 2982.9 cm^{-1}, E(6-3) = 2971.8 cm^{-1}, E(6-4) = 2960.7 cm^{-1}, compared to the values E(6-1) = 3002 cm^{-1}, E(6-2) = 2988 cm^{-1}, E(6-3) = 2979 cm^{-1}, E(6-4) = 2962 cm^{-1} obtained experimentally[30]. We have found that these systems, also, are strongly covalent. We have obtained the values of admixture coefficients in the neighborhood of $\lambda_{d,s} = 0.1$, $\lambda_{d,p_\sigma} = 0.6$, $\lambda_{d,p_\pi} = -0.4$ for InP:Fe^{2+}; $\lambda_{d,s} = 0.1$, $\lambda_{d,p_\sigma} = 0.5$, $\lambda_{d,p_\pi} = -0.3$ for GaAs:Fe^{2+}; and $\lambda_{d,s} = 0.0$, $\lambda_{d,p_\sigma} = 0.0$, $\lambda_{d,p_\pi} = -0.4$ for GaP:Fe^{2+}. Our results indicate that Fe^{2+} in GaP is relatively less covalent than Cr^{2+} and Fe^{2+} in GaAs and InP.

Previously, the experimental spectra of Fe^{2+}-doped III-V materials had been roughly interpreted by introducing two parameters, q and k[31,32,34]. The parameter q had been introduced as a reduction factor, multiplying the free-ion (subjected to a crystal field) formula for the energy spaicng K, due to spin-spin and spin-orbit interactions, of the split ground state (^5E) levels. The parameter k was also introduced as a reduction parameter of the spin-orbit coupling constant, associated with the impurity ion, from the free-ion value. These reduction factors, q and k, introduced in an ad hoc way, do not provide information about their origin, nor, more important, about the electronic structure of the impurity Fe^{2+} in III-V compounds. Our treatment provides a better insight into the covalency effects of the electronic structure of these systems, since we have derived the expressions of energy transitions using the wave functions of the cluster.

This work has been a first attempt to calculate the spin-

Hamiltonian parameters, transition energies, and transition intensities of the localized impurities in the III-V semiconductor systems, taking into account, explicitly, the effects of the overlap and charge transfer covalencies effects. The overlap and charge transfer effects reveal the nature of the defect centers, which are otherwise difficult to understand, since these systems involve large numbers of electrons, and consequently the exact wave functions are unknown. A similar approach could also be beneficial in explaining the experimental data for other impurities in III-V semiconductors. One could also follow the present treatment to calculate energy states for different charge states of Mn in GaAs, and for comparison with the X_α calculations performed by Srivastava, Sundaram, and Sharma[47].

For future improvement, we suggest an extension of the present cluster calculations. One should involve more atoms in forming the cluster wave functions. With larger clusters, one can expect not only a better agreement with the experimental data, but also a more realistic estimate of actual charge transfers. For large cluster calculations, however, one is required to expend considerable computational effort, which could be very costly. Also, one should include ligand-ligand interactions for overlap effects and spin-orbit interactions. Furthermore, the contributions arising from the non-local and distant terms due to spin-spin interactions should be included. Although such effects are expected to influence the covalency effects only slightly (less than 10%), their inclusion, following the procedure developed by Sharma, Das, and Orbach[52],

would be an improvement on the present treatment. For further improvement of the generalized treatment of d-electron interaction matrices, one should include the spin-orbit and spin-spin interactions. The generalized treatment of the electron-electron interaction matrices would also be useful for extending calculations appropriately to other systems. Also, it is expected that this work will provide the necessary stimulus to experimentalists to observe more refined and abundant lines in the spectra, and to theorists to make the first-principles calculations to compare with our results and explain the experimental data.

APPENDIX I

Jahn-Teller Distortion on Tetrahedral Configurations

According to a theorem by Jahn and Teller[87], when the orbital ground state of an ion in a solid is degenerate for reasons of symmetry, the ligands of this ion experience forces which act to displace them from their symmetry positions. As a result, a local distortion is induced which lowers the symmetry of the site, and the ion assumes an electronic configuration of lower symmetry and of lower energy, thereby removing the degeneracy.

The Hamiltonian, H, for the stationary states of a molecule contains as parameters the various nuclear coordinates. For small displacements of the nuclei from the symmetric configuration, we can expand H in a Taylor series in terms of the generalized coordinates Q_j which describe the displacements:

$$H = H_0 + \sum_j Q_j \frac{\partial H_0}{\partial Q_j} + \frac{1}{2} \sum_{j,k} Q_j Q_k \frac{\partial H_0}{\partial Q_j} \frac{\partial H_0}{\partial Q_k} + \ldots . \qquad \text{(A-1)}$$

where H_0 is the Hamiltonian of the unperturbed symmetry state of the molecule, with an orthonormal set of degenerate wave functions $\Psi_1^0 \ldots \Psi_n^0$. Q_j is a function of the nuclear displacement coordinates and $\frac{\partial H_0}{\partial Q_j}$ is a function of the electronic coordinates only. Both Q_j and $\frac{\partial H_0}{\partial Q_j}$ must transform in the same way, since the Hamiltonian is invariant under all symmetry operations. Taking the set Ψ_i^0 (i = 1, . . ., n) as zero-order wave functions, and the linear term in Q_j in Eq. (A-1) as the first-order perturbation, we must evaluate

matrix elements of the type

$$V_{in} = \mathcal{Q}_j \left\langle i \left| \frac{\partial H_0}{\partial \mathcal{Q}_j} \right| n \right\rangle \qquad \text{(A-2)}$$

If the initial degeneracy is retained, all the matrix elements V_{in} vanish. If this is not the case, a lifting of the degeneracy will occur. Also, if V_{in} is non-zero, the energy contains terms linear in $\mathcal{Q}_j$, and hence the initial configuration is not stable.

The degenerate set Ψ_i^0 spans the irreducible representation Γ of the point group of the site in the molecule, and $\frac{\partial H_0}{\partial \mathcal{Q}_j}$ transforms like $\mathcal{Q}_j$. The condition for a nonvanishing matrix element V_{in} is, therefore, that the symmetry product $[\Gamma]^2$ contain a representation also found in the normal vibrational modes. Jahn and Teller[87] were able to show, by going through all of the possible 34 molecular point groups, that in all cases where a degenerate electronic state can occur, there will always exist a vibrational mode which will destroy the degeneracy. The nuclei will be displaced in such a way as to remove the degeneracy; the symmetry of the molecule is lowered.

In the tetrahedral group, the symmetry species of the vibrational mode, apart from the totally symmetric mode (A_1), are the E and T_2 modes. The doubly degenerate mode (E) is the only active mode for a doubly degenerated level, as one can see by simple group-theoretical arguments. The degenerate electronic level T_2, on the other hand, may be split up by both E and T_2 vibrational modes. Under the vibrational mode E, the tetragonal symmetry (T_d) will distort in such a way as

to preserve its fourfold rotation-reflection symmetry axis. This distortion corresponds to an elongated or compressed tetrahedron, with axial symmetry (D_{2d}). The Jahn-Teller interaction due to the vibrational mode E may be expressed as[23,64,84]

$$V_{JT} = V_1(\mathcal{Q}_\theta \mathcal{E}_\theta + \mathcal{Q}_\varepsilon \mathcal{E}_\varepsilon) + V_2(\mathcal{Q}_\theta \mathcal{U}_\theta + \mathcal{Q}_\varepsilon \mathcal{U}_\varepsilon)$$

$$+ \frac{1}{2} k_E(\mathcal{Q}_\theta^2 + \mathcal{Q}_\varepsilon^2)\mathcal{I} \qquad \text{(A-3)}$$

where V_1 and V_2 are coupling coefficients of the lattice to the orbital electronic states T_2 and E, respectively. $\mathcal{Q}_\theta$ and $\mathcal{Q}_\varepsilon$ are normal coordinates of nuclear displacement. $\mathcal{E}_\theta$ and $\mathcal{E}_\varepsilon$ are electronic operators acting only on the orbital T_2 wave functions. $\mathcal{U}_\theta$ and $\mathcal{U}_\varepsilon$, similarly, apply to the orbital E wave functions. The matrix representations of $\mathcal{E}_\theta$, $\mathcal{E}_\varepsilon$, $\mathcal{U}_\theta$, and $\mathcal{U}_\varepsilon$ are[23,64]

$$\mathcal{E}_\theta = \begin{pmatrix} \frac{1}{2} & 0 & 0 \\ 0 & \frac{1}{2} & 0 \\ 0 & 0 & -1 \end{pmatrix} \qquad \text{(A-4)}$$

$$\mathcal{E}_\varepsilon = \begin{pmatrix} -\frac{\sqrt{3}}{2} & 0 & 0 \\ 0 & \frac{\sqrt{3}}{2} & 0 \\ 0 & 0 & 0 \end{pmatrix} \qquad \text{(A-5)}$$

$$\mathcal{U}_\theta = \begin{pmatrix} -1 & 0 \\ 0 & 1 \end{pmatrix} \tag{A-6}$$

$$\mathcal{U}_\varepsilon = \begin{pmatrix} 0 & 1 \\ 1 & 0 \end{pmatrix} \tag{A-7}$$

where the representation of $\mathcal{E}_\theta$ and $\mathcal{E}_\varepsilon$ is the T_2 electronic state (ξ,η,ζ) which transforms like (yz,xz,xy) respectively, and $\mathcal{U}_\theta$ and $\mathcal{U}_\varepsilon$ are given in terms of the electronic state $E_1(\theta,\varepsilon)$ which transforms like $(z^2, x^2 - y^2)$ respectively. The last term of Eq. (A-3) is the elastic energy associated with the distortion; k_E is the elastic constant; and $\mathcal{I}$ is the unit matrix.

For the state ζ, the minimization of Eq. (A-3),

$$\frac{\partial V_{JT}}{\partial \mathcal{Q}_\theta} = 0, \qquad \frac{\partial V_{JT}}{\partial \mathcal{Q}_\varepsilon} = 0 \quad ,$$

leads to a stable energy minimum in $\mathcal{Q}$ space at

$$\mathcal{Q}_\theta = \frac{V_1}{k_E} \tag{A-8}$$

$$\mathcal{Q}_\varepsilon = 0 \tag{A-9}$$

which is a pure tetragonal distortion along the z axis. The energy at this distortion has been lowered by the Jahn-Teller energy[23]

$$E_{JT}(E) = \frac{V_1^2}{2k_E} \tag{A-10}$$

The local symmetry is reduced to D_{2d} and the ground state

ζ is of symmetry $^5B_2$. The electronic wave functions ξ and η remain degenerate with symmetry $^5E_1$ and are 3 $E_{JT}(E)$ higher in energy with respect to the state ζ, as one can verify upon substitution of Eqs. (A-8) and (A-9) in Eq. (A-3) and by making use of Eqs. (A-4) and (A-5) for $\mathcal{E}_\theta$ and $\mathcal{E}_\varepsilon$. Fig. II.1 illustrates this Jahn-Teller splitting. The states θ and ε are also split by the tetragonal distortion. Upon substitution of Eqs. (A-8) and (A-9) into Eq. (A-3) and using Eqs.(A-6) and (A-7) for $\mathcal{U}_\theta$ and $\mathcal{U}_\varepsilon$, one verifies that the electronic state θ is lowered by the amount V_1V_2/k_E, whereas the state ε is raised by this same amount (see Fig. II.1).

For the T_2 vibrational mode, the Jahn-Teller interaction distorts the tetrahedron along one of the threefold axes, the energy of the system being lowered by[64]

$$E_{JT}(T_2) = \frac{2}{3}\frac{V_3^2}{k_{T_2}} \qquad \text{(A-11)}$$

where V_3 is the electron-lattice coupling coefficient for the mode T_2, and k_{T_2} is the elastic constant for this mode. The trigonal (D_{3d}) configuration is stable over the tetragonal (D_{2d}) if the energy gained by the system under D_{3d} distortion is larger than for the one under D_{2d} distortion. Or, from Eqs. (A-10) and (A-11), one has

$$\frac{V_3^2 k_E}{V_1^2 k_T} > \frac{3}{4} \qquad \text{(A-12)}$$

The tetragonal configuration is the stable one if

$$\frac{V_3^2 k_E}{V_1^2 k_{T_2}} < \frac{3}{4} \qquad \text{(A-13)}$$

If by accident the two stabilization energies (A-10) and (A-11) are equal, the complex will oscillate back and forth between a tetragonal and a trigonal configuration.

APPENDIX II

Sharma's expression for overlap integrals between Slater-type orbitals.

Sharma[60] derived the following expression for a two-center overlap integral between unnormalized Slater-type orbitals:

$$\left\langle r^{N'-1}\, e^{-\eta' r}\, Y_{L'}^{M'}(\theta,\phi) \,\middle|\, R^{N-1}\, e^{-\eta R}\, Y_{L}^{M}(\Theta,\Phi) \right\rangle =$$

$$\delta_{M',M}\, a^{N+N'+1} \sum_{k'=0}^{N+L'} \Bigg[e^{-\eta a} \left(- \frac{n!}{[a(\eta'+\eta)]^{n+1}} \right.$$

$$\left. + (-1)^{k'} g_n[a(\eta'-\eta)] \right) \sum_{k=0}^{k_{max}} \left(\frac{1}{\eta a} \right)^{k+1} F_{k',k}(NL'LM) -$$

$$e^{-\eta' a}\, (-1)^{L+N-k'}\, h_n[a(\eta'+\eta)] \sum_{k=0}^{k_{max}} \left(\frac{-1}{\eta a} \right)^{k+1} F_{k',k}(NL'LM) \Bigg]$$

where

$$n = N'-L'+k' \ ,$$

$$k_{max} = 2L'+L+N-k' \ ,$$

$$h_n(x) = \sum_{t=0}^{n} \frac{n!}{(n-t)!} \left(\frac{1}{x} \right)^{t+1} \ ,$$

and

$$g_n(x) = n!/x^{n+1} - e^{-x}\, h_n(x) \ .$$

When x is zero or very small, it is more accurate to use the limitting forms

$$g_n = \begin{cases} 1/(n+1) & , \quad \text{if } x=0 \\ \sum_{t=0}^{\infty} \frac{(-x)^t}{t!(n+t+1)} & , \quad \text{if } x \text{ is small.} \end{cases}$$

$$F_{k',k}(NL'LM) = \sum_{s=0}^{L'+L} \sum_{\gamma=0}^{\gamma_{max}} \frac{b_\gamma(sL'LM)\,(2s-L+N)!}{(k'-2\gamma)!\,(2s-L+N-k-k'+2\gamma)!}$$

with

$$\gamma_{max} = \min(L'+L-s,\ k'/2)\ ,$$

$$b_\gamma(sL'LM) = \frac{(-1)^L}{2} \sum_{p'=0}^{p'_{max}} \sum_{q'=q'_{min}}^{s} (-1)^{q'} \sum_{q=q_{min}}^{q_{max}} (-1)^q \cdot$$

$$\beta_{L',\,M}(p',q',\gamma-q-p') \sum_{p=0}^{p_{max}} \beta_{L,-M}(p,s-p-q',q)$$

where, in general

$$\beta_{\ell,m}(p,q,k) = \left[\frac{(2\ell+1)\,(\ell-m)!}{(\ell+m)!}\right]^{1/2} \frac{(2\ell-2p)!\,2^{2(p-\ell)}\,(-1)^p}{p!\,(\ell-p)!\,q!\,k!\,(\ell-m-2p-q-k)!}$$

and the various limits are:

$$p'_{max} = \min(L',\gamma) \quad , \quad q'_{min} = \max(0,s-L-M)\ ,$$

$$q_{min} = \max(0,p'+q'+\gamma-L'+M) \quad , \quad q_{max} = \min(\gamma-p',L+M-s+q')$$

and

$$p_{max} = \min(s-q',L+M-s+q'-q)\ .$$

REFERENCES

1. T. Instone and L. Eaves, J. Phys. C 11, L771 (1978)

2. W. H. Koschel, S. A. Bishop, and B. D. McCombe, Solid State Commun. 19, 521 (1976)

3. H. J. Stocker and M. Schmidt, J. Appl. Phys. 47, 2450 (1976)

4. K. Kocott and G. L. Pearson, Solid State Commun. 25, 113 (1978)

5. G. P. Peka and Yu. I. Karkhanin, Sov. Phys. Semicond. 6, 261 (1972)

6. N. V. Vorob'eva, Yu. V. Vorob'ev, and I. A. Kolomiets, Sov. Phys. Semicond. 8, 388 (1974)

7. V. V. Batavin and G. V. Popova, Sov. Phys. Semicond. 8, 1495 (1975)

8. S. A. Abagyan, G. A. Ivanov, Yu. N. Kuznetsov, Yu. A. Okuney, and Yu. E. Shanurin, Sov. Phys. Semicond. 7, 989 (1974)

9. D. Bois and P. Pinard, Phys. Rev. B 9, 4171 (1974)

10. A. L. Lin and R. H. Bube, J. Appl. Phys. 47, 1859 (1976)

11. H. J. Stocker, J. Appl. Phys. 48, 4583 (1977)

12. D. C. Look, Solid State Commun. 24, 825 (1977)

13. A. M. White, Solid State Commun. 32, 205 (1979)

14. N. Killoran, B. C. Cavenett, and W. E. Hagston, Solid State Commun. 35, 333 (1980)

15. J. J. Krebs and G. H. Stauss, Phys. Rev. B 15, 17 (1977)

16. G. H. Stauss and J. J. Krebs, Phys. Rev. B 22, 2050 (1980)

17. J. J. Krebs and G. H. Stauss, Phys. Rev. B 16, 971 (1977)

18. J. J. Krebs and G. H. Stauss, Phys. Rev. B 20, 795 (1979)

19. G. Martinez, A. M. Hennel, W. Szuszkiewicz, M. Balkanski, and B. Clerjaud, Phys. Rev. B 23, 3920 (1981)

20. U. Kaufmann and J. Schneider, Solid State Commun. 20, 143 (1976)

21. J. T. Vallin, G. A. Slack, S. Roberts, and A. E. Hughes, Phys. Rev. B 2, 4313 (1970)

22. B. Nygren, J. T. Vallin, and G. A. Slack, Solid State Commun. 11, 35 (1972)

23. J. T. Vallin and G. D. Watkins, Phys. Rev. B 9, 2051 (1974)

24. H. Tokumoto and T. Ishiguro, J. Phys. Soc. Japan, 46 (1979)

25. A. M. Hennel, W. Szuszkiewicz, M. Balkanski, G. Martinez, and B. Clerjaud, Phys. Rev. B 23, 3933 (1981)

26. U. Kaufmann and W. Koschel, Phys. Rev. B 17, 2081 (1978)

27. E. M. Ganapol'skii, Sov. Phys. Solid State 15, 269 (1973)

28. V. I. Fistul', L. Ya. Pereva, E. M. Omel'yanovskii, E. P. Rashevskaya, N. N. Solov'ev, and O. V. Pelevin, Sov. Phys. Semicond. 8, 311 (1974)

29. V. A. Bykoskii, V. A. Vil'kotskii, D. S. Domanevskii, and V. D. Tkachev, Sov. Phys. Semicond. 9, 1204 (1975)

30. G. K. Ippolitova and E. M. Omel'yanovski, Sov. Phys. Semicond. 9, 156 (1975)

31. G. H. Stauss, R. J. Wagner, and J. J. Krebs, Bull. Am. Phys. Soc. 27, 277 (1982)

32. C. L. West, W. Hayes, J. F. Ryan, and P. J. Dean, J. Phys. C 13, 5631 (1980)

33. G. H. Stauss, J. J. Krebs, and R. L. Henry, Phys. Rev. B 16, 974 (1977)

34. W. H. Koschel, U. Kaufmann, and S. G. Bishop, Solid State Commun. 21, 1069 (1977)

35. G. A. Slack, F. S. Ham, and R. M. Cherenko, Phys. Rev. 152, 376 (1966)

36. F. S. Ham and G. A. Slack, Phys. Rev. B 4, 777 (1971)

37. W. Low and M. Weger, Phys. Rev. 118, 1119 (1960)

38. W. Low and M. Weger, Phys. Rev. 118, 1130 (1960)

39. L. Hemstreet and J. Dimmock, Phys. Rev. B 20, 1527 (1979)

40. L. A. Hemstreet and J. O. Dimmock, Solid State Commun. 31, 461 (1979)

41. R. R. Sharma, M. H. deA. Viccaro, and S. Sundaram, Phys. Rev. B 23, 738 (1981)

42. L. A. Hemstreet, Phys. Rev. B 15, 834 (1977)

43. R. R. Sharma and S. Sundaram, Solid State Commun. 33, 381 (1980); Bull. Am. Phys. Soc. 24, 255 (1979)

44. Y. Tanabe and S. Sugano, J. Phys. Soc. Japan 9, 753 (1954); 766 (1954)

45. M. H. deA. Viccaro, R. R. Sharma, and S. Sundaram, Bull. Am. Phys. Soc. 25, 10 (1980)

46. J. S. Griffith, The Theory of Transition Metal Ions (Cambridge University Press, New York, 1961)

47. R. P. Srivastava, S. Sundaram, and R. R. Sharma, Bull. Am. Phys. Soc. 26, 287 (1981)

48. W. Schairer and M. Schmidt, Phys. Rev. B 10, 2501 (1974)

49. M. Ilegems, R. Dingle, and L. W. Rupp Jr., J. Appl. Phys. 46, 3059 (1975)

50. R. Bleekrode et al., Phys. Letters 2, 355 (1962)

51. J. Owen and J. H. M. Thornley, Rep. Prog. Phys. 29, 675 (1966)

52. R. R. Sharma, T. P. Das, and R. Orbach, Phys. Rev. 155, 338 (1967)

53. R. R. Sharma, Phys. Rev. B 6, 4310 (1972)

54. M. H. deA. Viccaro, S. Sundaram, and R. R. Sharma, Bull. Am. Phys. Soc. 25, 326 (1980)

55. M. H. deA. Viccaro, S. Sundaram, and R. R. Sharma, Phys. Rev. B 25, (1982)

56. M. H. deA. Viccaro, S. Sundaram, and R. R. Sharma, Twenty-ninth Midwest Solid State Conference, September 25-26, 1981

57. M. H. deA. Viccaro, S. Sundaram, and R. R. Sharma, Bull. Am. Phys. Soc. 26, 287 (1981)

58. M. H. deA. Viccaro, S. Sundaram, and R. R. Sharma, Bull. Am. Phys. Soc. 27, 277 (1982)

59. R. R. Sharma, Phys. Rev. 176, 467 (1968)

60. R. R. Sharma, Phys. Rev. A 13, 517 (1976)

61. W. A. Harrison, in Pseudopotentials in the Theory of Metals (Benjamin/Cummings, Menlo Park, California, 1966)

62. K. H. Johnson, in Advances in Quantum Chemistry, Vol. 7, edited by P. O. Löwdin (Academic Press, New York, 1973), p. 143

63. G. Bylander, in Materials for Semiconductor Functions (Hayden Book Co., Inc., New York,)

64. C. J. Ballhausen, in Introduction to Ligand Field Theory (McGraw-Hill Book Co., 1962)

65. F. Seitz, P. Turnbull, and H. Ehrenreich (editors), in Solid State Physics, Advances in Research and Applications, Vol. 20, 1967

66. E. Clementi, IBM J. Res. Develop. 9, 2 (1965)

67. P. S. Bagus, T. L. Gilbert, and C. C. J. Roothan, in "Hartree-Fock wavefunctions of nominal accuracy for He through Rb^+, calculated by the expansion method" (Argonne National Laboratory, Argonne, Illinois, February 1, 1972)

68. C. J. Ballhausen and H. B. Gray, in Molecular Orbital Theory (W. A. Benjamin, Inc., New York, 1965)

69. M. Thinkam, in Group Theory and Quantum Mechanics (McGraw-Hill Book Co., 1964)

70. H. Goldstein, in Classical Mechanics (Addison-Wesley Publishing Co., 1950)

71. E. Merzbacher, in Quantum Mechanics (John Wiley and Sons, Inc., 1961)

72. P. O. Löwdin, Adv. Phys. 5, 17 (1956)

73. R. R. Sharma, J. Math. Phys. 9, 4 (1968)

74. K. J. Duff, Int. J. Quantum Chem. 5, 1 (1971)

75. M. H. deA. Viccaro, Int. J. Quantum Chem. 10, 1081 (1976)

76. R. R. Sharma, class notes for Physics 428, University of Illinois at Chicago Circle, Chicago, Illinois, 1981

77. G. Racah, Phys. Rev. 62, 438 (1942); 63, 367 (1942); 76, 1352 (1949)

78. A. Abragam and B. Bleaney, in Electron Paramagnetic Resonance of Transition Ions (Clarendon Press, Oxford, 1970)

79. See also page 111 of Ref. 46.

80. M. H. Pryce, Phys. Rev. 80, 1107 (1950)

81. H. G. Kuhn, in Atomic Spectra (Academic Press, New York, 1962)

82. L. Pauling and S. Goudsmit, in Structure of Line Spectra (McGraw-Hill Book Co., New York, 1930)

83. M. Rotenberg, R. Bivins, N. Metropolis, and J. Wooten, Jr., in The 3-j and 6-j Symbols (Technology Press, MIT, Cambridge, Massachusetts, 1959)

84. F. S. Ham, Phys. Rev. 166, 307 (1968)

85. R. G. Barnes and W. V. Smith, Phys. Rev. 93, 95 (1954)

86. J. J. Krebs, private communication

87. H. A. Jahn and E. Teller, Proc. Roy. Soc. (London) A 161, 220 (1937)

VITA

Maria Helena de Azambuja Viccaro, née Maria Helena da Cruz Azambuja, was born in Palmas, Pr., Brazil, on July 15, 1950. She attended the "Colegio Israelita-Brasileiro" High School in Porto Alegre, Brazil. Following graduation, she attended the Universidade Federal do Rio Grande do Sul in Porto Alegre, Brazil, and received a B.S. in physics in 1972 and her M.S. in physics in 1975. In 1979 she received an M.S., also in physics, from the University of Illinois at Chicago Circle. Her teaching experience at the Universidade Federal do Rio Grande do Sul was in freshman physics lecture sections. At the University of Illinois at Chicago Circle, her teaching experience was in freshman physics laboratory sections. She has the following publications:

1. Dependence of Raman intensities on π-type covalency parameter in octahedral complexes, M. H. deA. Viccaro, Master's Thesis (1975) [in Portugese], UFRGS, Brazil
2. Symmetry property of Lowdin's "alpha" function, M. H. deA. Viccaro, Int. J. Quantum Chem. 10, 1081 (1976)
3. Theory of charge-transfer for the electronic structure of Cr^{2+} in GaAs, M. H. de A. Viccaro, R. R. Sharma, and S. Sundaram, Bull. Am. Phys. Soc. 25, 10 (1980)
4. Theory of g-factors and zero field splitting parameters including Jahn-Teller distortion in GaAs:Cr^{2+}, M. H. deA. Viccaro, S. Sundaram, and R. R. Sharma, Bull. Am. Phys. Soc. 25, 326 (1980)
5. Generalized d-electron interaction matrices—their derivation and impact on existing results, R. R. Sharma, M. H. deA. Viccaro, and S. Sundaram, Phys. Rev. B 23, 738 (1981)

6. Theory of EPR results of Cr^{2+} in InP, M. H. deA. Viccaro, S. Sundaram, and R. R. Sharma, Bull. Am. Phys. Soc. 26, 287 (1981)

7. Jahn-Teller distortion and covalency effects in GaAs:Cr^{2+}, M. H. deA. Viccaro, S. Sundaram, and R. R. Sharma, Twenty-ninth Midwest Solid State Conference, Argonne National Laboratory, Argonne, Illinois, Sept. 25-26, 1981

8. Electronic structure of Fe acceptor in InP, M. H. deA. Viccaro, S. Sundaram, and R. R. Sharma, Bull. Am. Phys. Soc. 27, 277 (1982)

9. Electron paramagnetic resonance parameters of substitutional Cr^{2+} impurity in GaAs by a cluster approach, M. H. deA. Viccaro, S. Sundaram, and R. R. Sharma, Phys. Rev. B 25, (1982)